

Electronic Thesis and Dissertation Repository

12-11-2013 12:00 AM

Glass-Ceramics for Non-Metallic Dental Implant Applications

Selma Saadaldin

The University of Western Ontario

Supervisor

Dr. Amin Rizkalla

The University of Western Ontario

Graduate Program in Medical Biophysics

A thesis submitted in partial fulfillment of the requirements for the degree in Doctor of Philosophy

© Selma Saadaldin 2013

Follow this and additional works at: <https://ir.lib.uwo.ca/etd>



Part of the [Dental Materials Commons](#)

Recommended Citation

Saadaldin, Selma, "Glass-Ceramics for Non-Metallic Dental Implant Applications" (2013). *Electronic Thesis and Dissertation Repository*. 1799.

<https://ir.lib.uwo.ca/etd/1799>

This Dissertation/Thesis is brought to you for free and open access by Scholarship@Western. It has been accepted for inclusion in Electronic Thesis and Dissertation Repository by an authorized administrator of Scholarship@Western. For more information, please contact wlsadmin@uwo.ca.

GLASS-CERAMICS FOR NON-METALLIC DENTAL IMPLANT APPLICATIONS

(Thesis format: Integrated Article)

by

Selma Saadaldin, BDS, M.Sc.

Graduate Program in Medical Biophysics

A thesis submitted in partial fulfillment
of the requirements for the degree of
Doctor of Philosophy

The School of Graduate and Postdoctoral Studies
The University of Western Ontario
London, Ontario, Canada

© Selma A Saadaldin 2013

ABSTRACT

Metallic dental implants are an important treatment for the replacement of missing teeth. However, for esthetic and environmental issues, there is a need to develop non-metallic dental implant materials. In this thesis, two novel glass-ceramics (GCs), miserite and wollastonite, were synthesized for one-piece dental implant applications. Glasses were synthesized by wet chemical methods, followed by calcination, melting and quenching. The crystallization kinetics of these glasses were determined by differential thermal analysis (DTA). GC specimens were produced by cold pressing of the glass powder and sintering using schedules determined by DTA. The crystalline phases and microstructure of the GC samples were characterized by X-ray diffraction (XRD) and scanning electron microscopy (SEM), respectively. Miserite GC displayed an interlocking lath-like crystalline morphology. Mechanical testing results showed Dynamic Young's modulus (E), 96 ± 3 GPa, true hardness (H_o), 5.27 ± 0.26 GPa, fracture toughness (K_{IC}), 4.77 ± 0.27 $\text{MPa}\cdot\text{m}^{0.5}$, and brittleness index (BI), 1.11 ± 0.05 $\mu\text{m}^{-0.5}$, indicating suitable mechanical properties and machinability. Miserite GC showed excellent bioactivity, with formation of a hydroxyapatite surface layer when soaked in simulated body fluid (SBF). Osteoblast-like cells exhibited attachment, spreading and proliferation on miserite GC surfaces, demonstrating biocompatibility. However, preliminary studies revealed that the chemical stability of miserite GC was not optimal, prompting us to modify the GC composition. Accordingly, wollastonite GC was synthesized; it consisted of dense acicular interlocking crystals and demonstrated excellent machinability. E, H_o and K_{IC} were 90 ± 3 GPa,

5.15±0.47 GPa and 4.91±0.26 MPa·m^{0.5}, respectively. Importantly, chemical durability of wollastonite GC satisfied ISO 6872 specification for dental ceramics. Furthermore, when evaluated according to ISO 10993-14, there was little chemical degradation. In addition, the chemical stability tests had no significant effect on K_{IC} (*p*>0.05). Bioactivity tests revealed that wollastonite GC induced the formation of bone-like carbonated hydroxyapatite when soaked in SBF. Moreover, wollastonite GC supported osteoblast attachment and proliferation. Osteoblast spreading, focal adhesion formation and alkaline phosphatase activity on this GC were comparable to those on a control zirconium-oxide-based ceramic, indicating excellent biocompatibility. In conclusion, wollastonite GC is a promising material for non-metallic dental implant applications based on five tested qualities: mechanical properties, chemical stability, machinability, excellent bioactivity and biocompatibility.

KEYWORDS

Dental implant, Glass-ceramic, Miserite, Wollastonite, Dynamic Young's modulus, Fracture toughness, True hardness, Machinability, Brittleness index, Chemical durability, Bioactivity, Cell attachment, Cell proliferation, Focal adhesion, Alkaline phosphatase

CO-AUTHORSHIP STATEMENT

Chapters 1 entitled “**Introduction**” was written by Selma Saadaldin, with help in editing and proofreading by Drs. P. Canham, S.J Dixon and A.S. Rizkalla. *Chapter 2* entitled “**Synthesis of Bioactive and Machinable Miserite Glass-Ceramics for Dental Implant Applications**“ is adapted from Saadaldin *et al*, 2013. Dental Materials 29(6): 645-655, and reproduced here with a permission from ELSEVIER (Appendix A). In my role as a PhD candidate, I participated in designing the study, synthesized the glasses and glass-ceramics, performed the experiments, analyzed all data, performed the statistical analysis, and wrote the manuscript text. Dr. S. Jeffrey Dixon and Daniel O. Costa advised on bioactivity and cell experimental design, reviewed the results and provided editorial feedback. Dr. Amin S. Rizkalla, as the candidate’s supervisor provided ongoing guidance, contributed to the study design, reviewing of results, provided mentorship and editorial assistance. All experiments were carried out in the laboratories of Drs. A. S. Rizkalla, S. J. Dixon and D. W. Hamilton with technical assistance for the cell experiments from Ms. Elizabeth Pruski in Dr. Dixon’s lab.

Chapter 3 is an original manuscript that has been accepted for publication in Dental Materials, entitled “**Synthesis and Characterization of Wollastonite Glass-Ceramics for Dental Implant Applications**”. The manuscript was co-authored by Selma A. Saadaldin and Amin S. Rizkalla. Selma Saadaldin performed all experiments, data and statistical analysis and wrote the manuscript text. Dr. Amin S. Rizkalla contributed through designing the study, reviewing the results, and providing editorial assistance. Dr. P. Canham provided valuable and constructive comments on the manuscript. All experiments were carried out in the laboratories of Dr. A.S. Rizkalla.

Chapter 4 is an original manuscript that has been submitted for publication, entitled ***“Bioactivity and Cell-Compatibility of Wollastonite Glass-Ceramics”***. The manuscript is co-authored by Selma A. Saadaldin, S. Jeffrey Dixon, and Amin S. Rizkalla. In my role as a PhD candidate, I participated in designing the study, performed all experiments, analyzed all data, performed the statistical analysis, and wrote the manuscript text. Amin S. Rizkalla and S. Jeffrey Dixon aided in designing the study, reviewing the results, and providing editorial assistance. All experiments were carried out in the laboratories of Drs. A. S. Rizkalla, D. W. Hamilton and S. Jeffrey Dixon.

Chapter 5 entitled ***“General Discussion”*** was written by Selma Saadaldin. Drs. Peter Canham and Amin S. Rizkalla reviewed and edited the Chapter.

ACKNOWLEDGMENTS

In the name of ALLAH, the most Merciful, the most Gracious and the Most Beneficent. First and foremost I praise and gratitude ALLAH, the Almighty, who blessed me and gave me the strength, ability and endurance on this rewarding academic journey to complete my PhD degree and to succeed in my life.

I would like to acknowledge my supervisor, Dr. Amin Rizkalla, for his constant guidance, support, and patience particularly during the early years of my PhD program. I appreciate his time and effort for teaching me new laboratory testing techniques and enhancing my research skills. I would like to extend my profound appreciation to my advisory committee, Dr. Peter Canham and Dr. Gildo Santos, for providing ongoing advice and encouragement in regards to my research and enhancing the significance of the research by their valuable suggestions. Special thanks to Dr. Peter Canham for helping in editing and proofreading the thesis and providing me with his insightful comments.

I am grateful to Dr. S. Jeffrey Dixon for his sustained enthusiasm, thoughtful criticism and endless assistance. I am also very thankful to him for allowing me to use his facilities and work with the excellent research team in his lab. His unique personality motivates students to do the best. I would like to express my thanks to Dr. Douglas Hamilton for generously donating primary osteoblast cells and allowing me to use his fluorescence microscope. I would like to express my genuine appreciation to the faculty and staff in Medical Biophysics, in particular to Wendy Hough and Dr. Dan Goldman for always being able to help.

I extend my thanks to all staff at Western University for their kindness, understanding and caring especially Olga Sauer from SOGS. I would like to acknowledge my colleagues including Daniel Costa, Paul Prowse, Bedilu Abaineh Allo, Barry Lai and Manal Dafar for their fruitful input and for their help and support. Special thanks to Grace C Yau and Kimberley R Law for their technical assistance with XRD, Elzibiete Pruski for the help with cell works, and Tim Goldhawk for his assistance with SEM. I am grateful for the financial support provided by the Schulich school of Medicine & Dentistry (Schulich Graduate Scholarship) and the Natural Sciences and Engineering Research Council of Canada (NSERC).

I am indebted to my late father who believed in my strength and my abilities, provided me tools to accomplish my goals in life and encouraged me to continue my postgraduate studies. I sincerely wish he were here to share this accomplishment. My wholehearted thanks to my mother, my siblings and their families for their unconditional love and continuous prayers. It means so much to be surrounded by so many people who love and care about you. To my daughters Sara, Leena and Mariam and to my son Saeed who went through all of the ups and downs of my research work, thank you for your understanding and patience, especially Sara for offering me a helping hand when needed.

TABLE OF CONTENTS

ABSTRACT.....	ii
CO-AUTHORSHIP STATEMENT.....	iv
ACKNOWLEDGEMENTS.....	vi
TABLE OF CONTENTS.....	viii
LIST OF TABLES.....	xiv
LIST OF FIGURES.....	xv
LIST OF ABBREVIATIONS AND DEFINITIONS.....	xvii
CHAPTER 1:	
INTRODUCTION.....	1
1.1 DENTAL IMPLANT.....	1
1.1.1 Historical Overview.....	2
1.1.2 Implant Biomaterials.....	3
1.1.2.1 Metallic Implants.....	3
1.1.2.2. Ceramics.....	5
1.1.3 Mechanical Parameters of Dental Implants.....	9
1.1.3.1 Modulus of Elasticity.....	11
1.1.3.2 Fracture Toughness.....	12
1.1.3.3 Fatigue Strength.....	13
1.2 GLASS-CERAMICS.....	15
1.2.1 Glass-Ceramic Properties.....	16
1.2.2 Medical Glass-Ceramics.....	17
1.2.3 Dental Glass-Ceramics.....	19
1.2.4 Machinable Dental Glass-Ceramics.....	23

1.3 BONE PROPERTIES FOR DENTAL IMPLANTOLOGY.....	25
1.3.1 Macroscopic Structure of Bone.....	26
1.3.2 Bone Cells.....	27
1.3.3 Bone Related Markers And Adhesion Proteins.....	30
1.4 OSSEOINTEGRATION OF DENTAL IMPLANTS.....	34
1.5 BIOACTIVITY IN DENTAL IMPLANTOLOGY.....	36
1.6 THESIS HYPOTHESES AND OBJECTIVES.....	39
1.7 THESIS ORGANIZATION.....	40
1.8 REFERENCES.....	42
CHAPTER 2:	
SYNTHESIS OF BIOACTIVE AND MACHINABLE MISERITE GLASS- CERAMICS FOR DENTAL IMPLANT APPLICATIONS	59
2.1 INTRODUCTION.....	59
2.2 MATERIALS AND METHODS.....	61
2.2.1. Glass Synthesis.....	61
2.2.2 Crystallization Kinetics.....	62
2.2.3 Preperation of Glass-Ceramics.....	63
2.2.4 X-Ray Diffraction.....	64
2.2.5 Microstructure.....	64
2.2.6 Dynamic Young’s Modulus of the Glass and Glass-Ceramics.....	64
2.2.7 True Hardness.....	65
2.2.8 Fracture Toughness.....	65

2.2.9 Machinability.....	66
2.2.10. Bioactivity.....	66
2.2.11 Cell Number and Morphology.....	67
2.2.12 Cell Proliferation Assay.....	68
2.2.13 Statistical Analyses.....	68
2.3 RESULTS.....	68
2.3.1 Differential Thermal Analysis (DTA) of Glass.....	68
2.3.2 XRD Analysis of Glass and GCs.....	69
2.3.3 Microstructure of Glass and GCs.....	70
2.3.4 Physical and Mechanical Properties.....	76
2.3.5 Bioactivity of GC4.....	77
2.3.6 Cell Morphology and Number on GC4 and Titanium.....	80
2.3.7 Cell Proliferation on GC4 and Titanium.....	83
2.4 DISCUSSION.....	83
2.5 CONCLUSIONS.....	86
2.6 REFERENCES.....	87

CHAPTER 3:

SYNTHESIS AND CHARACTERIZATION OF WOLLASTONITE GLASS-CERAMICS FOR DENTAL IMPLANT APPLICATIONS..... 92

3.1 INTRODUCTION..... 92

3.2 MATERIALS AND METHODS..... 95

3.2.1. Glass Synthesis..... 95

3.2.2 Differential Thermal Analysis.....	96
3.2.3 Glass-Ceramics Preparation.....	96
3.2.4 X-Ray Diffraction.....	97
3.2.5 Microstructure	97
3.2.6 Dynamic Elastic Constants of the Glass-Ceramics.....	98
3.2.7 True Hardness and Fracture Toughness Evaluation.....	98
3.2.8 Chemical Durability.....	99
3.2.9 Degradation Testing.....	99
3.2.10 Machinability.....	100
3.2.11. Statistical Analyses.....	100
3.3 RESULTS.....	100
3.3.1 Differential Thermal Analysis of the Glasses.....	101
3.3.2 XRD Analysis of GCs.....	103
3.3.3 Microstructure of GCs.....	105
3.3.4 Physical and Mechanical Properties.....	105
3.3.5 Chemical Durability.....	105
3.3.6 Degradation Test.....	107
3.4 DISCUSSION.....	109
3.5 CONCLUSIONS.....	113
3.6 REFERENCES.....	114

CHAPTER 4:

BIOACTIVITY AND BIOCOMPATIBILITY OF A NOVEL

WOLLASTONITE GLASS CERAMICS	118
4.1 INTRODUCTION	118
4.2 MATERIALS AND METHODS	120
4.2.1 Materials.....	120
4.2.2 Bioactivity.....	120
4.2.2.1 Scanning Electron Microscopy and Energy Dispersive X-Ray Spectroscopy.....	121
4.2.2.2 X-Ray Diffraction.....	121
4.2.3 Biocompatibility.....	121
4.2.3.1 Osteoblast Attachment and Morphology.....	121
4.2.3.2 Cell Proliferation Assay.....	123
4.2.3.3 Quantification of Alkaline Phosphatase Activity.....	123
4.2.4 Statistical Analyses.....	124
4.3 RESULTS	124
4.3.1 Bioactivity.....	124
4.3.1.1 Scanning Electron Microscopy and Energy Dispersive X-Ray Spectroscopy.....	124
4.3.1.2 X-Ray Diffraction.....	125
4.3.2 Biocompatibility.....	129
4.3.2.1 Osteoblast Attachment and Morphology.....	129
4.3.2.2 Cell Proliferation Assay.....	129

4.3.2.3 Alkaline Phosphatase Activity (ALP).....	130
4.4 DISCUSSION.....	133
4.5 CONCLUSIONS.....	136
4.6 REFERENCES.....	137
CHAPTER 5	
GENERAL DISCUSSIONS.....	143
5.1 LIMITATION OF THE RESEARCH AND FURUTE DIRECTIONS.....	151
5.1.1 Limitations.....	151
5.1.2 Future Directions.....	152
5.2 REFERENCES.....	154
APPENDICES.....	161
A. COPYRIGHT PERMISSIONS.....	161
B. CHEMICAL DURABILITY TESTS OF MISERITE GC.....	177
CURRICULUM VITAE.....	179

LIST OF TABLES

Table 1-1: Ionic Compositions (mM) of Human Blood Plasma and SBF.....	37
Table 2-1: Differential Thermal Analysis (DTA) Data for Experimental Glass.....	72
Table 2-2: Avrami Exponents and Activation Energies of the Glass Crystallization.....	73
Table 2-3: Heat Treatment Schedules for Experimental Glass-Ceramics.....	73
Table 2-4: Physical and Mechanical Properties of Experimental Glass and GCS.....	77
Table 2-5: Energy Dispersive X-Ray Spectroscopy (EDX) Analysis of GC4 and Molar Ca/P Ratio for Different Soaking Times in SBF.....	78
Table 3-1: Chemical Composition (wt %) of the Experimental Glasses.....	95
Table 3-2: Optimal Heat treatment Schedules for the Experimental Glass-Ceramics Based on the DTA Data.....	97
Table 3-3: Avrami Exponents and Activation Energies of the Experimental Glasses	101
Table 3-4: Physical, Mechanical And Chemical Properties of the Experimental Glass-Ceramics and Yttria-Stabilized Zirconia (YZ).....	106

LIST OF FIGURES

Figure 1-1: Comparison of Natural Tooth and Implant with Crown	2
Figure 1-2: Clinical Applications of Zirconia.....	7
Figure 1-3: Dental Applications of Glass-Ceramics.....	23
Figure 1-4: Sections Through the Diaphysis of a Long Bone.....	32
Figure 1-5: Cross-Section Through the Mandible.....	33
Figure 2-1: Differential Thermal Analysis (DTA) of the Experimental Glass Powder	71
Figure 2-2: X-Ray Diffraction (XRD) of the As-Quenched Glass and GCs.....	74
Figure 2-3: Microstructure of Fractured Surfaces of As-Quenched Glass and GCs and Macroscopic Image of Machined GC4 Specimens.....	75
Figure 2-4: Bioactivity of GC4.....	79
Figure 2-5: Osteoblast Attachment, Spreading and Morphology on GC4 and Titanium	81
Figure 2-6: Osteoblast Proliferation on GC4 and Titanium.....	82
Figure 3-1: (A) Representative DTA Curve of the Glasses. (B) Typical DTA Plots of $\ln T_p^2/\Delta$ vs. $1000/T_p$ For the First Peaks of the Glasses.....	102
Figure 3-2: XRD Analysis of GC-A, GC-B and GC-C.....	103
Figure 3-3: SEM Micrograph of Sintered GCs.....	104

Figure 3-4: Fracture Toughness Values Before and After Soaking GCs Specimens in 4% Acetic Acid and Tris Buffered Solution.....	107
Figure 3-5: (A) Degradation Test of the Experimental GCs. (B) Weight Loss Percentages of the GCs After 120 Days Soaking in Tris Buffered Solution.....	108
Figure 3-6: Representative Image of Machined GC-B Specimens.....	112
Figure 4-1: SEM Images of WGC and YZ Before and After Soaking in SBF.....	126
Figure 4-2: EDX Spectra Showing Elemental Analysis of WGC and YZ Surfaces Before and After Soaking in SBF.....	127
Figure 4-3: XRD Pattern of WGC and YZ Specimens Before and After Soaking in SBF.....	128
Figure 4-4: Representative Fluorescence Images of MC3T-E1 Cell Attachment, Morphology Spreading and Focal Adhesions on WGC and YZ Substrata	130
Figure 4-5: MC3T3-E1 Cell Count (A) and Focal Adhesion (B) Count on WGC and YZ specimens after 6 and 24 h incubation.....	131
Figure 4-6: MC3T3-E1 Cell Proliferation (A) and Alkaline Phosphatase Activity (B) on WGC and YZ on WGC and YZ. Specimens	132

LIST OF ABBREVIATIONS AND DEFINITIONS

ΔE	Activation energy
ΔT	Full width at the half maximum of the exothermic peak
Å	Angstrom (1 Å= 10 ⁻¹⁰ m)
A	Apatite
AC	Acetic acid
Al	Aluminum
ALP	Alkaline phosphatase
ANOVA	Analysis of variance
BI	Brittleness index
BSA	Bovine serum albumin
CAD-CAM	Computer-aided design/ computer-aided manufacturing
CPTi	Commercially pure titanium
DAPI	4',6 diamidino-2-phenylindole
DTA	Differential thermal analysis
E	Modulus of elasticity
ECM	Extracellular matrix
EDX	Energy dispersive X-ray spectroscopy
F-actin	Filamentous actin
FA	Focal adhesion
FBS	Fetal bovine serum
FTIR	Fourier transform infrared reflection spectroscopy
GC	Glass-ceramic

HA	Hydroxyapatite
HCA	Hydroxycarbonate apatite
H_0	True hardness
K_{IC}	Fracture toughness
N	Newton
n_A	Avrami exponent
\emptyset	Heating rate
PBS	Phosphate-buffered saline
$pNPP$	<i>p</i> -nitrophenol phosphate
RT	Room temperature
SBF	Simulated body fluid
SD	Standard deviation
STi	Sandblasted and acid-etched titanium
TBS	TRIS-HCl buffered solution
T_e	Liquidus temperature
T_g	Glass transition temperature
Ti	Titanium
T_p	Glass crystallization temperature (Exothermic peak)
V	Vanadium
V_L	Longitudinal wave velocity
V_S	Shear wave velocity
W	Wollastonite
wt/A	Weight loss/ unit area

XRD X-ray diffraction
Y-TZP Yttria-stabilized tetragonal zirconia polycrystals
YZ Yttria-stabilized zirconia
 α -MEM..... Minimum essential medium
 μg Microgram
 μm Micrometer
 ρ Density
 ν Poisson's ratio

CHAPTER 1

INTRODUCTION

Overview: This Chapter provides background information on dental implants, including an historical overview, a review of materials used for dental implants, and a description of the most relevant mechanical parameters of dental implants. The chapter also includes background information on glass-ceramics, including their properties and clinical applications, pertinent aspects of bone physiology, osseointegration of dental implants, and the bioactivity of biomaterials. It concludes with the study hypotheses and objectives of the study and an outline of the organization of the thesis.

1.1 DENTAL IMPLANTS

Dental Implant is defined as a “prosthetic device of alloplastic material(s) implanted into the oral tissues beneath the mucosal and/or periosteal layer, and/or within the bone to provide retention and support for a fixed or removable prosthesis”.¹ Part of most dental implants is projected into the oral cavity and therefore subjected to wide range of physical and biological environments, in contrast to medical implants that are placed totally inside the body e.g. artificial hip, knee and silicone breast.²

Theoretically, implants within bone would perform the same way as the natural tooth (Figure 1-1) through balancing between osteoblast and osteoclast activities, hence maintaining the health of the maxilla or mandible with minimal bone resorption.³ Dental implants must be capable of transferring occlusal forces to the adjacent bone through osseointegration as the bone anchors to the implant surfaces.⁴ In general, developing an optimal dental implant requires the collaboration among biomaterial, chemical, mechanical, physical, and biological interdisciplinary expertise.⁵

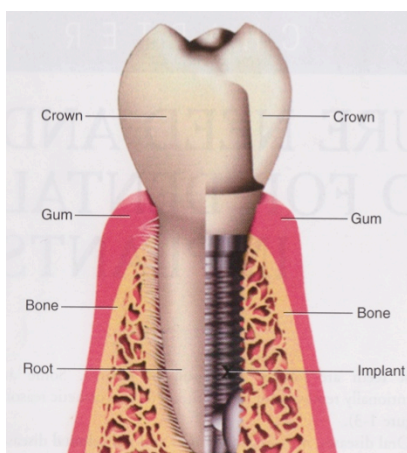


Figure 1-1: Comparison of natural tooth and implant with crown. Adapted with permission from *Dental Implants*, 2nd edition.⁶ (Appendix A)

1.1.1 Historical Overview

The replacement of missing teeth using dental implant restorations have been traced to ancient civilizations where seashells, wood, bone, ivory, gold and stone were used.¹ Throughout centuries, there were documentations of successful tooth transplantation for restoring missing teeth; human or animal teeth were used to replace missing teeth. In the early 19th century, cast gold tooth-root shaped implants were fixed into fresh extracted sockets and other materials were proposed such as platinum-lead implants, iridium and silver posts. However, complications were accompanied with different implant materials, designs and procedures leading to the beginning of “modern era” of dental restorations in 1950s. Vitallium, an inert cast alloy, composed of cobalt, chromium and molybdenum was proposed as a dental implant material. This alloy was used for different applications; such as sub periosteal implants and orthopedic plates, screws, nails and joints.⁷

The most important milestone in dental implants was the understanding of osseointegration phenomena by Brånemark⁸ in 1952. After 3 years, Brånemark and his team used the first titanium dental implant on a human subject⁸. In 1978, he reported the

breakthrough in Osseointegration Clinical Dentistry in a Toronto Conference with clinical insertion of 2768 implants soon after that.⁸

The global dental implant market was valued at approximately \$6.8 billion in 2011 and is predicted to increase by an average of 9.3% per year from 2011 to 2016.⁹ Over one million dental implants are inserted each year. These numbers continue to increase progressively, with almost \$550 million of implant products sold to North American dentists in 2005.⁶ Success rates for mandibular implants (96-98%) and for maxillary implants (94-96%) were reported; these appeared to depend on bone quality, surgical techniques and primary implant retention and stability.⁷

1.1.2 Implant Biomaterials

Metal alloys and ceramics are the two classes of biomaterials currently used for dental implants.

1.1.2.1 Metallic Implants

The current alloys used for dental implants belonged to two principal metallic systems: titanium-based alloys and cobalt-based alloys^{1,8,10}

Titanium-based alloys are considered as “materials of choice” due to their high strength-to-weight ratio, desired physical and chemical properties, high corrosion resistance, outstanding biocompatibility, excellent fatigue feature and relatively low cost.^{7,11} It can be presented either in a 99.75% pure form known as commercial pure titanium (CPTi) or as an alloy with 6% aluminum and 4% vanadium (Ti-6Al-4V). CPTi has been used since 1950 in medical applications due to its superior mechanical strength, corrosion resistance,

its welding ability and ease for shaping. CPTi alloys (monophasic- α) are available in four grades with disparate amounts of impurities of carbon, hydrogen, iron, nitrogen and oxygen. In spite of relatively small percentages of the interstitial impurities, they affect the mechanical properties of CPTi significantly. The limitations of CPTi lead to the development of biphasic α/β alloys (Ti-6Al-4V), which are currently the most commonly used alloys for medical applications.¹⁰

Titanium is considered biocompatible due to its low dissolution rate and non-reactivity of the titanium-dissolution products leading to bone thriving and osseointegration.^{12,13} Topography of the titanium surface can be modified, mechanically or chemically, to improve the rate and quality of osseointegration and to maximize bone-implant interaction such as sand blasting, plasma-spraying and chemical treatment of the implant surface.^{1,7,10,13} However, some titanium's modifications (e.g. screw threading or deposition of coating) will reduce its fatigue strength. Many studies believed that bioactive coatings on dental implants might disrupt the inter-facial attachment with bone.^{10,14-16}

Under physiological conditions, titanium-based implants are in a passive state because of the thin layer of titanium oxide, of nm thickness, that is formed immediately over implant surfaces. This layer will be in contact with the tissues of the body. The superior corrosion resistance, biocompatibility, and osseointegration of titanium were ascribed to the presence of this layer.¹⁷ Different oxides such as TiO, TiO₂, and Ti₂O₃ can be formed. Yet, TiO₂ is considered to be the most stable oxide and usually is found after exposure to physiological environments. The crystalline structures of the oxide layer are changed according to implant surfaces.^{1,7}

Even though titanium is considered as a material of choice for dental implants, its limitation has been investigated in several studies. Despite the long-term clinical success rate (10-16 years) of titanium dental implants, biological and technical complications did occur (48.03% up to 16 years).^{18,19} Sicilia *et al*¹⁹ found that diverse titanium allergic reactions were detected in some dental implant patient. Other studies and clinical reports addressed the relationship of titanium dental implant failures to allergic and hypersensitivity reactions, in spite of the deficiency of epidemiological studies.¹⁸⁻²³ Additionally, the cosmetic outcome of anterior dental implants might be unacceptable to the patients due to a greyish dark color line along the gingival tissues as a result of gingival resection or thin peri-implant gingival tissues.²⁴

1.1.2.2 Ceramics

Ceramics exhibited outstanding biocompatibility, owing to their chemical stability. The color of ceramics can match the color of bone, enamel and dentin. Ceramic implant materials are classified into two categories: “inert” and “bioactive”.¹

Bioactive ceramics react directly with bone tissue; the result of this reaction is a direct chemical bond between the implant surfaces accompanied with new bone formation.²⁵

Bioactive ceramics are relatively brittle and partially soluble, making it not suitable for use in high-stress situations. Therefore, it is mainly used as bone filler or as surface coating. There is a great emphasis on bioactive and bioresorbable ceramics to elicit normal tissue regeneration and form an intimate bond with bone tissues.^{1,7}

Hydroxyapatite, (HA), $\text{Ca}_{10}(\text{PO}_4)_6(\text{OH})_2$ and tricalcium phosphate ($\text{Ca}_3(\text{PO}_4)_2$) are some of the commonly used bioactive ceramics, which can possibly develop a cohesive chemical

bond with bone.²⁶ Accordingly, ceramic materials can be used as a coating onto other implant surfaces or it can make up the bulk of dental implant.

Inert ceramics like aluminum oxide (Al_2O_3), carbon (C) and zirconia (ZrO_2) are well tolerated by bone tissues similar to titanium-based alloys.⁷ Inert ceramics have high strength, stiffness and hardness, but their fracture resistance is poor, especially to bending forces. Inert ceramics can withstand relatively low tensile and shear stresses, with the high risk of catastrophic fractures.^{7,17} Several forms of carbon have been used including amorphous carbon, carbon fibers and carbon-silicate, but currently they are not used because of their defective osseointegration. Alumina, one of the inert ceramics, is brittle and tends to break when subjected to occlusal forces.¹⁷

Zirconia is the oxidized form of zirconium (ZrO_2). Currently it is the only used all-ceramic dental implant material, owing to its outstanding mechanical properties comparable to that of steel, in particular bending strength, fracture toughness, and Young's modulus. Zirconia has been used as implant biomaterial for hip replacement since the 1970s.²⁴ In Dentistry; zirconia has been used widely for different applications such as manufacturing high strength crown and bridge frameworks, endodontic posts, implant abutments, veneers, and orthodontic brackets.⁷

The first *in vivo* study of zirconia dental implants was in 1993, when a group of researchers inserted experimental zirconia in the mandibles of dogs.²⁷ However, the first clinical report of using zirconia dental implant in patients was published in 2004.²⁸ Zirconia dental implants showed satisfactory osseointegration that is comparable with the titanium dental implants,²⁹ and the stress distribution is also similar to that of titanium

implants.³⁰ Other study revealed that the fracture strength of the one-piece zirconia implants can be reduced following machining and during cyclic loading.³¹ Nevertheless, the current clinical data on the biomechanical behavior of the zirconia dental implants are inadequate.^{31,32} Currently zirconia is used for different application ranging from dental implant abutment, one-piece dental implant, dental posts and in hip arthroplasty (Figure 1-2).

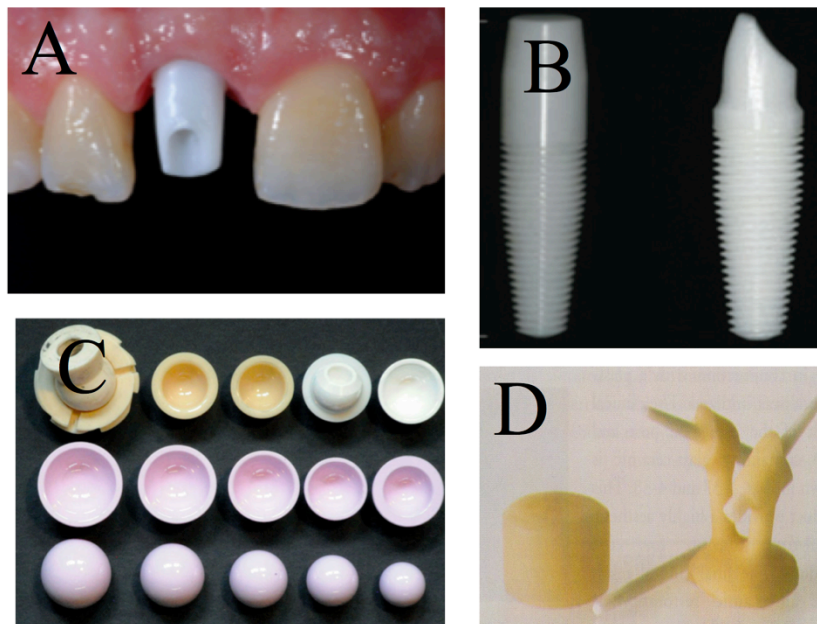


Figure1-2: Clinical applications of zirconia. A) Dental implant abutment.³³ B) One-piece dental implant.³⁴ C) Different generations of zirconia used in hip arthroplasty as bearing materials.³⁵ D) Zirconia-containing glass-ceramic ingots and zirconia posts.³⁶ Figures are adapted from the references with permission (Appendix A)

Zirconia is a polymorphic material since it can have more than one crystalline structure depending on the pressure conditions and temperature. Pure zirconia is monoclinic at room temperature (RT). As the temperature increases, the monoclinic phase transforms into the tetragonal form at 1170 °C and later into the cubic phase at 2370 °C.³⁷ As the temperature cools down to RT, phase transformation is accompanied with significant volumetric expansion (3-5 vol %) generating high internal stresses and cracks in pure zirconia.^{28,38}

Metal oxides such as CaO, MgO, CeO₂ and Y₂O₃ were added to pure zirconia, in small percentages (3-8 mass%), to stabilize the tetragonal phase at RT by allowing the generation of multiphase materials and to control the volumetric expansion.³⁸ Yet, the majority of dental researches focused on Y₂O₃ doped zirconia, which is known as yttrium tetragonal zirconia polycrystals (Y-TZP).³⁸ Y-TZP exhibits diverse interesting characteristics like high density, high compression and bending strength as well as low porosity that is usually associated with other oxides such as MgO.³⁷ The addition of small percentages of Y₂O₃ to zirconia results in the formation of a metastable tetragonal crystal structure at RT. When a crack is generated, it tends to progress and grow. In the meantime, the metastable tetragonal crystal structure of zirconia transforms to the more stable monoclinic form accompanied by an expansion of the material causing closure of the crack tip and consequently preventing it from advancing.³⁹ This phenomenon is known as stress-induced transformation toughening which gives Y-TZP ceramics its superior mechanical properties compared with other ceramics.

On the other hand, the ongoing progression of phase transformation might initiate surface flaws, followed by the ejection of grains, resulting in catastrophic effects and making the

material more vulnerable to aging.⁴⁰ Additionally, Y-TZP undergoes microstructural degradation at a relatively low temperature in humid environments leading to a significant decrease in flexural strength⁴¹ and reducing its functional lifetime as a result of increasing the susceptibility to crack growth.⁴²

Many researchers are concerned about the considerable concentration of radioactive impurities of uranium and thorium radionuclides in naturally occurring zirconia.⁴³ *Alpha* and *gamma* radiations are correlated with zirconia. Significant *alpha* radiations have been detected in zirconia-based ceramics used for surgical implants that can adversely affect hard and soft tissue cells.²⁷ *Gamma* radiation levels are not considered hazardous in zirconia.^{43,44} Since the radioactivity of Y-TZP ceramics can be effectively managed by carefully controlled purification procedures, Y-TZP can be safely considered for biomedical applications.^{24,43} Many published papers state that the radiation doses from highly purified zirconia powder ceramics form are significantly lower than the natural background dose.⁴⁰ Zirconia can be used as a dental implant by itself, or its particles can be used as coating materials for titanium dental implants to improve its osseointegration.⁴⁵

1.1.3 Mechanical Parameters of Dental Implant Materials

Dental endosteal implants are used to reconstruct and replace missing teeth to improve mastication, aesthetic and speech, stabilize and support removable dentures or create the abutments for fixed prostheses.¹¹ Therefore, the bone-implant interface should withstand forces generated during functional and para-functional forces for up to 40 years.¹⁷ The magnitude and spatial distribution of stresses on the implant, bone and the dental implant-

tissue interface will depend on several factors: dental implant shape, loading on the implant, quality and quantity of the surrounding bone and the mechanical properties of implant and interfacial bony tissues.⁴⁶ Listings of the materials' physical properties are not useful unless they are related to the physiological implications of the biomechanics.⁴⁷

Implants are subjected to compression, shear, bending and torsion loading leading to a wide range of normal and shear stresses. The force direction must be considered in addition to the magnitude of the loading. Since bone is 65% weaker when loaded in shear, shear forces that are transmitted from implant to bone should be reduced.¹³ Increased interfacial shear strength results in a better stress transfer from the implant to the surrounding tissues and lowers stresses in the implant.⁴⁸ Studies have shown that excessive forces compromise the osseointegration and biointegration of the implants.¹⁷ The occlusal forces are transferred from teeth to the surrounding bone via periodontal ligaments as tensile and compressive forces that favor the maintenance of the bone support by balancing between bone apposition and resorption in a process known as bone remodeling.⁴⁹ On the other hand, the occlusal loads from the dental implants are transmitted to the bone tissues mainly by compressive forces that tend to cause bone resorption.⁴ Modifying the material type, diameter and length of dental implants are considered as important factors to reduce the compressive forces in addition to the patients' factors including occlusal habits (clenching and bruxism) and the quality of the jawbone.¹⁷ Moreover, threaded dental implants have the tendency to reduce shear stress, convert occlusal loads into more favorable stresses at the bone interface, and reduce the risk of failure.¹³

During normal functioning, dental implants are subjected to various forces and moments that are transmitted to its internal structure. Thus they should tolerate these different masticatory loads without failures or fracture.⁵⁰ However, a quantitative evaluation of these loads is challenging, because it is determined by several factors such as magnitude of the usual chewing forces that range between 220-880 N, anatomical and physiological properties of surrounding bone and the mechanical properties of the dental implant.⁵⁰ Modulus of elasticity, fracture toughness, fatigue strength, yield and ultimate strengths are the more important mechanical properties for dental implant design.¹ In the current research project, we evaluated the modulus of elasticity and fracture toughness of the bioceramics that we synthesized.

1.1.3.1 Modulus of Elasticity

The young's modulus of elasticity (E) is an expression for material stiffness and an important property that influences the ability of the implant to transmit stresses to the adjacent bone and sustains tissue vitality over time.¹ It affects osseointegration and implant's compatibility with surrounding bone.⁵¹ The Young's modulus for titanium and dental zirconia are 100-116 GPa¹⁰ and 200-210 GPa⁵², respectively. These values are significantly higher than that of the human cortical bone ranging from 4 to 30 GPa.^{10,11,53} The extreme mismatch between the E values, of bone and implant materials can lead to a phenomenon known as stress shielding. As a result of the extremely stiff implant, disuse atrophy, bone resorption and implant complications can occur.⁵⁴⁻⁵⁶ The E value is used to evaluate bio-functionality of dental implants. The lower the Young's modulus of implant material, the better the load distribution to the surrounding tissue with the possible

beneficial result of new bone formation.¹¹ Porous titanium dental implants are used to decrease the E value, but the fatigue strength was diminished by at least 10%.¹¹

1.1.3.2 Fracture Toughness

The *fracture toughness* (K_{IC}) is a measure of energy needed to cause failure in the presence of a defect and it is important in evaluating implants with surface contours that can act as stress raiser.¹ K_{IC} is a critical value of the stress-intensity factors that causes failure of the material. K_{IC} values of materials are most useful when working with materials of limited toughness or ductility. Materials that show very little plastic deformation before fracture usually have relatively low K_{IC} .⁵⁷ Improvement of K_{IC} values of the dental implant materials have been established by various surface modification approaches, such as flaw modification (size or geometry), coating and heat treatment.⁵⁸ The microstructure of the materials has a considerable effect on the K_{IC} . For instance, dense interlocking crystals microstructure usually attributes to higher K_{IC} as a result of blunting microcracks and inhibiting crack propagation.³⁶

K_{IC} is usually measured using a four-point bend test with a single-edge or chevron-notched specimens or by compact tension through recording the tensile or bending force respectively⁵⁹. Another method for calculating K_{IC} is Vickers indentation tests.^{57,60} The Vickers indentation test has become common for brittle materials like glasses and ceramics because it is simple, quick, standardized by using Vickers diamond indenter and it can be used on a comparative basis for specimens with small surface area.⁶⁰ Yet, there are limitations to this technique including:

1. Presence of 19 different standardized equations in the literature to calculate K_{IC} . These equations are assuming the crack geometry as radial-median (halfpenny) or Palmqvist shaped.⁶⁰
2. Measurement of the crack length, that is used later to calculate the K_{IC} , should be accurate and standardized.⁶⁰
3. Young's modulus and hardness of the material should be known to be included in the K_{IC} equation.^{57,61}

Blendell, Evans and Lankford equations applied curve-fitting methods for median and Palmqvist crack patterns, which were applicable to both cracks systems.⁵⁷ In my thesis research, the Lankford equation was used to calculate K_{IC} since it combines both crack geometries.

1.1.3.3 Fatigue Strength

Dental implant materials can fail at a much lower stress, when subjected to cyclic loading, than that which the material can withstand under the application of a single maximum load. These failures are known in engineering terms as *fatigue failures*, while they are identified in clinical fields as *stress fracture*. *Stress concentration* (often known as stress raiser or stress riser) is the localization of high stresses at sharp notches, holes or corners, it is often the point of originating fatigue failure.⁶² Once initiated, the crack can propagate incrementally within the material under the cyclic or repeated loading.⁵⁹ Since fatigue fracture of dental implants does occur, fatigue resistance is considered an important property of dental implants. The most severe mechanical stress conditions are related to biodynamic fatigue when several factors are involved such as the surface

topography and presence of stress concentration and corrosive environments.⁵⁹ ISO 14801 standard was introduced to test the dynamic fatigue strength of dental implant materials with angled specimens to determine the survival functional threshold loads under “worse case” biological conditions.⁵⁰ Interestingly, it has been proven that fatigue strength especially due to fretting (where an overlapping of friction wears and cyclic loading occur between two bodies such as a screw and bone plate) was higher when the materials exhibited low Young’s modulus.⁶³ The passive oxide layer on titanium alloys can crack when bending forces were applied on the implant leading to corrosion fatigue in simulated body environments that accompany low oxygen content and degassing with nitrogen.⁶⁴ It was proven that the fatigue strength of dental implants decreased by 19% in simulated body environments compared with the laboratory dry conditions. Furthermore, corrosion fatigue can be initiated with the development of pits that act as sites of stress concentration.⁶⁵

Fatigue failure is infrequent in ceramics owing to the absence of inelastic (plastic) strain during cyclic loading.⁵⁹ However, inter-granular fatigue can cause reduction of mechanical strength as a result of the propagation of natural microcracks originally existing in the component’s microstructure. Although Y-TZP ceramic materials show significant subcritical crack propagation at extensively lower stress levels, but it could be used successfully in dentistry subjecting to the masticatory forces taking into consideration its initial high mechanical strength and special design of the material.⁶⁶

1.2 GLASS-CERAMICS

Glass-ceramics (GC) were first discovered in mid-1950s by a famous glass chemist, S.D. Stookey³⁶ who found that these materials combined the attractive properties of glasses and ceramics on top of the favorable properties superior to organic polymers and inorganic materials.³⁶ Later, in the late 1950s, Corning Glass Works developed diverse GCs for different applications.³⁹ MacCulloch^{7,39} in 1968 introduced the first dental GC based on the $\text{Li}_2\text{O-ZnO-SiO}_2$ system that was used to construct denture teeth. He suggested the possibility of using this GC to fabricate crowns and inlays by centrifugal casting of molten glass.³⁹

GC is a ceramic material formed by a process called *ceramming*. This process involves subjecting base glasses to controlled heat treatment, during which nucleation is initiated followed by the development of tiny and evenly distributed crystals throughout the glass structure. The crystalline phase will grow and can eventually occupy from 50% to nearly 100% of the material.^{7,39} Thus, a GC is a multiphase material containing a residual glass with a finely dispersed crystalline phase(s).³⁹ The number and size of the crystals and their growth rate are regulated by the ceramming time and temperature of the heat treatment. GCs have a wide variety of special microstructure that cannot be produced in any other material. These microstructures are related to the base glass, structure of the formed crystals and their mode of growth.³⁹ Currently, GCs based on leucite, lithium disilicate and HA have been used for dental applications. They are available as powders or as solid blocks that can be pressed, milled or prepared using computer-aided design/computer-aided manufacturing (CAD-CAM) technology.

1.2.1 Glass-Ceramic Properties

GCs with diverse and favorable properties were developed based on the chemical composition of the base glass and the microstructure of the GC. Regarding the processing properties; synthesis of parent glass is considered as a critical step in the GC development. In addition to producing bulk glasses by traditional melting and forming, it can be produced by sol-gel, chemical vapor deposition, rolling, spin-casting, thin-layer method, casting, drawing, pressing and press-blowing a glass melt. Technologies used to synthesize the base glass can be used for the production of the GC. Glass powder or grains can be converted to GCs by different methods. GCs are thermally stable; they can withstand high-temperature with limited and controllable shrinkage and expansion. Thus, GCs are manufactured on a large scale for industrial, technology and medical applications.³⁶

As GCs are non-porous and multi-phase materials, they demonstrate different levels of translucency, transparency, and opacity based on the type of crystals, microstructure of the material and the difference in the refractive index between the crystal and the parent glass.⁶⁷ GCs can be produced in any color by adding pigmentation. Other important optical properties for some GCs are fluorescence and opalescence.³⁶

Degradable or chemically durable GCs can be produced depending on their crystals, the glass and crystalline phases exist in the material and the interface between the crystals and the glass phase. Different microstructures of GCs permit the combination of resorbability of one specific phase and chemical stability of other phase(s). Some GCs

have good biocompatibility and have been developed for medical and dental applications; other GCs are bioactive and used in implantology.⁶⁸

The mechanical properties of GCs are improving; it has been possible to achieve flexural strength up to 500 MPa and K_{IC} higher than $3 \text{ MPa}\cdot\text{m}^{0.5}$. *Flexural strength* (also known as bend strength, fracture strength or modulus of rupture) is the material's ability to resist deformation under load when unsupported, while the *fracture toughness* is the estimation of the load required to cause crack propagation.⁶² No other material exhibited excellent mechanical properties combined with translucency and handling qualities as in the case of monolithic GCs. An additional advantage of certain GCs is their machinability, where the material can be milled, drilled or sawed into different shapes.⁶⁹ Furthermore, surface characterization of the GCs such as roughness, polishability, luster or abrasion can be controlled.⁶⁸ There are different GC systems, which are available in the market for medical or dental applications such as wollastonite, leucite, lithium disilicate, HA and mica GCs. Other GC systems are discussed in the literature but they are still not available for clinical applications such as miserite, fluorrichterite, fluorapatite and canasite GCs.³⁶

1.2.2. Medical Glass-Ceramics

GCs are used in implantology as medical prostheses to replace missing parts of body such as orthopedics, head and neck surgery, dental implants and root fillers. These materials should be biocompatible, and in most cases, bioactive to form a biologically active hydroxycarbonate apatite (HCA) layer that permits bonding with bone. Depending on the application, GC can be load bearing or non-load bearing to fulfill different requirements for each situation with respect to bending strength, toughness and Young's modulus.³⁶

Bioactive glasses such as BIOGLASS[®] was found to have multiple applications and are used in head and throat surgery in the form of middle-ear devices and implants for orbital floor of the skull.²⁵ The following bioactive GCs are used in human medicine for implantology: Cerabone[®], Ceravital[®] and Bioverit[®].

Cerabone[®] is a GC prepared from the parent glass in $3\text{CaO}\cdot\text{P}_2\text{O}_5\text{-CaO}\cdot\text{SiO}_2\text{-MgO}\cdot\text{CaO}\cdot 2\text{SiO}_2$ system. Both of, apatite (A) and wollastonite (W) crystalline phases are homogeneously distributed in a glass matrix, commercially known as cerabone[®]A-W.⁷⁰ Cerabone[®]A-W is the most widely and successfully bioactive GC used for bone replacement in human medicine.³⁶ Since 1983, A-W GC has been used in spine and hip surgery, in the form of vertebral prostheses, for iliac crest restorations⁷⁰ or as bone defect fillers.³⁶ A-W GC demonstrates high bioactivity.⁷⁰ The advantages of this GC provided by the combination of bioactivity and specific mechanical properties, such as compressive strength (215 MPa), Young's modulus (110 GPa) and K_{IC} ($2\text{ MPa}\cdot\text{m}^{0.5}$).³⁶ The GC can be used in non-bearing load areas, and it was successfully used for vertebra replacements in more than 10,000 patients between 1991-1996.³⁶

Ceravital[®] Apatite-devitrite GC contains mainly SiO_2 , $\text{Ca}(\text{PO}_2)_2$ and CaO with small amounts of oxides such as Na_2O , MgO , K_2O .⁷⁰ *In vitro* and *in vivo* investigations have proven the biocompatibility and bioactivity of ceravital[®] GC.^{71,72} However, because of its poorer mechanical properties, the only clinical application for this material is the replacement of the ossicular chain in the middle ear where the loads are minimal.^{36,70}

Bioverit[®]I is a mica-apatite GC with a chemical composition derived from the $\text{SiO}_2\text{-Al}_2\text{O}_3\text{-MgO-Na}_2\text{O-K}_2\text{O-F-CaO-P}_2\text{O}_5$ base glass system. **Bioverit[®]II** GC contains mica as

the main crystal phase. **Bioverit[®] III** is SiO₂-free, contains apatite, AlPO₄ and complex phosphate structure.⁷⁰ All these GCs are machinable and workable with standard metal tools and they can be modified during the surgical procedure. The machinability of these GCs depends on mica content and the morphology of the GCs – the higher mica contents the better machinability of the GC.³⁶ Adequate mechanical properties of Bioverit[®]I and Bioverit[®]II allow them to be used as medical bone substitution for different applications such as orthopedic, head and neck surgery especially middle ear implants. Bioverit[®]III is used in composites with certain metals as bioactive materials.⁷⁰

1.2.3 Dental Glass-Ceramics

Dental GC is the second category of GCs that used for restorative dental applications to fulfill the dental biomaterial standardization. They must be capable of simulating the natural teeth properties: show compatibility with oral environment, high strength, resistance to abrasion and wear, and excellent chemical durability to withstand the harsh oral circumstances of wide range of temperature and pH. Surface properties of the dental GCs should match those of natural teeth like shade, translucency, opalescence and fluorescence. Another important property of the dental GCs is their suitable handling techniques for both dentists and dental technicians.⁷³

Restorative dental materials are used to fabricate crowns, bridges, inlays, onlays and veneers by different techniques such as casting, hot pressing, moulding, centrifuge layering and sintering.⁷⁴⁻⁷⁶ The following dental GCs have these properties: Dicor[®], IPS Empress[®] Cosmo, IPS Empress[®], IPS Empress[®] 2, IPS d. SIGN[®], Pro CAD[®] and IPS e.max.

Dicor[®] was the first GC used for inlays and crowns production⁶⁸ synthesized from SiO₂-Al₂O₃-MgO-K₂O-ZrO₂-CeO₂ glass system.³⁶ The main crystalline phase present in this GC is tetrasilicic mica crystals produced by controlled volume crystallization. Crystals are 1 μm in length at approximately 55 vol %.^{75,77} Dicor[®] is a castable GC with which dental restorations are fabricated in the dental laboratory in a centrifugal casting procedure.⁶⁸ The optical quality of DICOR[®] produced by controlled translucency is based on the microstructure of mica crystals embedded in a glassy matrix.³⁶ There is a relationship between the clinical survival of Dicor[®]GC dental restorations (up to 20 years) to various physical and biological factors, such as tooth position, patient sex, core structure, acid etching and cementation.⁷⁸

Dicor[®]MGC is a machinable GC, where the dental restorations are produced using CAD-CAM technology. This GC is characterized by a high crystallinity, approximately 70 vol % of crystal content. The main crystalline phase is tetrasilicic fluromica, KMg_{2.5}Si₄O₁₀F₂, in a sandwich-like composite sheet.^{36,74} Interlocking, easily cleavable fluoromica flakes of average diameter of 2 μm and 0.5 μm thickness, are the key machinability factors in the microstructure of Dicor[®]MGC.^{36,69} Dicor[®]MGC have excellent properties, yet their clinical application is limited due to low K_{IC} (1.5 MPa·m^{0.5})⁷⁹ and low biaxial flexure strength (150 MPa).⁸⁰

IPS Empress[®]Cosmo is used for dental core construction where its strength is improved by incorporation of more than 15% ZrO₂ in P₂O₅-SiO₂-Li₂O-ZrO₂ base glass. The properties of GCs are influenced by the growth and formation of ZrO₂ rich (Li₂ZrSi₆O₁₅) crystals during the hot-press procedure. These GCs demonstrate a bending strength of maximum 160 MPa with high translucency.⁸¹ Two different materials: IPS

Empress[®]Cosmo and ZrO₂-sintered ceramic (CosmoPost) are used as a unique combination to form post and core for endodontic treated teeth. The advantages of using post and core combination include: improved esthetics, unified post and core, inert and stable materials, high bending stiffness resistance to fatigue loading and simple fabrication procedures.⁸²

IPS Empress[®] is an extremely homogeneous, leucite-based material (KAlSi₂O₆) fabricated from the SiO₂-Al₂O₃-K₂O base glass system using surface controlled crystallization.⁷⁴ The degree of crystallinity of IPS Empress[®]GC is 35±5 vol %.⁸³ Leucite crystals increase flexural strength of the GC; the GC exhibited biaxial flexural strength of 110-160 MPa^{36,83} and K_{IC} up to 1.3 MPa·m^{0.5}.⁸³ Flexural strength value can be increased to 200 MPa, by improving the surface quality⁷⁴ or by modifying its microstructure.⁸⁴ The GC demonstrates very good chemical durability, optical properties (Figure 1-3A), abrasion and wear resistance qualities, that are comparable to those of natural teeth.⁷⁶ From 1991-2004, this GC was used to produce 27 million dental restorations, and the success rate was higher than 90% over 14 years of clinical assessment.⁶⁸ However, the fracture rates were higher for posterior crowns than the anterior ones for different time periods ranging between 5-11 years.^{76,85} Consequently, IPS Empress[®] is recommended for producing metal free dental restorations such as inlays, onlays, crown and veneers, but not recommended for multi-unit dental bridges.³⁶

IPS Empress[®]2 is a pressed GC with lithium disilicate (Li₂Si₂O₅) crystal phase. It was developed in order to overcome the limitations of IPS Empress[®], by increasing its strength and toughness to extend the clinical applications to posterior multi-unit bridges.⁷⁵ The pressed GC is derived from the basic SiO₂-Li₂O system with other oxides additions

such as ZnO, P₂O₅, K₂O and La₂O₃. It is fabricated through a combination of the lost-wax and heat-press techniques. The GC has high crystal content (Figure 1-3B). Lithium disilicate crystals are precipitated in the base glass by epitaxial nucleation and crystallization until they reach up to 70±5 vol %, with randomly oriented interlocking microstructure that are attributed to its superior mechanical properties.⁹ The interlocking crystals deflect and blunt the developing cracks leading to increasing the toughness of the material⁷⁵ and substantial increasing in the flexural strength.³⁹ The mechanical properties of lithium disilicate GC are double or triple those of leucite GC.⁸³ The flexural strength value of IPS Empress[®]2 is around 400 MPa and the K_{IC} is about 3.3 MPa·m^{0.5}.⁸³ Moreover, the chemical durability of this GC is within the ISO requirements of dental ceramics and it is better than IPS Empress[®] GC by about fourfold.⁸³ Though, the GC cannot be machined or cut after pressing.⁶⁸

IPS e.max Ceram is a low fusing nano-fluorapatite GC, and it is applied as veneering of restoration produced by press technology and/or CAD-CAM technology to improve its optical properties. Apatite needle-like crystals can be precipitated in SiO₂-Al₂O₃-CaO-Na₂O-LiO₂-K₂O-P₂O₅-F system.⁶⁸ The abrasion characteristics of the fluorapatite-containing GC are similar to lithium disilicate GC, but its chemical durability is higher than IPS Empress[®]2. Dental restorations can be fabricated in a special combination design; framework made of the high strength GC to absorb the load peaks, and the veneer apatite GC to produce optical properties such as fluorescence and opalescence with excellent chemical durability.³⁶

IPS d.SIGN[®]: a leucite-apatite composite containing GC derived from the SiO₂-Al₂O₃-Na₂O-K₂O-CaO-P₂O₅-F system. This GC is developed by combining two different

mechanisms: controlled surface nucleation that precipitates leucite crystals, and controlled bulk nucleation that precipitates fluoroapatite crystal phase, $\text{Ca}_5(\text{PO}_4)_3\text{F}$.⁶⁸ It is used to veneer metal framework of multi-unit bridges owing to the combinations of appropriate translucency, color, and brightness, with proper mechanical and chemical properties.⁷⁵ This GC is the most frequently used GC materials; around 55 million units were clinically delivered from 1998-2004.⁶⁸ IPS d.SIGN[®] GCs can be presented in different categories according to their usage to restore different tooth structures.³⁶

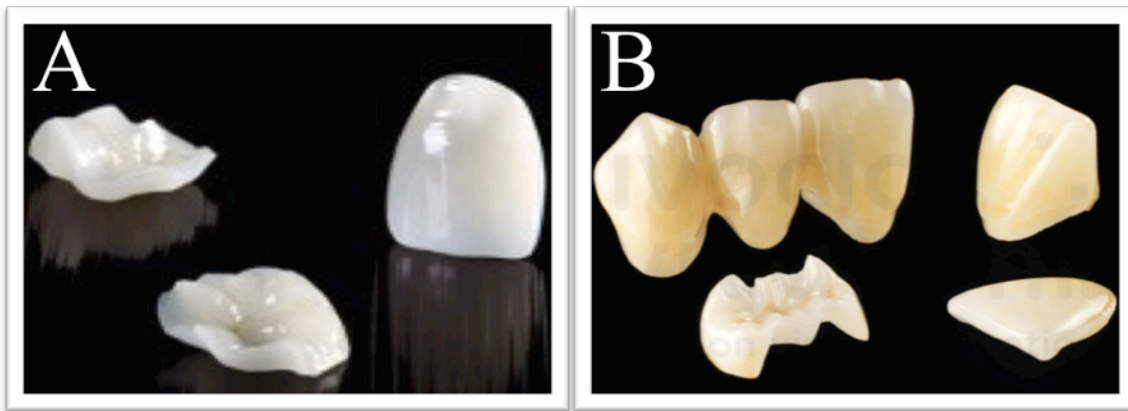


Figure 1-3: Dental applications of glass ceramic A) IPS Empress[®] GC inlays and veneer. B) IPS Empress[®]2 (3 unit bridge, crown, veneer and inlay). Adapted with permission from Glass-Ceramics Technology.³⁶ (Appendix A)

1.2.4 Machinable Dental Glass-Ceramics

CAD-CAM has become a commonplace fundamental technology in an industry used to design and fabricate virtually various products such as automobile, airplanes and jet engines.⁸⁶ CAD-CAM was introduced to dentistry in 1970s, followed by the development of CEREC[®] system in 1980s.⁸⁷ CAD-CAM provides advanced, highly qualified, state-of-the-art services to dental patients.⁸⁸

Machinable dental materials can be milled into their final form without condensation, sintering or melting. For direct restoration, a camera scans the replica of the prepared tooth to produce digital impression. Data are processed to software that guides machining tools to mill the ceramic blocks to the final restorations within a short time. Dental restorations are delivered in a single clinical appointment minimizing postoperative sensitivity and preventing tooth contamination. In the most advanced techniques, captured digital impressions are sent electronically to the lab for milling and production of the restorations. CAD-CAM restorations have several advantages over other restorations. First, shrinkage is not associated with CAD-CAM restorations due to the absence of heating, casting, condensing and melting. Second, the properties of the restorations are more predictable because of the machinable dental blocks.¹⁷ Currently, the innovation of CEREC[®]3 system is reflected in technical improvement of processing quality of ceramic restorations that are produced with natural morphology, fine surfaces and improved adaptation to the restored teeth.⁸⁹

ProCAD[®]: is a leucite-reinforced GC derived from the system $\text{SiO}_2\text{-Al}_2\text{O}_3\text{-K}_2\text{O-Na}_2\text{O}$, similar to IPS empress[®] with a finer particle size. It is characterized by excellent chemical durability, outstanding esthetic outcomes with different degrees of translucency that is available in several shades.⁹⁰ Mechanical properties of ProCAD[®] are acceptable, K_{IC} was determined to be $1.3 \text{ MPa}\cdot\text{m}^{0.5}$ with flexural strength of 135-160 MPa, that may be as high as 180-240 MPa after polishing the restoration surface or applying ProCAD[®] glaze.³⁶

IPS e.max[®]: is a machinable lithium disilicate GC that can be used with CAD-CAM systems. An intermediate lithium metasilicate GC containing dendritic crystals was developed, where the crystals are smaller and more homogenous than lithium disilicate.⁹¹

Lithium metasilicate GC is blue in color, and it can be machined easily and quickly to produce dental restorations which subsequently are heat-treated at 850 °C to be converted into a lithium disilicate GC. Subsequently, the restorations are additionally veneered with a fluoroapatite GC to imitate the optical properties of natural teeth.⁹² Clinical studies reviewing IPS e.max[®] dental restorations showed up to 8 years survival rates up to 93% for dental crowns and small bridges.⁹³ Other clinical studies disclosed that IPS e.max[®] all-ceramic three-unit bridges exhibited survival and success rates comparable to those of metal-ceramic bridges.⁹¹

1.3 BONE PROPERTIES FOR DENTAL IMPLANTOLOGY

Bone is a highly organized, mineralized connective tissue that has fundamental physical functions. It is one of the few mammalian tissues that can resist compressive and shear loading. Because of its stiffness and rigidity, it is suited for different functions including locomotion, standing and withstanding the mastication forces that can reach 1000 N.⁹⁴

Two primary functions are provided by bone: mechanical and metabolic. From the mechanical point of view, bone supports different structures and organisms, protects vital organs such as brain and heart and acts as leverage for musculoskeletal locomotion.⁹⁵

Bone consists of a biphasic extracellular matrix (ECM), cells, blood vessels and nerves. Bone matrix is composed of 30 vol % organic and 70 vol % inorganic materials.⁹⁶ The organic part consists mainly (98%) of a network of collagen type I fibers that contribute to tensile strength and toughness.^{97,98} The remaining 2% of the organic content includes structural and biologically active proteins, glycoproteins, peptides, lipid materials and adsorbed serum proteins.⁹⁵ The inorganic portion of bone ECM is composed of minerals, primarily carbonated hydroxyapatite, that include a complex of calcium phosphate,

calcium carbonate and small amounts of calcium fluoride and magnesium fluoride⁴ that contribute to compressive and shear strength and hardness.⁹⁷ The crystals in bone are small (an approximate diameter of 25-75 Å and length of 200 Å), and primarily presented in the form of poorly crystalline carbonate-apatite structure.⁹⁵

1.3.1 Macroscopic Structure of Bone

The mammalian skeleton is composed of two distinct kinds of bone based on porosity: dense cortical bone (also known as compact bone) and trabecular bone (also known as spongy or cancellous bone). Both cortical and trabecular bone are found in every bone site, but their quantity and distributions vary. The non-mineralized spaces within trabecular bone contain marrow, blood vessels, nerves and various cells. The main function of marrow is to generate the cells present in blood. Marrow is a highly osteogenic tissue that can lead to bone formation if placed in extracellular skeletal locations.⁴

Dense cortical bone comprises about 80-85 vol % of total bone in the body, it forms a shell around vertebral bodies and most bones. Cortical bone has two surfaces: outer periosteal and inner endosteal surfaces⁴⁹ (Figure 1-4). Cortical bone is organized in bony cylinders consolidated around a central blood vessels, called a Haversian system or osteon.⁴ The structure and microstructure of cortical bone provide the principal mechanical strength of the skeleton; the cortical thickness and cross sectional areas are strong indicators of gross bone strength and fracture resistance.⁹⁷ Trabecular bone comprises about 15-20 vol % of the body's total bone, is found in cuboidal, flat bones and in the end of long bones. When compared with cortical bone, it is lesser in density and has a greater degree of macro-porosity (medullary cavities) that is interconnected and

filled with hematopoietic marrow or fatty marrow in older adults.

Periosteum, the outer surface of cortical bone, forms a boundary between bone tissue and the covering soft tissue. The endosteum is fibrous and delicate membrane consisting of progenitor cells with slight amount of connective tissue. It acts as a lining of medullary and inner cavities of bone. Periosteum and endosteum are the sites of metabolic, cellular and biomechanical activities that modulate bone growth and shape.⁴⁹ They also contribute to new bone formation in the case of bone fracture.⁹⁶

Wolff's law stated that there are specific strain values that maintain the form and mass of the bone; values above this range will stimulate bone apposition while strains below the maintenance limit lead to bone resorption.⁹⁹ A study showed that these dynamic changes in the alveolar ridges primarily occur in cortical bone.¹⁰⁰

1.3.2 Bone Cells

A brief overview of bone cells is provided in the thesis because knowledge of the role of different bone cells and matrix molecules in bone formation and resorption is important for understanding the body's reaction to dental implants. This knowledge is helpful for evaluating the biological performance of different materials used as dental implants. Three major types of cells are involved in bone metabolism and physiology: osteoblasts, osteocytes and osteoclasts (Figure 1-5).

Osteoblasts are mononuclear, cuboidal and highly secretory cells. They are derived from multi-potential mesenchymal progenitor cells; mesenchymal stem cells or marrow-derived stromal cells.⁹⁵ Mature osteoblasts are responsible for producing bone's organic matrix that subsequently mineralizes extracellularly.¹⁰¹

Bone deposition continues in an active growth area, with osteoblasts laying down new bone in sequential layers. Osteoblasts produce phospholipids and proteoglycans that are important in the mineralization process.⁴ They produce paracrine growth factors that influence osteoprogenitor cells, the growth of preosteoblasts, and resorption of the mineralized bone matrix by osteoclasts during bone remodeling.⁹⁵ Mature osteoblasts affect osteoclastogenesis that in turn controls the degree of resorption at different bone sites.¹⁰³ Moreover, osteoblasts may act as helper cells for osteoclasts during normal bone resorption.⁴ When osteoblasts have successfully produced bone matrix, a fraction of osteoblasts that had become embedded transform into osteocytes, while the majority of the cells undergo programmed cell death (apoptosis).⁹⁵

Osteocytes are mature, post-synthetic osteoblasts; they are the most abundant bone cells (90-95% of all bone cells) and are the longest living type of bone cell.¹⁰⁴ Osteocytes are involved in mineral homeostasis⁹⁵ and coordination of metabolic activities.¹⁰⁴ Osteocytes act as mechanosensory cells by responding to internal and associated local strains from external loads on bone and, thus, osteocytes help to sustain the ECM.⁹⁶ Mechanical stimulation regulates gene expression in osteocytes, and affects their survival and apoptotic death. Some studies indicated that osteocyte apoptosis might stimulate or inhibit signals regulating the localized function of osteoclasts and osteoblasts.¹⁰⁵ Additionally, osteocytes can induce osteoclast activity, where the osteocytes orchestrate bone resorption as a result of expression of a rate-limiting factor required for osteoclast formation and function.^{104,106}

Osteoclasts are large motile, multinucleated cells (containing as many as 50 nuclei), and are responsible for bone resorption.⁴ They originate from hematopoietic stem cells in the

non-adherent part of the bone marrow.¹⁰⁷ Osteoclasts are located in shallow excavations (Howship's lacunae) along mineralized bone surfaces.⁴ The mechanism of the osteoclastic bone resorption is unique and efficient. Bone resorption requires a number of steps: 1) migration of osteoclast precursors to the bone surface; 2) fusion of precursors to form multinucleated osteoclasts; 3) attachment of the osteoclast to the bone surface; 4) polarization of the osteoclast to form three distinct membrane domains – a ruffled border, a sealing zone and a functional secretory domain; 5) pumping of HCl to lower the pH in the resorption lacuna, leading to dissolution of bone mineral; 6) secretion of hydrolytic enzymes to degrade the organic phase of the bone matrix; and 7) removal of degradation products from the resorption lacuna. Afterwards, osteoclasts undergo apoptosis or return to the non-resorbing stage.¹⁰⁸

In healthy adults, there is a continuous balanced interaction between bone-forming osteoblasts and bone-resorbing osteoclasts to sustain skeletal remodeling and maintain bone mass. Discrepancies of this balanced relationship are a feature of pathological disorders such as osteoporosis.⁹⁵

Bone-lining cells are a fourth type of bone cells. They are retired osteoblasts that do not embed in newly formed bone like osteocytes; instead, they adhere to the outer bone surfaces. Bone-lining cells are responsible for regulating the transfer of mineral ions in and out of bone, for sensing mechanical strains and for initiating bone remodeling in response to various chemical or mechanical stimuli.⁴ Bone-lining cells also have important function of cleaning bone surfaces before osteoclastic resorption.¹⁰⁹

1.3.3 Bone Related Markers and Adhesion Proteins

Different ECM molecules and other proteins have been proposed in the literature as bone markers. Cell-dental implant interactions such as cell attachment, adhesion, proliferation and differentiation involve collagen I, alkaline phosphatase, osteopontin, and bone sialoprotein.¹¹⁰ It is important to understand the expression of specific bone-related markers, involved in osteoblast development, osseointegration and dental implant biocompatibility. Below, we briefly discuss the marker that was used in this thesis as well as the adhesion proteins used to assess osteoblast attachment and spreading.

Alkaline phosphatase (ALP) is a hydrolytic enzyme that removes phosphate groups from proteins and other types of molecules. It is present in bone (produced by osteoblasts) and several other organs of the human body. ALP is a common biochemical marker used to evaluate osteoblast differentiation¹¹¹ and is considered as a sensitive and reliable indicator of osteoblast activity.¹¹² It can be bound to the surface of osteoblasts via a phosphoinositol linkage and can be free floating within the mineralizing matrix.⁴⁹ ALP is abundant in matrix vesicles that are thought to contribute to ECM calcification¹¹³. The levels of ALP are increased before bone mineralization to generate free phosphate (needed for formation of HA) and to degrade mineralization inhibitors such as pyrophosphate.¹¹¹

Adhesion proteins: Cell adhesion on implant materials is required for successful osseointegration of the implanted material. Moreover, cell adhesion to ECM is crucial for modulation of numerous critical cellular events; examples include gene expression, cell locomotion and subsequently cell differentiation, proliferation and survival.¹¹⁴ Cell

adhesion is dependent on integrin-mediated signal transduction and cytoskeleton proteins that form specialized structures known as focal adhesions (FA).¹¹¹ At FA sites, bundles of actin filaments are attached to transmembrane receptors of the integrin family. Some FA components provide a structural link between actin filaments and membrane receptors. Other components are signaling molecules including different protein kinases and phosphatases, their substrates and many adaptor proteins. These complexes include focal adhesion kinase, vinculin, integrins and actin filaments.¹¹⁵

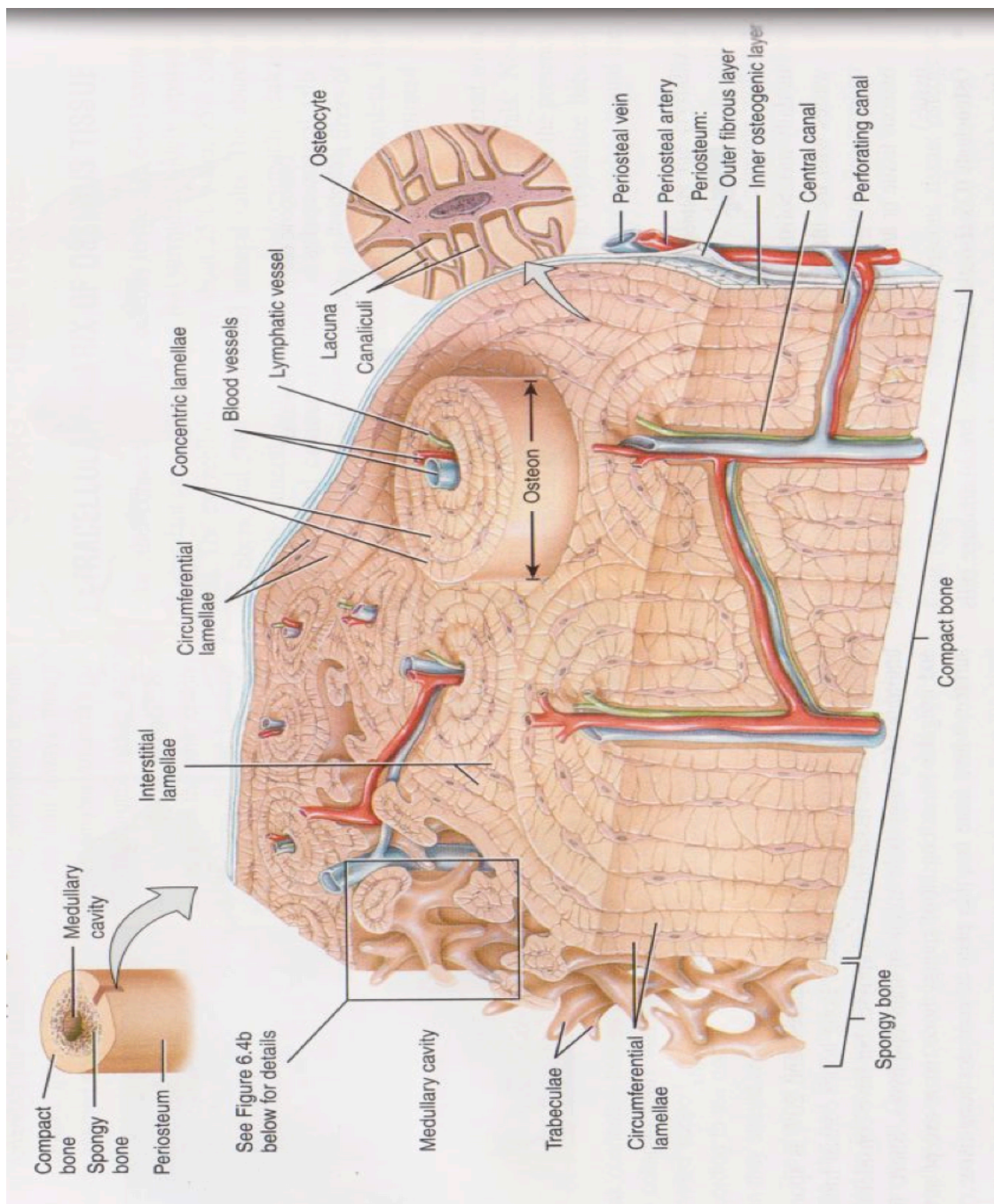


Figure 1-4: Sections through the diaphysis of a long bone, from the periosteum on the right, to compact bone tissue in the middle, to spongy bone tissue and the medullary cavity on the left. The inset at the upper right shows an osteocyte in its lacuna. Reproduced from *Anatomy and Physiology: From Science to Life*, 2nd edition with permission of John Wiley & Sons, Inc.¹⁰² (Appendix A).

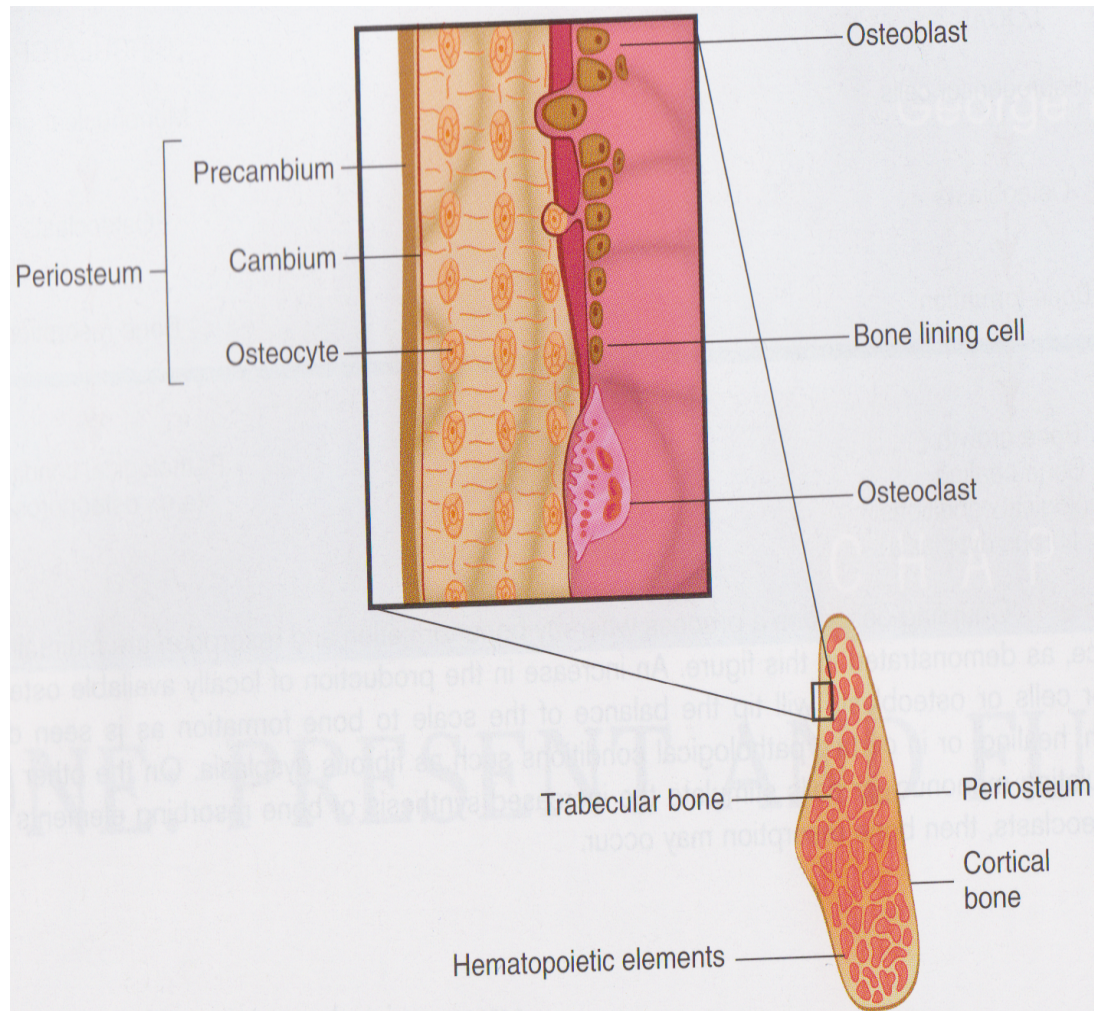


Figure 1-5: Schematic view of a cross-section through the mandible. An outer cortical shell encases the inner trabecular bone containing the hematopoietic elements. When examined at higher magnification, as in the upper drawing, the various cellular elements of bone (osteoblasts, osteoclasts, osteocytes and bone lining cells) may be identified. Adapted with permission from Dental Implant, 2nd edition⁶ (Appendix A).

1.4 OSSEOINTEGRATION OF DENTAL IMPLANTS

Osseointegration is the formation of a direct interface between an implant material surface and the host bone tissues without intervening connective tissue.¹¹⁶ Brånemark¹¹⁷ developed the concept of osseointegration in the 1950s when he discovered the formation of strong bond between bone and titanium. The bone-implant interaction and the conditions that favor osseointegration depend on various factors: implant material, implant design and shape, chemical and physical surface quality, status of the bone, surgical technique, and mechanical loading conditions.^{118,119} For a successful osseointegration, the implant must be inserted with a low-trauma surgical technique to avoid bone overheating during preparation of the precise recipient site. Implant must be placed with initial stability and should be non-functional during the healing period of 3-6 months.²

Interfacial micromotion is a periodic development of μm displacement of an implant body relative to the surrounding tissue as result to a shear or tensile force.¹²⁰ Micromotion has destructive effects on osseointegration; it will replace the early bony healing process by scar tissues through damaging the fibrin network and the new vasculature.¹²¹ The long-term osseointegration of dental implants relies on their placement within bone that has adequate trabecular density, ridge height and width. Trabecular bone that is not sufficiently dense will either fail to osseointegrate or lose its osseointegration over time.⁴

Many researchers showed that surface modification and roughness of dental implants such as porous plasma-spray,^{26,122} sand blasting,^{122,123} ultraviolet treatment,¹²⁴ acid etching^{125,126} or anodic oxidation¹³ have direct effects on cellular proliferation and

differentiation. Other studies revealed that porosity provides favorable environments for bone interlocking and in-growth. Titanium implants with a micro rough surfaces accomplish faster bone integration and superior percentage of bone implant contact with shorter healing periods compared with titanium implants with a polished or smooth surface.^{3,119,122,125} It has also been demonstrated that surface treatments such as biomimetic coatings (e.g. calcium phosphate) promote greater osseointegration.^{14,116,125}

Ceramic implants promote biointegration *versus* osseointegration that are related to titanium-based dental implants. Successful osseointegrated/biointegrated dental implants should show clinical stability without any kind of mobility that can be maintained throughout the lifetime of the implant. Biointegration can be defined as the continuity of ceramic implant to the surrounding bone without any intervening space.¹⁷ In this case, corrosion products will enclose the implant surfaces and there will be a chemical bond between the implant material and the bone.¹²⁷

Biointegration, although not fully understood, is considered to be a chemical degradation of the ceramic material that integrates with the surrounding bone and stimulates bone formation. Yet, the advantages of biointegration over osseointegration are not clear, but in both cases, surrounding bone should remain vital.¹⁷ To combine both osseointegration and biointegration properties at the osteotomy site, plasma-spray coating of HA is used as the most common method for surface modification of metallic dental implants with a coating thickness of 50-100 μm .^{26,45,128} In this case a combination of high strength alloy and favorable biointegrated characteristics of the ceramic material is achieved.^{17,25} These bioactive coatings will enhance bone apposition and reduce healing time.¹²⁹ Many studies disclosed that these ceramic coatings promote greater bone-implant contact and

biointegration rather than osseointegration and showed a greater bone-implant contact.^{5,130,131}

The bond strength of ceramic coatings to alloys is a significant concern. For example, some studies have observed that non-uniform and partial degradation of the ceramic coatings interferes with the cellular reactions at the implant-bone interface.¹³² Other studies considered the coating dissolution as an adverse factor on the long-term integration of the dental implants.^{129,133} Debonding of the coatings from the base alloys could affect the long-term performance of the implant.¹⁴ The mismatch of the Young's moduli between the implant and the coating material can cause local loading with high stress value at the interface leading to a reduction in the fatigue stress of the implant.⁶⁵

It is advantageous to accelerate bone apposition onto dental implant surfaces because a steady interface must be achieved before starting the implant loading. Different implant surface configurations can improve the osseointegration, leading to the full transfer of occlusal loads to the adjacent tissue and minimizing relative motion between implant and bone to avoid creation of fibrous integration, thereby lengthening the service life of the implant.^{13,118}

1.5 BIOACTIVITY IN DENTAL IMPLANTOLOGY

There is a group of glasses and GCs that exhibit bioactivity by bonding to living bone with the formation of an apatite layer. Bioactive materials are used clinically for the replacement and reconstruction of bone defects resultant from diseases or trauma.¹³⁴ To assess the bioactivity of biomaterials, *in vitro* testing is usually carried out to confirm the formation of HA layer on the material surfaces. Kokubo *et al*¹³⁵ and Hench *et al*¹³⁶

introduced acellular solutions with ion concentrations nearly equal to those of human blood plasma known as simulated body fluid (SBF), but they are richer in Cl^- ion and poorer in HCO_3^- (Table 1-1).

Table 1-1: Ionic compositions (in mM) of human blood plasma and SBF.¹³⁷

Ion	Na^+	K^+	Mg^{2+}	Ca^{2+}	Cl^-	HCO_3^-	HPO_4^{2-}	SO_4^{2-}
Human blood plasma	142.0	5.0	1.5	2.5	103.0	27.0	1.0	0.5
SBF	142.0	5.0	1.5	2.5	147.8	4.2	1.0	0.5

Many researchers have used SBF to investigate the bioactivity of biomaterials. Specimens are soaked in SBF at body temperature for different time-points, and the material surfaces are investigated later. A material that shows apatite formation on its surface in SBF in a short time, usually bonds to living bone.¹³⁷

The mechanism of bioactivity is time-dependent as discussed in the literature. Several stages are included in this mechanism:^{25,138}

- i. Rapid exchange of Na^+ or K^+ with H^+ or H_3O^+ from the solution.
- ii. Loss of soluble silica in the form of $\text{Si}(\text{OH})_4$ to the solution, resulting from breakage of the Si-O-Si bond and formation of Si-OH (silanols) at the material solution interface. The SiO_2 -rich layer is condensed and repolymerized on the surface depleted in alkalis and alkaline cations.

- iii. Ca^{2+} and PO_4^{3-} groups are migrated to the material surface through the SiO_2 -rich layer to form a $\text{CaO-P}_2\text{O}_5$ -rich film on top of the SiO_2 -rich layer.
- iv. Amorphous $\text{CaO-P}_2\text{O}_5$ -rich film grows by incorporation of soluble calcium and phosphates from SBF.
- v. Finally, Amorphous hydroxycarbonate apatite (HCA) film crystallizes by incorporation of OH^- , CO_2^- , or F^- anions from the solution.

The last two stages are critical for controlling the biological activity of different biomaterials. If these stages are extremely slow, the material is considered as non-bioactive because there will be little or no bonds formed on the surface of bone. On the contrary, in a case of a very fast reaction, a resorption will be observed and the material is considered as biodegradable and resorbable. With a bioactive material that exhibits bone-bond formation, these stages must closely match the time of bone biomineralization.²⁵

The process of apatite formation can be characterized by different tests such as X-ray diffraction (XRD), Fourier transform infrared reflection spectroscopy (FTIR), energy dispersive X-ray spectroscopy (EDX) and scanning electron microscopy (SEM). Studies showed that apatite started to nucleate on the silica gel layer, and then they grew to make a spherulitic form by consuming the calcium and phosphate ions from the surrounding fluid. Each spherulitic structure consisted of plenty of flakes of HCA. The Ca/P ratio of the apatite was estimated around 1.5-1.6. Thus, the apatite formed was able to induce secondary nucleation of the apatite.¹³⁹

The commercially available dental implants (titanium and zirconia) are bioinert. Several bioactive materials such as BIOGLASS[®] 140 HA and wollastonite^{130,141} have been used as

coatings on the implant substrate, to modify their surfaces and make them bioactive. Various techniques have been used to prepare the bioactive coatings like plasma-spraying,¹³⁰ micro-arc oxidation,¹⁴² electro-hydrodynamics spray deposition, sputter technique,¹⁴³ sol-gel and vacuum deposition.¹⁴ There are some limitations to bioactive coatings. They could fail during cooling from the fabrication temperature, under service stresses, or due to lack of adhesion between the coating and the substrate.¹⁴⁴ Some coating materials such as HA exhibited microstructural changes that lead to a very slow osseointegration rate and could jeopardize the long-term stability of an implant.¹⁴¹

The development of bioactive GCs for dental implant applications with suitable mechanical properties is considered as a substantial challenge for researchers and yet remarkable progress in the dental implantology field is occurring. The motivation of this research is to synthesize bioactive, machinable and biocompatible with suitable mechanical properties as an alternative to metallic non-bioactive dental implant material.

1.6 THESIS HYPOTHESES AND OBJECTIVES

The overlying hypothesis of this study is that GCs can be synthesized with properties suitable for use in non-metallic, one-piece dental implant applications. In particular, our aim was to produce bioactive, biocompatible and machinable GCs that exhibited appropriate mechanical, physical, optical and chemical properties to overcome the limitations associated with current commercial dental implant systems (titanium or zirconia). We also hypothesized that one could synthesize transparent precursor glass with wet chemistry methods and then sintering the glass powder to produce GC. A further hypothesis was that modification of glass composition and heat treatment schedules

would improve the mechanical, physical and chemical properties of resultant GCs. Overall, we proposed that multiphase GCs constituted of miserite or wollastonite as the main crystalline phases are suitable materials for non-metallic, one-piece dental implant applications owing to their superior mechanical properties, excellent chemical durability, machinability, osteogenic potential and biocompatibility.

In order to test these hypotheses, the specific objectives of the research were:

1. To fabricate dental transparent glasses in different systems by wet chemistry.
2. To study the crystallization kinetics of the glasses.
3. To synthesize a miserite GC by cold pressing and sintering, and to characterize its mechanical, physical and biological properties.
4. To investigate the effect of modifying heat treatment schedules on the mechanical properties of miserite GC.
5. To synthesize a wollastonite GC by cold pressing and sintering, and to characterize its mechanical, physical, chemical and biological properties.
6. To investigate the effect of modifying the parent glass chemical composition on the mechanical and chemical properties of wollastonite GC.

1.7 THESIS ORGANIZATION

The work presented in this thesis focuses on synthesis and characterization of novel GCs for dental implant applications. *Chapter 1* presented the rationale, background and pertinent literature review. *Chapter 2* (Saadaldin *et al*¹⁴⁵) describes the synthesis of base glass, characterization of the crystallization kinetics of the glass, and synthesis of four GCs from the glass powder using different heat treatment schedules. Characterization of

the crystalline phases, microstructure, mechanical properties and machinability of the GCs are presented. Finally, testing bioactivity in SBF and biocompatibility (osteoblast morphology, attachment and proliferation) of the miserite GC that exhibited the best mechanical properties are presented. **Chapter 3** (Saadaldin *et al*¹⁴⁶) describes the synthesis of precursor glasses, characterization of their crystallization kinetics, and synthesis of three wollastonite GCs from glass powders that had variable weight percentages of their chemical constituents. The mechanical properties, machinability and chemical durability of the wollastonite GCs are presented. Fracture toughness values of the wollastonite GCs before and after chemical degradation testing is reported. The GC that showed the best mechanical properties and excellent chemical durability was selected for the following study. **Chapter 4** (Saadaldin *et al*¹⁴⁷) describes evaluation of the bioactivity in SBF and biocompatibility (including osteoblast attachment, focal adhesion formation, proliferation and ALP activity) of the wollastonite GC, which was synthesized as described in Chapter 3. **Chapter 5** includes the general discussion, overall conclusions, significances, limitations of the study and a brief description of potential areas for future studies.

1.8 REFERENCES

1. O'Brien WJ. Dental Materials and Their Selection. 4th ed. Hanover Park, IL: Quintessence Pub. Co.; 2008.
2. Ferracane JL. Materials in Dentistry: Principles and Applications. 2nd ed. Philadelphia: Lippincott Williams & Wilkins; 2001.
3. Cooper LF. A Role for Surface Topography in Creating and Maintaining Bone at Titanium Endosseous Implants. *J Prosthet Dent.* 2000 11; 84(5):522-34.
4. Garg AK. Bone Biology, Harvesting, Grafting for Dental Implants: Rationale and Clinical Applications. Chicago: Quintessence Pub. Co.; 2004.
5. Ellingsen JE, Thomsen P, Lyngstadaas P. Advances in Dental Implant Materials and Tissue Regeneration. *Periodontol 2000.* 2006; 41(1):136-56.
6. Babbush CA. Dental implants: The Art and Science. 2nd ed. Maryland Heights, Mo.: Saunders/Elsevier; 2011.
7. Anusavice KJ, Phillips RW, Shen C, Rawls HR. Phillips' Science of Dental Materials. 12th ed. St. Louis, Mo.: Elsevier/Saunders; 2013.
8. Ratner BD. Biomaterials Science: An Introduction to Materials in Medicine. San Diego: Academic Press; 1996.
9. Parker C. The Growth of Implant Dentistry. *Dentist Magazine.* 2012; 28(9).
10. Natali AN. Dental Biomechanics. London; New York: Taylor & Francis; 2003.
11. Leyens C, Peters M. Titanium and Titanium Alloys; Fundamentals and Applications. Weinheim: Wiley-VCH; 2003.

12. Wang RR, Li Y. In Vitro Evaluation of Biocompatibility of Experimental Titanium Alloys for Dental Restorations. *J Prosthet Dent.* 1998 10; 80(4):495-500.
13. Misch CE. *Contemporary Implant Dentistry.* 3rd ed. St. Louis: Mosby Elsevier; 2008.
14. Gross KA, Berndt CC. Biomedical Application of Apatites. *Rev Mineral Geochem.* 2002; 48(1):631-72.
15. Jayaswal GP, Dange SP, Khalikar AN. Bioceramic in Dental Implants: A Review. *J Ind Pros Society.* 2010; 10(1):8-12.
16. Rosenstiel SF, Land MF, Fujimoto J. *Contemporary Fixed Prosthodontics.* 4th ed. St. Louis, Mo.: Mosby Elsevier; 2006.
17. Powers JM, Wataha JC. *Dental Materials: Properties and Manipulation.* 10th ed. St. Louis, Mo.: Mosby/Elsevier; 2013.
18. Mine Y, Makihira S, Nikawa H, Murata H, Hosokawa R, Hiyama A, *et al.* Impact of Titanium Ions on Osteoblast, Osteoclast and Gingival Epithelial-like Cells. *J Prosthodont Res.* 2010; 54(1):1-6.
19. Sicilia A, Cuesta S, Coma G, Arregui I, Guisasola C, Ruiz E, *et al.* Titanium Allergy in Dental Implant Patients: A Clinical Study on 1500 Consecutive Patients. *Clin Oral Implants Res.* 2008; 19(8):823-35.
20. Siddiqi A, Payne AGT, De Silva RK, Duncan WJ. Titanium allergy: Could it Affect Dental Implant Integration? *Clin Oral Implant Res.* 2011; 22(7):673-80.

21. Olmedo DG, Paparella ML, Brandizzi D, Cabrini RL. Reactive Lesions of Peri-Implant Mucosa Associated with Titanium Dental Implants: A report of 2 Cases. *Int J Oral Maxillofac Surg.* 2010; 39(5):503-7.
22. Makihira S, Mine Y, Nikawa H, Shuto T, Iwata S, Hosokawa R, *et al.* Titanium Ion Induces Necrosis and Sensitivity to Lipopolysaccharide in Gingival Epithelial-Like Cells. *Toxicol In Vitro.* 2010; 24(7):1905-10.
23. Egusa H, Ko N, Shimazu T, Yatani H. Suspected Association of An Allergic Reaction With Titanium Dental Implants: A Clinical Report. *J Prosthet Dent.* 2008; 100(5):344-7.
24. Wenz HJ, Bartsch J, Wolfart S, Kern M. Osseointegration and Clinical Success of Zirconia Dental Implants: A Systematic Review. *Int J Prosthodont.* 2008; 21(1):27-36.
25. Hench L. Bioceramics-From Concept to Clinic. *J Am Ceram Soc.* 1991;74(7):1487-510.
26. Sykaras N, Iacopino AM, Marker VA, Triplett RG, Woody RD. Implant Materials, Designs, and Surface Topographies: Their Effect on Osseointegration. A Literature Review. *Int J Oral Maxillofac Implants.* 2000;15(5):675-90.
27. Volpato CÂM, Garbelotto LGDA, Fredel M.C.and Bondioli F. Application of Zirconia in Dentistry: Biological, Mechanical and Optical Considerations. In: Sikalidis C, editor. *Advances in Ceramics - Electric and Magnetic Ceramics, Bioceramics, Ceramics and Environment.* 1st ed. Croatia: InTech; 2011. p. 397-420.

28. Kohal R, Klaus G. A Zirconia Implant-Crown System: A Case Report. *Int J Periodontics Restorative Dent.* 2004;24(2):147-53.
29. Bächle M, Butz F, Hübner U, Bakaliniš E, Kohal RJ. Behavior of CAL72 Osteoblast-Like Cells Cultured on Zirconia Ceramics with Different Surface topographies. *Clin Oral Implants Res.* 2007; 18(1):53-9.
30. Kohal R-, Papavasiliou G, Kamposiora P, Tripodakis A, Strub JR. Three-Dimensional Computerized Stress Analysis of Commercially Pure Titanium and Yttrium-Partially Stabilized Zirconia Implants. *Int J Prosthodont.* 2002; 15(2):189-94.
31. Silva NRFA, Coelho PG, Fernandes CAO, Navarro JM, Dias RA, Thompson VP. Reliability of One-Piece Ceramic Implant. *J Biomed Mater Res B Appl Biomater.* 2009; 88(2):419-26.
32. Aydın C, Yılmaz H, Bankođlu M. A Single-Tooth, Two-Piece Zirconia Implant Located in the Anterior Maxilla: A Clinical Report. *J Prosthet Dent.* 2013; 109(2):70-4.
33. Manicone PF, Rossi Iommetti P, Raffaelli L. An Overview of Zirconia Ceramics: Basic Properties and Clinical Applications. *J Dent.* 2007; 35(11):819-26.
34. Andreiotelli M, Kohal RJ. Fracture Strength of Zirconia Implants after Artificial Aging. *Clin Implant Dent Relat Res.* 2009; 11(2):158-66.
35. Knahr K. *Total Hip Arthroplasty.* Berlin; New York: Springer; 2013.
36. Höland W, Beall GH. *Glass-Ceramic Technology.* Westerville, USA: American Ceramic Society; 2002.

37. Hisbergues M, Vendeville S, Vendeville P. Zirconia: Established Facts and Perspectives for a Biomaterial in Dental Implantology. *J Biomed Mater Res.* 2009; 88B(2):519-29.
38. Cavalcanti AN, Foxton RM, Watson TF, Oliveira MT, Giannini M, Marchi GM. Y-TZP ceramics: Key Concepts for Clinical Application. *Operative Dentistry.* 2009; 34(3):344-51.
39. Van Noort R. *Introduction to Dental Materials.* 4th ed. Edinburgh; New York: Mosby/Elsevier; 2013.
40. Piconi C, Maccauro G. Zirconia as a Ceramic Biomaterial. *Biomaterials.* 1999; 20(1):1-25.
41. Flinn BD, deGroot DA, Mancl LA, Raigrodski AJ. Accelerated Aging Characteristics of Three Yttria-Stabilized Tetragonal Zirconia Polycrystalline Dental Materials. *J Prosthet Dent.* 2012 10; 108(4):223-30.
42. Tinschert J, Natt G, Mohrbotter N, Spiekermann H, Schulze KA. Lifetime of Alumina and Zirconia Ceramics Used for Crown and Bridge Restorations. *J Biomed Mater Res.* 2007; 80B (2):317-21.
43. Vagkopoulou T, Koutayas S, Koidis P, Strub J. Zirconia in Dentistry: Part 1. Discovering the Nature of An Upcoming Bioceramic. *Eur J Esthet Dent.* 2009; 4(2):130-51.
44. Cales B. Zirconia as a Sliding Material-Histologic, Laboratory, and Clinical data. *Clin Orthop Relat Res.* 2000; 13(379):94-112.

45. Özkurt Z, Kazazoglu E. Zirconia Dental Implants: A Literature Review. *J Oral Implant.* 2011;37(3):367-76.
46. Brunski JB. Biomechanical Factors Affecting the Bone-Dental Implant Interface. *Clin Mater.* 1992; 10(3):153-201.
47. Weiss C, Weiss A. *Principles and Practice of Implant Dentistry.* St. Louis, Mo.: Mosby; 2001.
48. Ratner B. Replacing and Renewing: Synthetic Materials, Biomimetic, and Tissue Engineering in Implant Dentistry. *J Dent Edu.* 2001; 65(12):1340-7.
49. Clarke B. Normal Bone Anatomy and Physiology. *Clin J Am Soc Nephrol.* 2008; 3(S3):131-9.
50. Zonfrillo G, Pratesi F. Mechanical Strength of Dental Implants. *J of Appl Biomater.* 2008 05; 6(2):110-8.
51. Zhang Y, Wang J, Wang P, Fan X, Li X, Fu J, *et al.* Low Elastic Modulus Contributes to the Osteointegration of Titanium Alloy Plug. *J Biomed Mater Res.* 2013; 101B (4):584-90.
52. Andreiotelli M, Wenz HJ, Kohal R. Are Ceramic Implants a Viable Alternative to Titanium Implants? A Systematic Literature Review. *Clin Oral Implants Res.* 2009; 20(S4):32-47.
53. Park JB, Lakes RS. *Biomaterials: An Introduction.* 3rd ed. New York; London: Springer; 2007.

54. Lee W, Koak J, Lim YJ, Kim S, Kwon H, Kim M. Stress Shielding and Fatigue Limits of Poly-Ether-Ether-Ketone Dental Implants. *J Biomed Mater Res.* 2012; 100B (4):1044-52.
55. Pattanayak D, Rao B, Mohan T. Calcium Phosphate Bioceramics and Bioceramic Composites. *J Sol-Gel Sci Techn.* 2011; 59(3):432-47.
56. Koleganova VA, Bernier SM, Dixon SJ, Rizkalla AS. Bioactive Glass/Polymer Composite Materials with Mechanical Properties Matching those of Cortical Bone. *J Biomed Mater Res.* 2006; 77A (3):572-9.
57. Li Z, Ghosh A, Kobayashi AS, Bradt RC. Indentation Fracture Toughness of Sintered Silicon Carbide in the Palmqvist Crack Regime. *J Am Ceram Soc.* 1989; 72(6):904-11.
58. Chan RN, Stoner BR, Thompson JY, Scattergood RO, Piascik JR. Fracture Toughness Improvements of Dental Ceramic Through Use of Yttria-Stabilized Zirconia (YSZ) Thin-Film Coatings. *Dent Mater.* 2013 8; 29(8):881-7.
59. Smith WF, Hashemi J. *Foundations of Materials Science and Engineering.* 5th ed. Boston: McGraw-Hill Higher Education; 2010.
60. Ponton CB, Rawlings RD. Vickers Indentation Fracture Toughness Test Part 1 Review of Literature and Formulation of Standardized Indentation Toughness Equations. *Mat Sci Tech.* 1989; 5(9):865-72.
61. Lankford J. Indentation Microfracture in the Palmqvist Crack Regime: Implications for Fracture Toughness Evaluation by the Indentation Method. *J Mater Sci Mater Lett.* 1982; 1(11):493-5.

62. Bonsor SJ, Pearson GJ. A Clinical Guide to Applied Dental Materials. Amsterdam; Boston: Elsevier/Churchill Livingstone; 2013.
63. Niinomi M. Fatigue Characteristics of Metallic Biomaterials. *Int J Fatigue*. 2007;29(6):992-1000.
64. Niinomi M. Mechanical Properties of Biomedical Titanium Alloys. *Mat Sci Eng A*. 1998;243(1-2):231-6.
65. Kim MG. Fatigue Properties on the Failure Mode of a Dental Implant in a Simulated Body Environment. *Met Mater Int*. 2011;17(5):705-11.
66. Studart AR, Filser F, Kocher P, Gauckler LJ. Fatigue of Zirconia Under Cyclic Loading in Water and its Implications for the Design of Dental Bridges. *Dent Mater*. 2007; 23(1):106-14.
67. Varshneya AK. Fundamentals of Inorganic Glasses. London: Academic Press Limited; 1994.
68. Höland W, Rheinberger V, Apel E, Hoen C, Höland M, Dommann A, *et al*. Clinical Applications of Glass-Ceramics in Dentistry. *J Mater Sci Mater Med*. 2006; 17(11):1037-42.
69. Grossman DG. Machinable Glass-Ceramics Based on Tetrasilicic Mica. *J Am Ceram Soc*. 1972; 55(9):446-9.
70. Wang M. Biomaterials and Tissue Engineering. In: Shi D, editor. *Bioactive Materials and Processing*. Berlin; New York: Springer; 2004. p. 1-72.

71. Neo M, Kotani S, Nakamura T, Yamamuro T, Ohtsuki C, Kokubo T, *et al.* A Comparative Study of Ultrastructures of the Interfaces between Four Kinds of Surface-Active Ceramic and Bone. *J Biomed Mater Res.* 1992; 26(11):1419-32.
72. Ohtsuki C, Kushitani H, Kokubo T, Kotani S, Yamamuro T. Apatite Formation on the Surface of Ceravital-Type Glass-Ceramic in the Body. *J Biomed Mater Res.* 1991; 25(11):1363-70.
73. Denry I, Holloway JA. Ceramics for Dental Applications: A Review. *Materials (1996-1944).* 2010; 3(1):351-68.
74. Höland W. Biocompatible and Bioactive Glass-Ceramics — State of the Art and New directions. *J Non Cryst Solids.* 1997; 219(0):192-7.
75. Höland W, Schweiger M, Rheinberger VM, Kappert H. Bioceramics and Their Application for Dental Restoration. *Adv Appl Ceram.* 2009; 108(6):373-80.
76. Höland W, Schweiger M, Watzke R, Peschke A, Kappert H. Ceramics as Biomaterials for Dental Restoration. *Expert Rev Med Devices.* 2008; 5(6):729-45.
77. Kelly JR, Benetti P. Ceramic Materials in Dentistry: Historical Evolution and Current Practice. *Aust Dent J.* 2011; 56(1):84-96.
78. Malament KA, Socransky SS. Survival of Dicor Glass-Ceramic Dental Restorations Over 20 Years: Part IV. The Effects of Combinations of Variables. *Int J Prosthodont.* 2010; 23(2):134-40.
79. Rizkalla AS, Jones DW. Mechanical Properties of Commercial High Strength Ceramic Core Materials. *Dent Mater.* 2004;20(2):207-12.

80. Qin F, Zheng S, Luo Z, Li Y, Guo L, Zhao Y, *et al.* Evaluation of Machinability and Flexural Strength of a Novel Dental Machinable Glass-Ceramic. *J Dent.* 2009; 37(10):776-80.
81. Koutayas SO, Kern M. All-ceramic Posts and Cores: The State of the Art. *Quintessence Int.* 1999; 30(6):383-92.
82. Sorensen J.A., Mito W.T. Rationale and Clinical Technique for Esthetic restoration of Endodontically Treated Teeth with the Cosmopost and IPS Empress Post System. *Quintessence Dent Technol.* 1998; 12(21):80-91.
83. Holand W, Schweiger M, Frank M, Rheinberger V. A Comparison of the Microstructure and Properties of the IPS Empress[®]2 and the IFS Empress[®]Glass-Ceramics. *J Biomed Mater Res.* 2000; 53(4):297-303.
84. Chen X, Chadwick TC, Wilson RM, Hill RG, Cattell MJ. Crystallization and Flexural Strength Optimization of Fine-Grained Leucite Glass-Ceramics for Dentistry. *Dent Mater.* 2011; 27(11):1153-61.
85. Heintze SD, Rousson V. Fracture Rates of IPS Empress All-Ceramic Crowns. A Systematic Review. *Int J Prosthodont.* 2010; 23(2):129-33.
86. Teicholz E. CAD-CAM handbook. New York; Montreal: McGraw-Hill; 1985.
87. Van Noort R. The Future of Dental Devices is Digital. *Dent Mater.* 2012; 28(1):3-12.
88. CAD/CAM in Dentistry. *Oral Health.* 1997; 87(3):17-20.

89. Mormann WH, Bindl A. The cerec 3 - A Quantum Leap for Computer-Aided Restorations: Initial Clinical Results. *Quintessence Int.* 2000; 31(10):699-712.
90. Conrad HJ, Seong W, Pesun IJ. Current Ceramic Materials and Systems with Clinical Recommendations: A Systematic Review. *J Prosthet Dent.* 2007 11; 98(5):389-404.
91. Kern M, Sasse M, Wolfart S. Ten-year Outcome of Three-Unit Fixed Dental Prostheses Made from Monolithic Lithium Disilicate Ceramic. *JADA.* 2012; 143(3):234-40.
92. Höland W, Rheinberger V, Apel E, Ritzberger C, Rothbrust F, Kappert H, *et al.* Future Perspectives of Biomaterials for Dental Restoration. *J Eur Cera Soc.* 2009; 29(7):1291-7.
93. Wolfart S, Eschbach S, Scherrer S, Kern M. Clinical Outcome of Three-Unit Lithium-Disilicate Glass–Ceramic Fixed Dental Prostheses: Up to 8 Years Results. *Dent Mater.* 2009; 25(9):63-71.
94. Ferguson DB. *Physiology for Dental Students.* London; Boston: Wright; 1988.
95. Bueno EM, Glowacki J. *Biologic Foundations for Skeletal Tissue Engineering.* 1537 Fourth Street, San Rafael, CA; 2011.
96. Fanghänel J, Gedrange T, Proff P. Bone Quality, Quantity and Metabolism in Terms of Dental Implantation. *Biomed Tech (Berl).* 2008; 53(5):215-19.
97. Augat P, Schorlemmer S. The Role of Cortical Bone and its Microstructure in Bone Strength. *Age Ageing.* 2006; 35:27-31.

98. Gelse K, Pöschl E, Aigner T. Collagens-Structure, Function, and Biosynthesis. *Adv Drug Deliv Rev.* 2003; 55(12):1531-46.
99. Frost H. Wolff's Law and Bone's Structural Adaptations to Mechanical Usage: An Overview for Clinicians. *Angle Orthod.* 1994; 64(3):175-88.
100. Horner KA, Behrents RG, Kim KB, Buschang PH. Cortical Bone and Ridge Thickness of Hyperdivergent and Hypodivergent Adults. *Am J Orthod Dentofacial Orthop.* 2012 8; 142(2):170-8.
101. Tripuwabhrut P, Mustafa M, Gjerde CG, Brudvik P, Mustafa K. Effect of Compressive Force on Human Osteoblast-Like Cells and Bone Remodeling: An In Vitro Study. *Arch Oral Biol.* 2013; 58(7):826-36.
102. Jenkins GW, Kemnitz CP, Tortora GJ. *Anatomy and Physiology: From Science to Life.* Hoboken, N.J.: Wiley; 2007.
103. Thomas GP, Baker SUK, Eisman JA, Gardiner EM. Changing RANKL/OPG mRNA Expression in Differentiating Murine Primary Osteoblasts. *J Endocrinol.* 2001; 170(2):451-60.
104. Bonewald LF. The Amazing Osteocyte. *J Bone Miner Res.* 2011; 26(2):229-38.
105. Kogianni G, Noble BS. The Biology of Osteocytes. *Curr Osteoporos Rep.* 2007; 5(2):81-6.
106. O'Brien CA, Nakashima T, Takayanagi H. Osteocyte Control of Osteoclastogenesis. *Bone.* 2013; 54(2):258-63.
107. Suda T, Takahashi N, Martin TJ. Modulation of Osteoclast Differentiation. *Endocr Rev.* 1992; 13(1):66-80.

108. Vaananen HK, Zhao H, Mulari M, Halleen JM. The Cell Biology of Osteoclast Function. *J Cell Sci.* 2000; 113(3):377-81.
109. Everts V, Delaissé JM, Korper W, Jansen DC, TigchelaarGutter W, Saftig P, *et al.* Bone Lining Cell: Its Role in Cleaning Howship's Lacunae and Initiating Bone Formation. *J Bone Miner Res.* 2002;17(1):77-90.
110. Rosa V, Della Bona A, Cavalcanti BN, Nör JE. Tissue Engineering: From Research to Dental Clinics. *Dent Mater.* 2012; 28(4):341-8.
111. Pivodova V, Frankova J, Ulrichova J. Osteoblast and Gingival Fibroblast Markers in Dental Implant Studies. *Biomed Pap.* 2011;155(2):109-16.
112. Leung KS, Fung KP, Sher AH, Li CK, Lee KM. Plasma Bone-Specific Alkaline Phosphatase as an Indicator of Osteoblastic Activity. *J Bone Joint Surg Br.* 1993; 75(B):288-92.
113. Harris H. The Human Alkaline Phosphatases: What We Know and What We Don't know. *Clin Chim Acta.* 1990; 186(2):133-50.
114. Pelham RJ, Wang Y. Cell Locomotion and Focal Adhesions Are Regulated by Substrate Flexibility. *Proc Nati Acad Sci USA.* 1997; 94(25):13661-5.
115. Petit V, Thiery J. Focal adhesions: Structure and Dynamics. *Biol Cell.* 2000; 92(7):477-94.
116. Hobkirk JA, Watson RM, Searson LJJ. *Introducing Dental Implants.* Edinburgh; New York: Churchill Livingstone; 2003.
117. Palmer R. Dental Implants: Introduction to Dental Implant. *Br Dent J.* 1999; 187(3):127-32.

118. Barbucci R. *Integrated Biomaterials science*. New York: Kluwer Academic/Plenum; 2002.
119. Vasconcellos LMR, Oliveira MV, Graça MLA, Vasconcellos LGO, Cairo CAA, Carvalho YR. Design of Dental Implants, Influence on the Osteogenesis and Fixation. *J Mater Sci Mater Med*. 2008; 19(8):2851-7.
120. Winter W, Klein D, Karl M. Micromotion of Dental Implants: Basic Mechanical Considerations. *J Med Eng*. 2013; 2013:1-9.
121. Albrektsson T, Brånemark PI, Hansson HA, Lindström J. Osseointegrated titanium implants: Requirements for Ensuring a Long-Lasting, Direct Bone-to-Implant Anchorage in Man. *Acta Orthopaedica*. 1981; 52(2):155-70.
122. Le Guehennec L, Soueidan A, Layrolle P, Amouriq Y. Surface Treatments of Titanium Dental Implants for Rapid Osseointegration. *Dent Mater*. 2007; 23(7):844-54.
123. Li HF, Wang YB, Zheng YF, Lin JP. Osteoblast Response on Ti- and Zr-Based Bulk Metallic Glass Surfaces After Sand Blasting Modification. *J Biomed Mater Res B Appl Biomater*. 2012; 100 B (7):1721-8.
124. Att W, Takeuchi M, Suzuki T, Kubo K, Anpo M, Ogawa T. Enhanced Osteoblast Function on Ultraviolet Light-Treated Zirconia. *Biomaterials*. 2009; 30(7):1273-80.
125. Conner KA, Sabatini R, Mealey BL, Takacs VJ, Mills MP, Cochran DL. Guided Bone Regeneration around Titanium Plasma-Sprayed, Acid-Etched, and Hydroxyapatite-Coated Implants in the Canine Model. *J Periodontol*. 2003; 74(5):658-68.

126. Li D, Ferguson SJ, Beutler T, Cochran DL, Sittig C, Hirt HP, *et al.* Biomechanical Comparison of the Sandblasted and Acid-Etched and the Machined and Acid-etched Titanium Surface for Dental Implants. *J Biomed Mater Res.* 2002; 60(2):325-32.
127. Wataha, J.C. Materials for Endosseous Dental Implants. *J Oral Rehabil.* 1996; 23(2):79-90.
128. Palmquist A, Omar OM, Esposito M, Lausmaa J, Thomsen P. Titanium Oral implants: Surface Characteristics, Interface Biology and Clinical Outcome. *J R Soc Interface.* 2010; 7(s):S515-27.
129. Chen C, Huang T, Kao C, Ding S. Characterization of Functionally Graded Hydroxyapatite/Titanium Composite Coatings Plasma-sprayed on Ti Alloys. *J Biomed Mater Res.* 2006; 78B (1):146-52.
130. Cao H, Liu X. Plasma-Sprayed Ceramic Coatings for Osseointegration. *Int J Appl Ceram Technol.* 2013; 10(1):1-10.
131. Ripamonti U, Roden LC, Renton LF. Osteoinductive Hydroxyapatite-Coated Titanium Implants. *Biomaterials.* 2012; 33(15):3813-23.
132. Dalton JE, Cook SD. In Vivo Mechanical and Histological Characteristics of HA-Coated Implants Vary With Coating Vendor. *J Biomed Mater Res.* 1995; 29(2):239-45.
133. Gottlander M, Johansson CB, Albrektsson T. Short and Long-Term Animal Studies with a Plasma-Sprayed Calcium Phosphate-Coated Implant. *Clin Oral Implants Res.* 1997; 8(5):345-51.

134. Kokubo T. Bioactive Glass Ceramics: Properties and Applications. *Biomaterials*. 1991; 12(2):155-63.
135. Kokubo T, Kushitani H, Sakka S, Kitsugi T, Yamamuro T. Solutions Able to Reproduce In Vivo Surface-Structure Changes in Bioactive Glass-Ceramic A-W. *J Biomed Mater Res*. 1990; 24(6):721-34.
136. Filgueiras MR, La Torre G, Hench LL. Solution Effects on the Surface Reactions of A Bioactive Glass. *J Biomed Mater Res*. 1993; 27(4):445-3.
137. Kokubo T, Takadama H. How Useful is SBF in Predicting *In Vivo* Bone Bioactivity? *Biomaterials*. 2006; 27(15):2907-15.
138. Han YJ, Loo SCJ, Lee J, Ma J. Investigation of the Bioactivity and Biocompatibility of Different Glass Interfaces with Hydroxyapatite, Fluorohydroxyapatite and 58S Bioactive Glass. *BioFactors*. 2007; 30(4):205-16.
139. Li P, Ohtsuki C, Kokubo T, Nakanishi K, Soga N, Nakamura T, *et al*. Process of Formation of Bone-Like Apatite Layer on Silica Gel. *J Mater Sci: Mater-Med*. 1993; 4(2):127-31.
140. Hench LL. The Story of Bioglass®. *J Mater Sci Mater Med*. 2006; 17(11):967-78.
141. Mistry S, Kundu D, Datta S, Basu D. Comparison of Bioactive Glass Coated and Hydroxyapatite Coated Titanium Dental Implants in the Human Jaw Bone. *Aust Dent J*. 2011; 56(1):68-75.
142. Song H, Kim J, Kook M, Moon W, Park Y. Fabrication of Hydroxyapatite and TiO₂ Nanorods on Microarc-Oxidized Titanium Surface Using Hydrothermal Treatment. *Appl Surf Sci*. 2010; 256(23):7056-61.

143. Best SM, Porter AE, Thian ES, Huang J. Bioceramics: Past, Present and For the Future. *J Euro Cora Soc.* 2008; 28(7):1319-27.
144. Rawlings RD. Bioactive Glasses and Glass-Ceramics. *Clinic Mat.* 1993; 14(2):155-79.
145. Saadaldin SA, Dixon SJ, Costa DO, Rizkalla AS. Synthesis of Bioactive and Machinable Miserite Glass-Ceramics for Dental Implant Applications. *Dent Mater.* 2013; 29(6):645-55.
146. Saadaldin SA, Rizkalla AS. Synthesis and Characterization of Wollastonite glass-Ceramics for Dental Implant Applications. *Dent Mater*, 2013, *Accepted for publication*, DEMA-D-00398.
147. Saadaldin SA, Dixon SJ, Rizkalla AS. Bioactivity and Biocompatibility of a Novel Wollastonite Glass-Ceramic. *Submitted for publication*, 2013

CHAPTER 2

SYNTHESIS OF BIOACTIVE AND MACHINABLE MISERITE GLASS-CERAMICS FOR DENTAL IMPLANT APPLICATIONS

This chapter describes a novel approach for the synthesis of miserite GC with mechanical, physical and biological properties required for non-metallic dental implant applications. The contents of this chapter have been reproduced (with modifications) from: Saadaldin, SA; Dixon, SJ; Costa, DO and Rizkalla, AS. Synthesis of bioactive and machinable miserite glass-ceramics for dental implants applications. Dental Materials. 2013 Jun; 29(6): 645-655. doi: 10.1016/j.dental.2013.03.013, with permission from Elsevier (Appendix A).

2.1 INTRODUCTION

Dental implantology has become a predictable treatment for patients with missing teeth. Titanium (Ti) is the material most widely used for dental implants due to its superior mechanical properties, biocompatibility and resistance to corrosion. However, a long term clinical study revealed biological and technical complications with Ti dental implants.¹ Hypersensitivity and allergic reactions to Ti dental implants occur, although these reactions are under-reported, and the etiological factors of implant failure are poorly understood.²⁻⁴ In addition, the esthetic outcomes of Ti dental implants can be compromised in cases of gingival tissue recession, especially when replacing anterior teeth.⁵

Ceramics were introduced as potential materials for non-metallic dental implants. Among a variety of choices, the material currently used is yttria-stabilized tetragonal zirconia (Y-TZP).⁶ Advantages of zirconia include tooth-like color, good mechanical properties, biocompatibility, low affinity for plaque, and osseointegration comparable with Ti dental

implants.^{5,7} However, zirconia undergoes accelerated aging under stress in the presence of moisture, leading to surface deterioration, nucleation and propagation of microcracks that can result in spontaneous catastrophic failure.⁸⁻¹⁰

Bioactivity is defined as the ability of biomaterials to promote the formation of a crystalline HA layer from physiological fluid.¹¹ In implantology, there is considerable interest in bioactive materials to establish strong chemical bonding between the implant and bone, as well as to accelerate implant anchorage by inducing an HA layer on the implant surface.^{12,13} Ti and zirconia are considered bioinert; therefore, to improve their osseointegration, different bioactive coatings such as plasma-sprayed HA have been developed.^{5,14} However, such coatings do not degrade uniformly, giving rise to weak points at the bone-coating-implant interfaces.¹¹

GCs are produced by controlled nucleation and crystallization of glasses, and their properties can be tailored for specific applications.¹⁵ Glass crystallization can be determined by differential thermal analysis (DTA), which is thermoanalytic technique that is universally accepted as a rapid and convenient mean for determining the nucleation and crystallization temperature of glasses.¹⁶ Experimental glass and an inert reference (α -Al₂O₃) are made to undergo identical thermal cycles, the temperature differences between sample and the reference are used to get DTA curve that provide data on glass transition, crystallization and melting.¹⁷ The appearance of endothermic and exothermic peaks in the DTA curve corresponds to nucleation and crystallization temperature, respectively.¹⁸

There is great interest in GCs that possess appropriate physical, mechanical and biological properties for biomedical applications. These properties can be improved and

modified by varying the base glass composition or heat treatment conditions.¹⁵ Currently, several bioactive GCs are used for orthopaedic applications, including vertebral prostheses, middle ear devices and bone defect fillers.¹⁵ Miserite is a triclinic potassium calcium silicate mineral $[\text{KCa}_5(\text{Si}_2\text{O}_7)(\text{Si}_6\text{O}_{15})(\text{OH})\text{F}]$, which has a lath or rod-like crystal shape.¹⁹ Miserite was introduced in 1999 as the predominant crystal phase in multi-phase GCs that showed high bending strength (175 MPa) and high fracture toughness ($>3.5 \text{ MPa}\cdot\text{m}^{0.5}$).²⁰ It is anticipated that miserite GC is biocompatible and bioactive; however, it has not been evaluated previously as a material for dental implant applications.²⁰

Machinable biomaterials allow dentists to design and fabricate customized dental restorations with a high level of accuracy and precision through CAD-CAM technology.²¹ Introducing CAD-CAM technology in dental implantology offers dental clinicians a variety of treatment plans, with customized implants for each individual patient. The objective of this study was to synthesize and characterize bioactive and machinable miserite GCs, with physical, mechanical and biological properties appropriate for dental implant materials.

2.2 MATERIALS AND METHODS:

2.2.1 Glass Synthesis

Preliminary unpublished work conducted in our laboratory involved the synthesis of a range of multicomponent glass compositions in the system (SiO_2 - Al_2O_3 - CaO - CaF_2 - K_2O - B_2O_3 - La_2O_3) by wet chemical synthesis using sol-gel chemistry followed by spray-drying, calcinations and melting. The glass composition (wt %) that was selected for the

present study was 57.8 SiO₂, 0.5 Al₂O₃, 18.4 CaO, 12.6 CaF₂, 6.8 K₂O, 1.0 B₂O₃ and 2.9 La₂O₃. The rationale for using this composition was based on getting transparent glass, lowering the glass melting in addition to optimizing its mechanical properties. We made sure that the reagents used were of high purity and soluble in water to insure the homogeneity of the final product. The glass was synthesized through the following four steps:

- 1) Hydrolysis and polycondensation of metal alkoxides by mixing appropriate amounts of Si(C₂H₅O)₄, Al(NO₃)₃·9H₂O, Ca(NO₃)₂·4H₂O, CaF₂, KNO₃, H₃BO₃ and La(NO₃)₃·6H₂O in aqueous solution using excess deionized water.
- 2) Spray-drying with feed flow rate of 10 ml/min, inlet air temperature of 160 °C and outlet air temperature of 80 °C using a 190 mini spray-dryer (BÜCHI, Switzerland), yielding a spray-dried powder.
- 3) Calcination of the powder by heating incrementally at 200 °C, 500 °C and 700 °C for 2 h each in a Ney 650 vacuum oven (Ney-Barkmeyer, USA).
- 4) Melting of the calcined powder in an uncovered platinum crucible at 1150 °C for 3 h and 1250 °C for 1 h in a high temperature furnace (Thermolyne Corporation, USA), followed by quenching in iced water to obtain transparent glass frits.

2.2.2 Crystallization Kinetics

Transition and crystallization temperatures of experimental glasses were determined by DTA using a SDT Q600 V20.5 Build 15 system (TA Instruments, USA) under air atmosphere at five different heating rates (10-50 °C/min), starting from room temperature

up to 1200 °C. The average sample weight was 20 mg and an equivalent weight of α -Al₂O₃ was used as a reference. The activation energy (ΔE) was calculated from the plot of $\ln((T_p)^2/\dot{\Theta})$ vs $1000/T_p$ using the Kissinger equation,¹⁷ where T_p is the exothermic peak as determined from the DTA spectra and $\dot{\Theta}$ is the heating rate (°C/s). The Avrami exponent (n_A) was determined from the DTA exothermic peak using the Augis-Bennett equation¹⁶

$$\text{Avrami Exponent } (n_A) = \frac{(2.5/\Delta T)}{(RT_p^2/\Delta E)} \dots \dots \dots \text{(Eq 2-1)}$$

where ΔT is the full width at the half maximum of the exothermic peak determined at heating rate 20 °C/min, R is the universal gas constant (8.314 J/mol·K) and ΔE (kJ/mol) is the activation energy of crystallization.

2.2.3 Preparation of Glass-Ceramics

Glass powders were ground using a planetary ball mill, Pulverisette 7 (Laval Lab, USA) and mixed with 4% polyethylene glycol as a binder. Cylindrical ingots (6 mm X 10 mm) and disk specimens (12 mm X 1 mm) of the glass powder were produced by cold pressing by means of a Carver laboratory cold press (Carver, USA) in stainless steel dies at 40 MPa.

To study the effect of heat treatment on mechanical properties and crystallization of GCs, four different heating schedules were performed to produce four different GCs from the precursor glass (GC1, GC2, Gc3 and GC4). Pressed glass specimens were heated to 600 °C (glass transition temperature T_g) for 1 h, after which the temperature was subsequently increased to the crystallization temperatures determined from the DTA

exothermic peaks. The firing shrinkage of the resultant GCs was calculated from the values of the specimen diameters before and after sintering.

2.2.4 X-Ray Diffraction (XRD)

Crystalline phases within the GCs were studied by XRD using a Rotaflex RTP 300 RC (Rigaku Corp., Japan) operating on $\text{CoK}\alpha$ radiation at 45 kV and 160 mA. Spectra were collected in the 2θ range between 2 and 82° , with 0.05° step and $10^\circ/\text{min}$ scan speed. 2θ for equivalent $\text{CuK}\alpha$ radiation was calculated using Bragg's Law.²²

2.2.5 Microstructure

The fracture surfaces of the GCs were examined using LEO 1540XB FIB/SEM (Zeiss, Germany) equipped with an energy dispersive X-ray spectroscopy (EDX) system. Prior to SEM analysis, samples were mounted on aluminum stubs and then coated with 3 nm osmium metal (Filgen OPC 80T).

2.2.6 Dynamic Young's Modulus of the Glass and GCs

Poisson's ratio and dynamic Young's moduli of the glass and GCs were measured using a pulsed ultrasonic method. Lithium niobate crystals were used for transmitting and receiving signals, which were generated at 10 MHz resonant frequencies. The elastic parameters were calculated using the following equations.²³

$$\text{Poisson's ratio } (\nu) = \frac{0.5(V_L/V_S)^2 - 1}{(V_L/V_S)^2 - 1} \dots\dots\dots(\text{Eq1-2})$$

$$\text{Young's Modulus } (E) = \frac{(1 + \nu)(1 - 2\nu)}{(1 - \nu)} \rho V_L^2 \dots\dots\dots(\text{Eq1-3})$$

where V_L and V_S are the longitudinal and shear wave velocities, respectively, which were calculated from the thickness of each specimen and the travelling time of the waves across the specimen as determined using a V-66S oscilloscope at 60 MHz (Hitachi, Japan). The density of each specimen (ρ) was determined using the Archimedes method in distilled water at room temperature.

2.2.7 True Hardness

The true hardness (H_0) of the glass and GCs specimens was determined using a Buehler Micromet 5114 Knoop micro hardness indenter (Buehler, USA). Glass and GCs specimens were embedded in resin and polished. A series of Knoop indentations were performed on each specimen at six different loads (0.49-9.9 N). The average diagonal lengths of the Knoop indentations were measured using Buehler OmniMet MHT 7.2 Rev.2 optical microscope equipped with a digital camera and computer software (Buehler, USA). Indentation lengths were plotted vs the square root of the different load values, and H_0 was calculated from the slope of the linear regression line (S) using the following equation.²⁴

$$\text{True hardness } (H_0) = 14229/S^2 \dots\dots\dots (\text{Eq2-4})$$

2.2.8 Fracture Toughness

The fracture toughness (K_{IC}) of the glass and GCs were assessed using Micromet 5114 Vickers micro hardness indenter (Buehler, USA). The diagonals of the Vickers indentation and the crack lengths were measured to calculate the K_{IC} using the Lankford equation.²⁵

$$\text{Fracture Toughness } (K_{IC}) = 0.0782(H_o(a)^{0.5})(E/H_o)^{0.4}(c/a)^{-1.56} \dots\dots\dots(\text{Eq2-5})$$

where H_o is the true hardness (GPa), a is half the diagonal of the Vickers indentation (μm), E is the dynamic Young's modulus (GPa), and c is the crack length from the corner of the Vickers indentation (μm). The average K_{IC} was calculated from 15 indentations performed on each specimen at a load of 9.8 N.

2.2.9 Machinability

The machinability of the GCs was assessed qualitatively by drilling holes and preparing the samples by cutting shoulder finish lines, bevels and grooves with different depths. Quantitative evaluation of the machinability of the GCs was performed by calculating the brittleness index, which is the ratio of hardness to fracture toughness.²⁶

$$\text{Brittle Index } (BI) = H_o / K_{IC} \dots\dots\dots(\text{Eq2-6})$$

2.2.10 Bioactivity

The GC that exhibited the best mechanical properties was selected for bioactivity and cell compatibility studies. The ability of GC4 to induce formation of an apatite surface layer was evaluated by means of soaking in SBF *in vitro*.²⁷ Specimens were immersed in SBF at 37 °C for 1, 2 and 4 weeks. At predetermined times, specimens were thoroughly rinsed and dried. The surface layer formed on each specimen was assessed using SEM, EDX and XRD.

2.2.11 Cell Number and Morphology

MC3T3-E1 Subclone 4 (ATCC/CRL-2593, USA) osteoblast-like cells are a clonal non-transformed cell line originally established from newborn mouse calvariae.²⁸ These cells exhibit properties of osteoblasts, including elevation of cyclic AMP in response to parathyroid hormone, expression of transcripts for Runx2, bone sialoprotein and osteocalcin, and formation of bone-like matrix *in vitro* and *in vivo*.²⁹ GC4 discs were compared to sandblasted and acid-etched titanium (STi) as a positive control. STi discs were generously supplied by Institut Straumann AG. GC4 (12 mm X 1 mm) and STi (15 mm X 1 mm) discs were cleaned and sterilized using an argon-based plasma cleaner PDC-32G (Harrick plasma, USA), placed in 24-well plates, and seeded with 5,000 cells per well. Culture medium consisted of α -minimum essential medium (α -MEM, Invitrogen, CA) buffered with HCO_3^- , and supplemented with 10% heat-inactivated fetal bovine serum (FBS) and 1% antibiotic solution (10,000 U/ml penicillin, 10,000 $\mu\text{g}/\text{ml}$ streptomycin, and 25 $\mu\text{g}/\text{ml}$ amphotericin B). After 6, 24 and 72 h incubation at 37 °C in a humidified atmosphere of 5% CO_2 in air, cells were fixed with 4% paraformaldehyde. After fixation, cells were stained for filamentous actin (F-actin) using rhodamine phalloidin (1:100 in 3% BSA in PBS). Images were obtained using an Axiovert inverted fluorescence microscope (Carl Zeiss, Germany). Samples were mounted on glass coverslips using Vectashield (Vector Laboratories, CA) with 4', 6-diamidino-2-phenylindole dihydrochloride (DAPI) for visualization of cell nuclei. The number of cells present at 6, 24 and 72 h was calculated from 10 randomly selected fields from each specimen.

2.2.12 Cell Proliferation Assay

MC3T3-E1 cells were seeded at 5,000 cells per well on GC4 and STi discs and the culture medium was refreshed every other day. At 1, 3, 5 and 7 days, culture medium was removed and specimens with cells were frozen at -80 °C. MC3T3-E1 cell numbers were determined using CyQuant[®] cell proliferation assay kit (Invitrogen, USA). All specimens were thawed at room temperature, then 400 μ L of the CyQuant[®] GR dye/cell lysis buffer was added to each sample surface. A fluorescence microplate reader (Tecan Safire, USA) was used to measure fluorescence intensity of the dye/buffer at emission of 520 nm and excitation of 480 nm. Fluorescence intensity was converted to cell number using a standard curve. Cell numbers were normalized to account for the difference in surface area between the GC4 and STi specimens.

2.2.13 Statistical Analyses

Differences between two groups were evaluated by *t* tests. Differences among three or more groups were evaluated by one-way analysis of variance (ANOVA) followed by Tukey's multiple comparisons test. Differences were accepted as statistically significant at $p < 0.05$; *N* indicates the number of independent experiments.

2.3 RESULTS

2.3.1 Differential Thermal Analysis (DTA) of Glass

The crystallization kinetics of the experimental glass that was synthesized by wet chemical methods was determined by DTA. When the glass was heated, the DTA spectrum displayed three important features (Figure 2-1A). The first shoulder

endothermic peak corresponds to the glass transition temperature (T_g). The exothermic peaks (T_p^1 and T_p^2) demonstrate the crystallization temperatures of the glass. The second endothermic peak reveals the liquidus temperature (T_e), which resulted from decomposition and dissolution of the crystalline phases.

DTA was performed at five different heating rates (Table 2-1). T_g , T_p^1 , T_p^2 and T_e increased as the heating rate was increased. The Avrami exponent (n_A) at the crystallization temperature was calculated from the full width at the half maximum of the exothermic peak(s) at 20 °C/min (Figure 2-1B). The n_A values for the two crystallization temperatures are displayed in Table 2-2. The n_A value for T_p^1 was 1.1 (consistent with surface crystallization), whereas the n_A value for T_p^2 was 2.8 (consistent with bulk crystallization).¹⁸ The activation energies of crystallization of the two exothermic peaks (Table 2-2) were calculated from the slope of the regression lines ($\ln((T_p)^2/\theta)$ vs. $1000/T_p$) displayed in Figure 2-1C. Based on the DTA data, four heating schedules were selected for crystallization of four different GCs (Table 2-3).

2.3.2 XRD Analysis of Glass and GCs

XRD spectrum of the as-quenched glass confirmed its amorphous nature as revealed by the shallow hump at $2\theta = 25^\circ - 35^\circ$ (Figure 2-2A). The glass specimens were sintered using four heating schedules (Table 2-3), yielding GC1, GC2, GC3 and GC4. XRD of GC1 revealed crystalline phases consisting predominately of calcium fluoride silicate $\text{Ca}_2\text{SiO}_2\text{F}_2$ (ICDD-PDF # 35-2), accompanied by xonotolite $\text{Ca}_6\text{Si}_6\text{O}_{17}(\text{OH})_2$ (ICDD-PDF # 29-379), hydroxyapatite $\text{Ca}_5(\text{PO}_4)_3\text{OH}$ (ICDD-PDF # 9-432) and miserite $\text{KC}_5(\text{Si}_2\text{O}_7)(\text{Si}_6\text{O}_{15})(\text{OH})\text{F}$ (ICDD-PDF # 22-806) (Figure 2-2B).³⁰ GC2 exhibited

greater peak intensity at $2\theta = 28.1^\circ$, indicative of an increase in miserite content (Figure 2-2C). GC3 displayed an XRD spectrum (Figure 2-2D) similar to that of GC2. Finally, the GC4 spectrum showed a predominantly miserite crystalline phase, accompanied by other minor phases (Figure 2-2E). The XRD spectra indicated the successful synthesis of various GCs, consisting of variable amounts of calcium fluoride silicate, xonotolite, hydroxyapatite and miserite.

2.3.3 Microstructure of Glass and GCs

SEM of fracture surfaces of glass did not reveal any indication of crystalline phases (Figure 2-3A). Fracture surfaces of the GCs varied greatly with differences in the heating schedule (Figure 2-3B-E). GC1 showed a mixture of spherulitic and acicular crystals (Figure 2-3B). GC2 and GC3 showed predominant long laths with spherulitic crystals (Figure 2-3C,D). In contrast, the principal microstructural features of GC4 were long laths and logs with different aspect ratios (Figure 2-3E), consistent with the miserite crystalline phase.

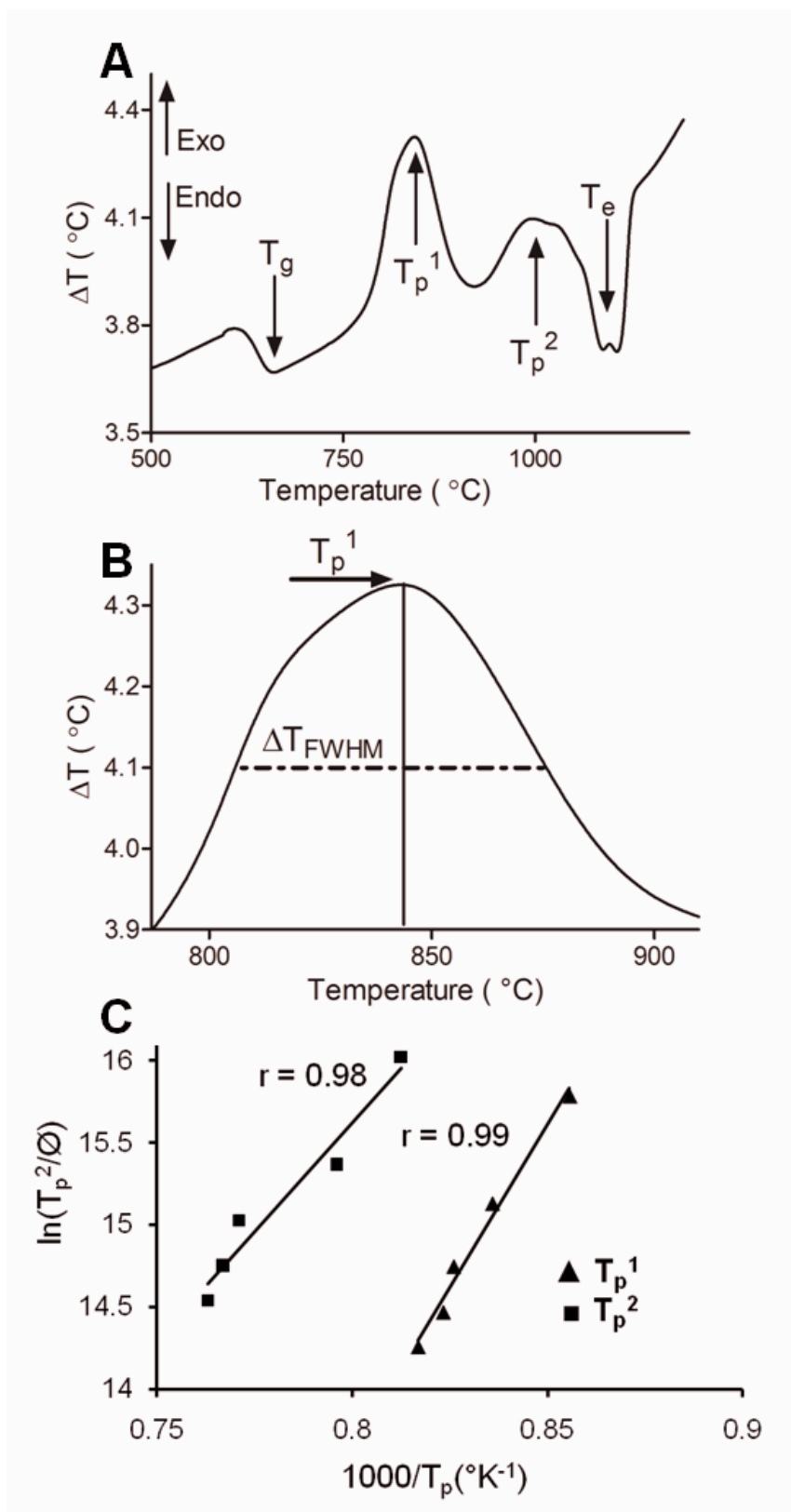


Figure 2-1: Differential thermal analysis (DTA) of the experimental glass powder. (A) Representative data from DTA of the experimental glass powder at 20°C/ min heating rate shows the glass transition (T_g), first and second exothermic peaks (T_p^1 , T_p^2) and liquidus temperatures (T_e). (B) Expanded exothermic peak for the glass at 20 °C/min heating rate. ΔT_{FWHM} is the full width at half maximum of the exothermic peak. (C) Typical DTA plots of $\ln(T_p)^2/\Delta$ vs. $1000/T_p$ for the first and second peaks of the glass at heating rates ranging between 10-50 °C/min, r is the correlation coefficient determined from linear regression. Data are representative of 3 independent determinations.

Table 2-1: Differential thermal analysis (DTA) data for experimental glass fired from RT to 1200 °C at five different heating rates ranging between 10 -50 °C/min. Data are means (SD), $n = 3$.

Heating rate (°C/min)	T_g (°C)	T_p^1 (°C)	T_p^2 (°C)	T_e (°C)
10	601 (2.7)	821 (1.9)	958 (2.1)	1073 (3.1)
20	603 (2.2)	841 (1.7)	983 (12.7)	1075 (1.4)
30	606 (3.4)	854 (1.3)	1024 (6.1)	1080 (25.7)
40	613 (2.2)	859 (1.6)	1031 (3.4)	1087 (28.8)
50	615 (2.5)	866 (1.4)	1038 (2.9)	1090 (4.5)

Table 2-2: Avrami exponents and activation energies of the glass crystallization. Calculated from the first and second DTA exothermic peaks. Data are means (SD), $n = 3$.

	T_p^1	T_p^2
Avrami Exponent (n_A)	1.1 (0.1)	2.8 (0.3)
Activation Energy (ΔE, kJ/mole)	354 (24)	217 (6)

Table 2-3: Heat treatment schedules for experimental glass-ceramics.

Heating Schedules	Samples	Heating rate* (°C/min)	Heat Treatment	
			Temperature (°C)	Holding time* (h)
1	GC1	20	600	1
			850	4
2	GC2	20	600	1
			850	4
			1000	2
3	GC3	5	600	1
			850	4
4	GC4	5	600	1
			850	4
			1000	2

*Heating rate and holding time are experimental and not based on DTA data

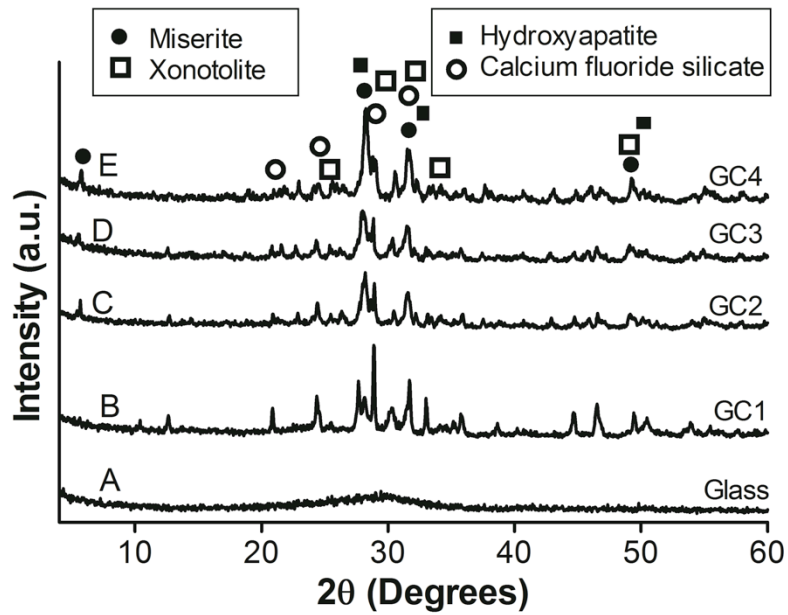


Figure 2-2: X-ray diffraction (XRD) of the as-quenched glass (A), GC1 (B), GC2(C), GC3 (D) and GC4 (E). GCs were treated at different heating rates, temperatures and holding times, as specified in Table 3

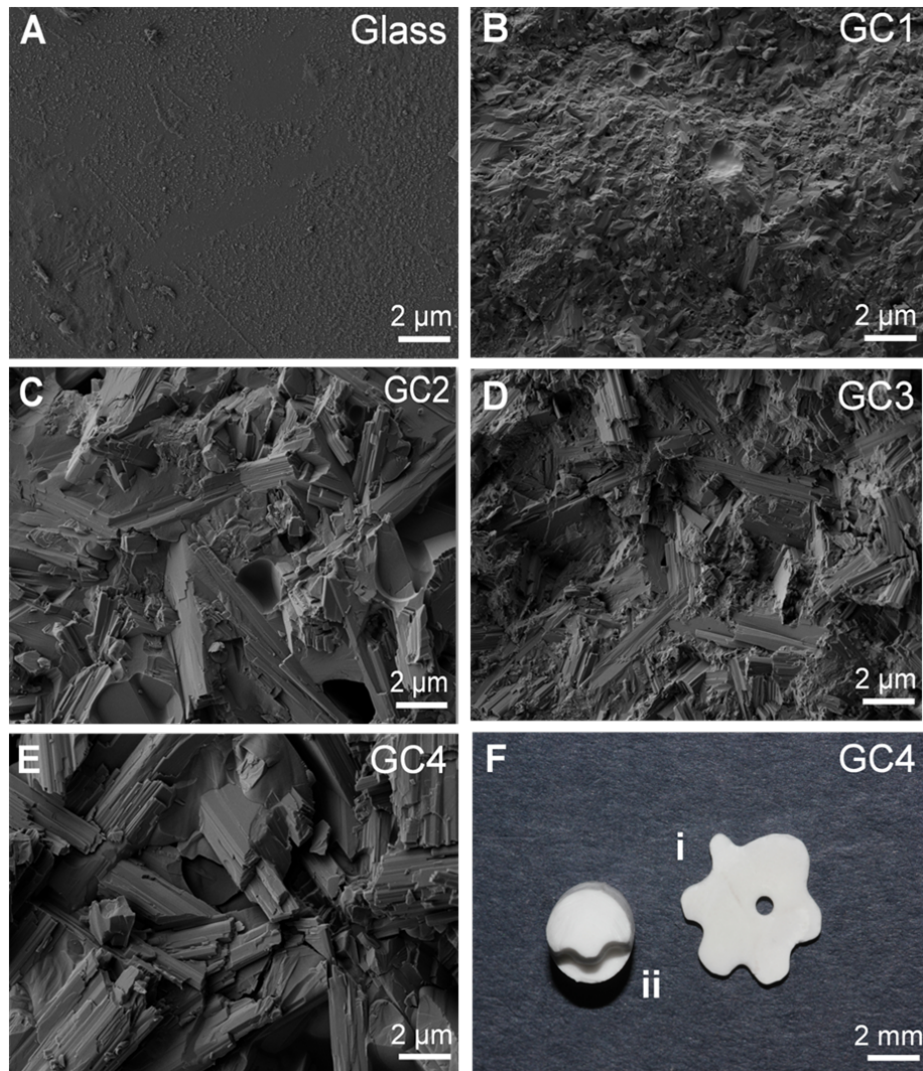


Figure 2-3: (A-E) Microstructure of fractured surfaces of as-quenched glass and GCs as determined by scanning electron microscopy (SEM). (A) Amorphous glass. (B) Microstructure of GC1 shows mixture of spherulitic and acicular crystals that represent calcium fluoride silicate crystalline phase and other secondary crystalline phases. (C, D) Microstructures of GC2 and GC3 reveal mixture of spherulitic and dominant long laths crystals. (E) Microstructure of GC4 showing the principal phase of randomly oriented long laths and logs with different aspect ratio that represent miserite crystalline phase. (F) Macroscopic image of machined GC4 specimens: (i) drilled hole and grooves cut along specimen perimeter, and (ii) shoulder preparation free of cracking and chipping. Images are representative of 3 independent preparations.

2.3.4 Physical and Mechanical Properties

The firing shrinkage of the GCs ranged between 14-18 %. The mean density and Poisson's ratio values for the as quenched glass and GCs ranged between 2666-2868 kg/m³ and 0.17-0.22, respectively (Table 2-4). The Young's moduli (E values) for the GC2, GC3 and GC4 were significantly higher than the as quenched glass ($p < 0.05$). These values ranged between 90-96 GPa, and GC4 exhibited the greatest E. The true hardness (H_o) and fracture toughness (K_{IC}) values of the GCs were significantly increased by heat treatment of the glass. These values ranged between 4.33-5.27 GPa, and 3.81-4.77 MPa·m^{0.5}, respectively. Additionally, the brittleness index (BI) values for the GCs were significantly lower than that of the glass ($p < 0.05$). GC4 exhibited the lowest value at 1.10 $\mu\text{m}^{-0.5}$ (Table 2-4). Moreover, GC4 could be prepared smoothly and it did not exhibit any surface cracking or chipping as a result of machining (Figure 2-3F). GC4 was selected for further studies to assess its bioactivity in SBF and biocompatibility with cultured cells, because of its excellent mechanical properties and machinability and it exhibited miserite as the main crystalline phase compared to other GCs.

Table 2-4: Physical and mechanical properties of experimental glass and glass-ceramics. Data are means (SD), $n = 3$. Different superscript letters denote that values are significantly different ($p < 0.05$) based on ANOVA and Tukey's multiple comparisons test.

Properties	Glass	GC1	GC2	GC3	GC4
Density (ρ, kg/m³)	2706 (3)	2666 (18)	2868 (12)	2818 (16)	2859 (37)
Poisson's ratio (ν)	0.22 (0.30)	0.20 (0.02)	0.20 (0.03)	0.18 (0.02)	0.17 (0.01)
Young's modulus (E, GPa)	78.1 (0.5) ^a	80.1 (4.2) ^a	94.9 (2.4) ^b	89.8 (0.5) ^b	95.9 (2.5) ^b
True hardness (H₀, GPa)	3.83 (0.09) ^a	4.33 (0.12) ^b	5.20 (0.42) ^c	4.84 (0.24) ^c	5.27 (0.26) ^c
Fracture toughness (K_{IC}, MPa·m^{0.5})	1.46 (0.14) ^a	3.81 (0.55) ^b	4.53 (0.60) ^c	3.90 (0.22) ^b	4.77 (0.27) ^c
Brittleness index (BI, $\mu\text{m}^{-0.5}$)	2.62 (0.05) ^a	1.14 (0.13) ^b	1.14 (0.18) ^b	1.24 (0.07) ^b	1.10 (0.05) ^b

2.3.5 Bioactivity of GC4

The SEM and EDX analyses of the GC4 specimens before and after soaking in SBF demonstrated successful deposition of a calcium phosphate surface layer (Figure 2-4A, B). As early as 1 week after immersion in SBF, the surface of the GC4 was covered with a distinct coating (Figure 2-4Aii). Immersion of GC4 specimens for 4 weeks resulted in the formation of a uniform surface layer having morphology similar to that of biomimetic HA (Figure 2-4Aiv). EDX elemental analysis revealed an increase in the intensity of the peaks attributed to Ca and P and gradual diminution of the Si peak after soaking in SBF for increasing times (Figure 2-4B and Table 2-5). The calcium to phosphorous ratio

(Ca/P) of the surfaces was in the range of 1.50-1.64, which is similar to bone-like apatite (Ca/P \approx 1.50) and approaching that of stoichiometric HA (Ca/P = 1.67).³¹

XRD spectra of the GC4 samples after immersion in SBF confirmed the formation of an HA layer on the GC surfaces (Figure 2-4Cii-iv). The results showed attenuation of the XRD peaks associated with GC4 after 1 and 2 weeks soaking in SBF, and the appearance of peaks at $2\theta = 26^\circ$ and 32° , indicative of a poorly crystalline HA (ICDD-PDF # 09-432). Moreover, after 4 weeks soaking in SBF, only peaks ascribed to HA were visible, consistent with the formation of a thick apatite layer. Taken together, the SEM, EDX, and XRD results confirmed the deposition of an HA surface layer after immersion of GC4 in SBF, indicating its bioactivity.

Table 2-5: Energy dispersive X-ray spectroscopy (EDX) analysis of GC4 and molar Ca/P ratio for different soaking times in SBF. Data are means (SD), $n = 3$.

Soaking time (Week)	Si Atomic %	Ca Atomic %	P Atomic %	Molar Ca/P ratio
0	21.38 (0.47)	17.19 (0.52)	0.12 (0.08)	-----
1	0.83 (0.25)	14.36 (0.21)	9.15 (0.07)	1.57 (0.01)
2	1.04 (0.33)	14.61 (0.33)	9.73 (0.14)	1.50 (0.03)
4	-----	18.68 (0.65)	11.37 (0.28)	1.64 (0.02)

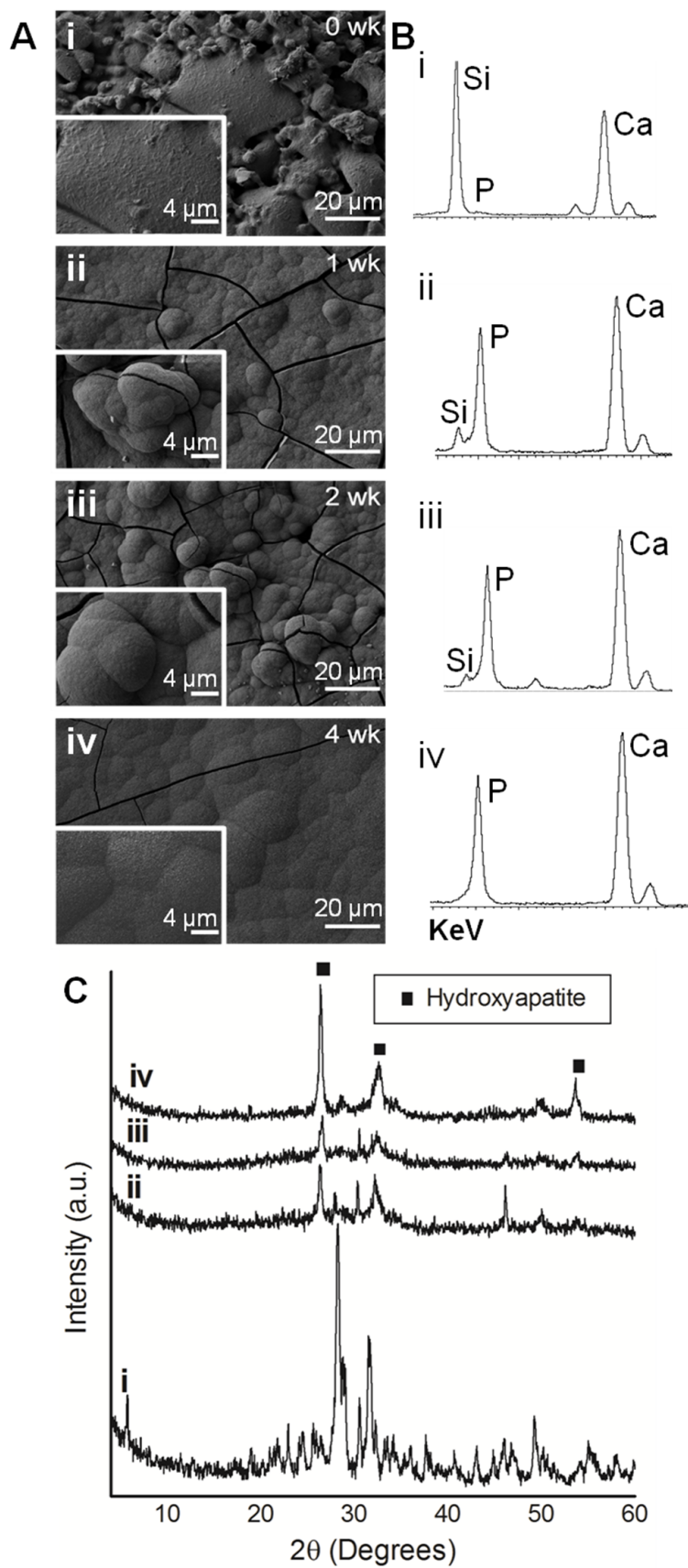


Figure 2-4: Bioactivity of GC4. (A) SEM surface morphologies, (B) EDX spectra and (C) XRD of GC4 before (i) or after soaking in SBF for 1 (ii), 2 (iii) or 4 (iv) weeks. (A) SEM micrographs illustrate the surface morphology of the GC4 before soaking in SBF and the formation of HA layer on the GC4 surfaces at low and high magnifications at different times. (B) EDX spectra show the Si, Ca and P peaks before and after soaking in SBF. (C) XRD confirmed the gradual formation of HA surface layer on the GC4 surfaces at different soaking times in SBF. At 4 weeks, the XRD showed the spectrum of HA only (PDF#19-272), indicating that GC4 is totally covered with HA layer (Civ).

2.3.6 Cell Morphology and Number on GC4 and Titanium

MC3T3-E1 osteoblast-like cells were cultured for 6, 24 and 72 h on GC4 and titanium surfaces. Sand-blasted and acid-etched titanium (STi) was used as a positive control as it is a biocompatible material approved for clinical implant applications.³² Fluorescence images at different incubation times showed that cells attached to both GC4 and STi, but spreading was markedly greater on GC4 at 6 h (Figure 2-5A-D). Cells on GC4 surfaces were flattened and well spread with polygonal shapes. Higher magnification images revealed the formation of stress fibers and few filopodia. In contrast, at 6 h the cells on STi were spindle-shaped with distinct filopodia along the periphery of cells and longer cytoplasmic extensions. There was no significant difference between the number of cells present on GC4 and STi after 6 and 24 h incubation. However, by 72 h, there was a significant increase in cell numbers on both GC4 and STi (Figure 2-5M, $p < 0.05$), consistent with proliferation of MC3T3-E1 cells on both surfaces. Also we note, there were significantly greater cell numbers on GC4 than on STi at 72 h (Figure 2-5M, $p < 0.05$).

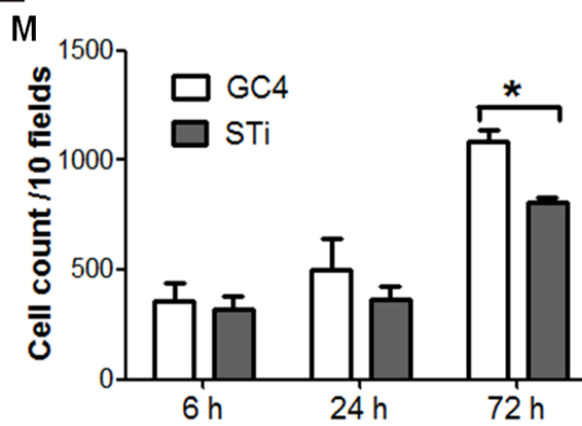
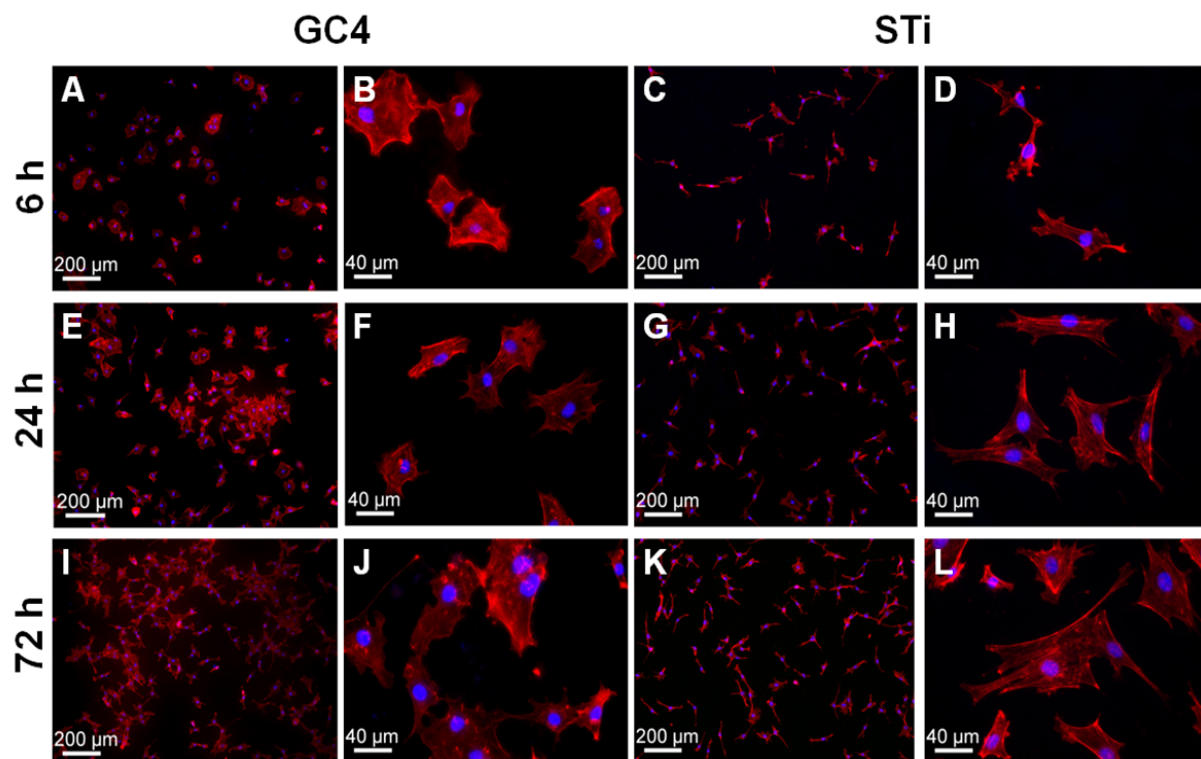


Figure 2-5: Osteoblast attachment, spreading and morphology on GC4 and titanium. MC3T3-E1 osteoblast-like cells were cultured for 6, 24 and 72 h on GC4 and titanium (STi, control) substrata. Cells were then fixed and stained for filamentous actin (F-actin, red) and nuclei (blue). (A-L) Images were obtained by fluorescence microscopy at low and high magnifications. (M) Cell number was quantified by counting cells on GC4 and STi discs after 6, 24 and 72 h. Cells were counted on 10 randomized fields on each sample. Cell count data are means (SD) based on 3 independent experiments each performed on triplicate samples. There was no significant difference between osteoblast attachment to GC4 and titanium at 6 and 24 h. On the other hand, at 72 h, the cell number was significantly greater on GC4 compared to STi ($p < 0.05$) based on ANOVA and Tukey's multiple comparison tests.

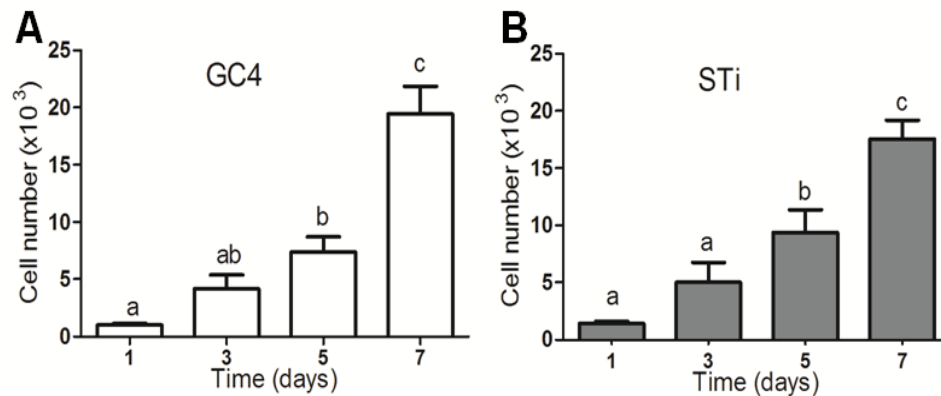


Figure 2-6: Osteoblast proliferation on GC4 (A) and titanium (B). Cell numbers were quantified after 1-7 days incubation using the CyQUANT[®] proliferation assay. Data are means (SD) based on 3 independent experiments each performed on triplicate samples. Because of different surface areas of GC4 and STi (113 mm² and 177 mm², respectively), cell numbers on GC4 were normalized to the cell numbers on STi. Different lowercase letters denote significant differences ($p < 0.05$) based on ANOVA and Tukey's multiple comparisons tests.

2.3.7 Cell Proliferation on GC4 and Titanium

To further investigate the ability of these surfaces to support cell proliferation, MC3T3-E1 cells were cultured for 1 to 7 days on GC4 and STi. Cell numbers were quantified using the CyQuant[®] cell proliferation assay (Figure 2-6). Both GC4 and titanium supported cell proliferation, with significant increases at days 5 and 7 on both substrata ($p < 0.05$). Taken together, results of the cell studies established that GC4 is at least comparable to titanium in terms of its ability to support the attachment, spreading and proliferation of osteoblast-like cells.

2.4 DISCUSSION

GCs are typically produced by melting glasses at high temperature (~1500 °C), which results in significant fluorine loss and adversely influences the glass mechanical properties.¹⁵ In the present study, the combination of wet-chemistry and spray-drying resulted in a more homogeneous glass with lower melting point (1250 °C) compared to similar compositions prepared by conventional methods.²⁰ Maintaining the fluorine content in the glass improves its sinterability and mechanical properties.^{33,34}

The GCs synthesized in this study displayed good sintering characteristics by maintaining the initial sample shape and integrity, features which are attributable in part to the homogeneity of the precursor glass produced by wet chemistry.³⁵ Additionally, the glass powder was calcined at low temperature (200-700 °C) to remove adsorbed moisture and impurities remaining from the synthesis stage.¹¹

Biomaterials are considered bioactive when a strong interfacial bond forms between the implant and the surrounding bone tissue; through the formation of a carbonated HA layer at the interface.¹³ This HA layer is similar in composition and structure to the apatite in bone.³⁶ The presence of an HA layer prevents fibrous tissue formation around the implant that could hinder bone integration. In addition, the interfacial bond improves the load distribution between the biomaterial and the surrounding bone and, as a result, diminishes stress shielding.³⁷ The GCs synthesized in this study are bioactive as evidenced by the complete coverage of the GC4 surfaces with HA after 4 weeks of soaking in SBF. The molar Ca/P ratio of the apatite surface layer ranged between 1.57 and 1.64, in good agreement with the characteristics of biological HA.³¹

To our knowledge, there are currently no bioactive machinable non-metallic materials used for dental implants. Therefore, it is relevant to compare characteristics of the experimental miserite GC described in the present study to those of titanium (used extensively for dental implants) and zirconia (recently introduced to the oral implantology field).^{1,5} Both titanium and zirconia lack the bioactivity of miserite

The high stiffness of titanium dental implants (105-116 GPa) and dental zirconia (~200 GPa) do not match that of human bone (4-20 GPa).^{6,38} This mismatch gives rise to stress shielding,³⁹ where the bone is inadequately loaded leading to bone resorption and subsequent implant failure.^{37,39} Although, the stiffness of the miserite GCs developed in the present study are still high (80-96 GPa), they are less than that of Ti and zirconia, and could potentially reduce stress shielding.

Currently, zirconia dental implants have poor machinability as they undergo accelerated aging due to development of micro cracks.⁸⁻¹⁰ Moreover, milling and machining of zirconia implants negatively impact the final implant fracture strength.^{9,40} The good machinability of the experimental GCs is attributed to the randomly oriented, interlocking lath crystals.³⁴

When miserite GC is machined, micro cracks developed at the glass/crystal interfaces will be hindered by the interlocking lath crystals, which act as a barrier against catastrophic crack propagation.²¹ BI has been proposed as a quantitative measure of machinability, where ceramics with a BI value less than $4.3 \mu\text{m}^{-0.5}$ are considered machinable.²⁶ This was the case for GC4, with a BI of only $1.1 \mu\text{m}^{-0.5}$. Moreover, GC4 could be milled into different shapes without cracking, indicating its potential for the production of dental implants by CAD-CAM technology.

Attachment of cells of the osteoblast lineage to the biomaterial surface is an initial step towards the formation of new bone tissue surrounding the implant.³² The osteoblast-like cell line, MC3T3-E1, used in the present study has been widely used to assess the biocompatibility of Ti dental implant materials.³² Osteoblast-like cells attached, spread and proliferated on GC4, which indicates that GC4 is biocompatible. Interestingly, cell morphology differed on the relatively smooth surface of GC4 and the rougher surface of STi, likely reflecting differences in surface chemistry and topography. These results are in agreement with previous studies, which demonstrated that osteoblasts attach, spread and proliferate differently on smooth surfaces as compared to rough surfaces.^{32,41} At 24 and 72 h, cells exhibited specific morphology and actin stress fibers were clearly visible. Moreover, both the GC4 and STi surfaces supported cell proliferation.

When the synthesized transparent glass was heat treated and crystallized to form GCs, it became white opaque. It likely lost transparency as a result of random light scattering and the difference in refractive index between the crystal and the parent glass.⁴² Regardless, GC4 is esthetically acceptable as a dental implant when compared with Ti dental implants that may show a grayish line at the gingival margin. The metal-free GC dental implant preserves the natural color of the soft tissue surrounding the dental implant and improves the esthetic outcome of treatment.

Preliminary studies were performed on these GC, assessing their chemical durability in acetic acid and degradation in tris-buffered solution (Appendix B). Results of these initial studies suggested that miserite GC was not sufficiently stable to meet the requirements of dental restorations exposed to the oral environment or implanted in bone. These data motivated us to modify the GC composition, keeping the favorable mechanical, physical and biological properties, while improving chemical durability. Synthesis and characterization of the resulting wollastonite glass-ceramics are described in *Chapters 3 and 4*.

2.5 CONCLUSIONS

Glass ceramic containing miserite $[\text{KCa}_5(\text{Si}_2\text{O}_7)(\text{Si}_6\text{O}_{15})(\text{OH})\text{F}]$ as the dominant phase was prepared by wet chemistry, spray-drying and sintering (bulk crystallization). The microstructure of GC4 was primarily interlocked log and lath crystals, which contributed to high K_{IC} ($4.77 \text{ MPa}\cdot\text{m}^{0.5}$), as well as excellent machinability. *In vitro* tests showed that miserite GC is bioactive and supports the attachment and proliferation of osteoblast-like cells comparable to clinically proven titanium surfaces.

2.6 REFERENCES

1. Simonis P, Dufour T, Tenenbaum H. Long-Term Implant Survival and Success: A 10–16-Year Follow-Up of Non-Submerged Dental Implants. *Clin Oral Implants Res.* 2010; 21(7):772-77.
2. Sicilia A, Cuesta S, Coma G, Arregui I, Guisasola C, Ruiz E, *et al.* Titanium Allergy in Dental Implant Patients: A Clinical Study on 1500 Consecutive Patients. *Clin Oral Implant Res.* 2008; 19(8):823–35.
3. Siddiqi A, Payne AGT, De Silva RK, Duncan WJ. Titanium Allergy: Could it Affect Dental Implant Integration? *Clin Oral Implant Res.* 2011; 22(7):673-80.
4. Tolstunov I. Dental Implant Success-Failure Analysis: A Concept of Implant Vulnerability. *Implant Dent.* 2006(4):341-46.
5. Özkurt Z, Kazazoglu E. Zirconia Dental Implants: A Literature Review. *J Oral Implant.* 2011; 37(3):367-76.
6. Andreiotelli M, Wenz HJ, Kohal R. Are Ceramic Implants a Viable Alternative to Titanium Implants? A Systematic Literature Review. *Clin Oral Implant Res.* 2009; 20(S4):32-47.
7. Hisbergues M, Vendeville S, Vendeville P. Zirconia: Established Facts and Perspectives for a Biomaterial in Dental Implantology. *J Biomed Mater Res.* 2009; 88B (2):519-29.
8. Al-Amleh B, LYons K, Swain M. Clinical Trials in Zirconia: A Systematic Review. *J Oral Rehabil.* 2010; 37(8):641-52.

9. Manicone PF, Rossi Iommetti P, Raffaelli L. An Overview of Zirconia Ceramics: Basic Properties and Clinical Applications. *J Dent.* 2007; 35(11):819-26.
10. Jayaswal GP, Dange SP, Khalikar AN. Bioceramic in Dental Implants: A Review. *J Ind Pros Society.* 2010; 10(1):8-12.
11. Gross KA, Berndt CC. Biomedical Application of Apatites. *Rev Mineral Geochem.* 2002; 48(1):631-72.
12. Kokubo T, Kushitani H, Sakka S, Kitsugi T, Yamamuro T. Solutions Able to Reproduce In Vivo surface-Structure Changes in Bioactive Class-Ceramic A-W. *J Biomed Mater Res.* 1990; 24(6):721-34.
13. Hench L. Bioceramics-From Concept to Clinic. *J Am Ceram Soc.* 1993;74(7):1487-510.
14. Palmquist A, Omar OM, Esposito M, Lausmaa J, Thomsen P. Titanium oral implants: Surface Characteristics, Interface Biology and Clinical Outcome. *J R Soc Interface.* 2010;7(s):S515-27.
15. Höland W, Beall GH. *Glass-Ceramic Technology.* Westerville, USA: American Ceramic Society; 2002.
16. Augis J, Bennett J. Calculation of the Avrami Parameters for Heterogeneous Solid State Reactions Using a Modification of the Kissinger method. *J Therm Analysis.* 1978;13(2):283-92.
17. Kissinger, H. Variation of Peak Temperature With Heating Rate in Differential Thermal Analysis. *J Rs Nat Bur Stand.* 1956;57(4):217-21.

18. Rizkalla AS, Jones DW, Clarke DB, Hall GC. Crystallization of Experimental Bioactive Glass Compositions. *J Biomed Mater Res.* 1996;32(1):119-24.
19. Scott JD. Crystal Structure of Miserite, a Zoltai Type 5 Structure. *Can Mineral.* 1976;14: 515-28.
20. Pinckney LR, Beall GH, and Andrus RL. Strong Sintered Miserite Glass-Ceramics. *J Am Ceram Soc.* 1999; 82(9):2523-28.
21. Alizadeh P, Eftekhari Yekta B, Javadi T. Preparation of Machinable Bioactive Mica Diopside-Fluoroapatite Glass-Ceramics. *Adv Appl Ceram.* 2010; 109(1):56-61.
22. Fultz B, Howe JM. Diffraction and the X-ray Powder Diffractometer. In: *Transmission Electron Microscopy and Diffractometry of Materials.* 3rd ed. New York: Springer; 2008. p. 1-59.
23. Schreiber E, Anderson O, Naohiro S. *Elastic Constants and Their Measurement.* New York: McGraw-Hill; 1973.
24. Rizkalla A, Jones D. Indentation Fracture Toughness and Dynamic Elastic Moduli for Commercial Feldspathic Dental Porcelain Materials. *Dental Materials.* 2004; 20(2):198-206.
25. Lankford J. Indentation Microfracture in the Palmqvist Crack Regime: Implications for Fracture Toughness Evaluation by the Indentation Method. *J Mater Sci Lett.* 1982; 1(11):493-5.
26. Boccaccini AR. Machinability and Brittleness of Glass-Ceramics. *J Mater Process Tech.* 1997; 65(1):302-4.

27. Kokubo T, Takadama H. How Useful is SBF in Predicting In Vivo Bone Bioactivity? *Biomaterials*. 2006; 27(15):2907-15.
28. Sudo H, Kodama H, Amagai Y, Yamamoto S, Kasai S. In Vitro Differentiation and Calcification in a New Clonal Osteogenic Cell Line Derived from Newborn mouse Calvaria. *J Cell Biol*. 1983 Jan.; 96(1):191-8.
29. Wang D, Christensen K, Chawla K, Xiao G, Krebsbach P, and Franceschi R. Isolation and Characterization of MC3T3-E1 Preosteoblast Subclones With Distinct In Vitro and In Vivo Differentiation/Mineralization Potential. *J Bone Miner Res*. 1990; 14(6):893–903.
30. Joint Committee on Powder Diffraction Standards, American Society for Testing and Materials. *Selected Powder Diffraction Data for Minerals*. 1st ed. Swarthmore, Pa: 1974.
31. LeGeros RZ. *Calcium Phosphates in Oral Biology and Medicine*. Basel; New York: Karger; 1991.
32. Le Guehennec L, Lopez-Heredia MA, Enkel B, Weiss P, Amouriq Y, Layrolle P. Osteoblastic Cell Behavior on Different Titanium Implant Surfaces. *Acta Biomater*. 2008; 4(3):535-43.
33. Banijamali S, Eftekhari Yekta B, Rezaie H, Marghussian VK. Effect of Fluorine Content on Sintering and Crystallization Behavior of CaO–Al₂O₃–SiO₂ Glass Ceramic System. *Advances in Applied Ceramics*. 2008; 107(2):101-5.
34. Molla A, Basu B. Microstructure, Mechanical, and In Vitro Properties of Mica Glass-Ceramics with Varying Fluorine Content. *J Mater Sci*. 2009; 20(4):869-82.

35. Dorozhkin SV. Amorphous Calcium (Ortho) Phosphates. *Acta Biomater.* 2010; 6(12):4457-75.
36. Kokubo T. Apatite Formation on Surfaces of Ceramics, Metals and Polymers in Body Environment. *Acta Materialia.* 1998; 46(7):2519-27.
37. Ratner B. Replacing and Renewing: Synthetic Materials, Biomimetics, and Tissue Engineering in Implant Dentistry. *J Dent Edu.* 2001; 65(12):1340-7.
38. Natali AN. *Dental Biomechanics.* London; New York: Taylor & Francis; 2003.
39. Koleganova VA, Bernier SM, Dixon SJ, Rizkalla AS. Bioactive Glass/Polymer Composite Materials with Mechanical Properties Matching Those of Cortical Bone. *J Biomed Mater Res.* 2006; 77A (3):572-79.
40. Andreiotelli M, Kohal RJ. Fracture Strength of Zirconia Implants after Artificial Aging. *Clin Implant Dent Relat Res.* 2009; 11(2):158-66.
41. Martin JY, Schwartz Z, Hummert TW, Schraub DM, Simpson J, Lankford J, et al. Effect of Titanium Surface Roughness on Proliferation, Differentiation, and Protein Synthesis of Human Osteoblast-Like Cells (MG63). *J Biomed Mater Res.* 1995;29(3):389-401.
42. Varshneya AK. *Fundamentals of Inorganic Glasses.* London: Academic Press Limited; 1994.

CHAPTER 3

SYNTHESIS AND CHARACTERIZATION OF WOLLASTONITE GLASS-CERAMICS FOR DENTAL IMPLANT APPLICATIONS

This chapter describes a novel approach for the synthesis of GCs with mechanical, physical and chemical properties required for non-metallic dental implant applications. The contents of this chapter have been reproduced (with modifications of the glasses and glass-ceramics nomenclature) from a manuscript that has been accepted for publication in Dental Materials (Saadaldin et al, Dental Materials, DEMA-D-13-00398R1).

3.1 INTRODUCTION

Glass-ceramics are polycrystalline materials with an inorganic-inorganic microstructure that were prepared from base glass by controlled crystallization. This was achieved by subjecting glasses to regulated heat treatment, which resulted in the nucleation and growth of one or more crystal phases within the glass. GCs have diverse physical, chemical, mechanical, optical and biological properties that can be modified with glass composition and heat treatment conditions.¹ As a consequence of the continuous need of the general public as well as the dental professionals to eliminate dental metal-based products, there is a trend towards GCs and ceramic-based materials in the biomedical field.² Yttrium-stabilized tetragonal zirconia polycrystalline has been used extensively as a material of choice for ball heads in total hip replacement since 1980s, and it became commercially available as non-metallic dental implants in 2000s, owing to its strength, fracture resistance and appropriate optical properties.³ However, zirconia undergoes aging through low-temperature degradation phenomenon that is moisture/water related and unfavorably affects its physical properties. In 2000, several hundreds of hip prosthesis failed over a short period of time. These failures were ascribed to an accelerated aging of

the zirconia femoral head in particular batches.⁴ Additionally, literatures showed that zirconia is correlated with two types of radiation impurities, alpha and gamma. Alpha radiation has been observed in a significant amounts and it could harm soft and hard tissues' cell due to their high ionization.^{5,6}

The wollastonites (CaSiO_3) are white glassy silicate minerals that occur as masses or tabular crystals of metamorphosed limestone. A silica chain GC that contains crystalline apatite and β -wollastonite (AW) was introduced in an $\text{MgO-CaO-SiO}_2\text{-P}_2\text{O}_5$ glassy matrix and it showed an excellent bioactivity, biocompatibility, machinability and adequate mechanical properties such as Young's modulus (117 GPa), compressive strength (1080 MPa), and bending strength (215 MPa).⁷ AW has been used for orthopedic applications—artificial vertebrae, intervertebral discs and iliac crest prostheses.^{7,8} Kokubo proved that the mechanical strength of the AW was significantly unaffected in simulated body fluid at 36.5 °C and presumed that it can withstand a bending stress of 65 MPa in the human body environment for over 10 years.⁷ Yet, the fracture toughness of the AW had relatively low values (2-2.5 $\text{MPa}\cdot\text{m}^{0.5}$); therefore it's limited to non-load bearing applications. And we note that, a custom AW prostheses production by conventional lost wax casting can be difficult as a result of the surface crystallization.⁷ However, because of its excellent bioactivity, AW was used as a coating on different substrates such as titanium alloys⁹ or as a composite scaffold by incorporation of AW with other materials.^{10,11}

Fracture toughness (K_{IC}) measures the resistance of a material to cracks propagation and the ability to prevent the initiation of catastrophic fracture. Indentation test has been considered as an accurate procedure to measure the fracture toughness for brittle

materials, like ceramics and GCs. The indentation method has the advantages of simplicity and economy; where only small specimen area is needed, hence the technique is suited for comparative evaluation.¹²

Chemical durability affects the clinical performance of dental materials. With a wide range of pH and temperature, dental materials should resist chemical degradation and dissolution. Chemical degradation of ceramic dental materials could lead to structure's weakening and surface roughness as a result of surface-ion exchange. This phenomenon leads to increased plaque attachment onto the biomaterials and intensify abrasion potential against opposing natural teeth and other restorative materials.¹³

The brittle behavior of the GCs makes them sensitive to milling and machining; therefore the development of machinable GCs for dental implant applications is considered a significant progress. A machinable dental implant material can be introduced to CAD-CAM technology and customized implants for different clinical cases can be fabricated, in addition to the possibility of the modification and adjusting of the implant at the time of surgical insertion. Machinable GCs can be used as one-piece dental implants where the upper part can be prepared to produce the abutment unit and get rid of multiple component implants i.e. fixture, screw and abutment.

The objectives of this study were to synthesize machinable wollastonite GCs with mechanical properties suitable for dental implant applications, to assess their chemical durability using acetic acid and tris buffered solution at different time points and evaluate their fracture toughness following chemical degradation testing.

3.2 MATERIAL AND METHODS:

3.2.1 Glass Synthesis

Transparent glass frits were synthesized by wet chemical methods through four steps. In the beginning, the desired glass compositions in weight % (Table 3-1) were prepared by mixing batch ingredients { $\text{Si}(\text{C}_2\text{H}_5\text{O})_4$, $\text{Al}(\text{NO}_3)_3 \cdot 9\text{H}_2\text{O}$, $\text{Ca}(\text{NO}_3)_2 \cdot 4\text{H}_2\text{O}$, CaF_2 , KNO_3 , H_3BO_3 , $\text{Ce}(\text{NO}_3)_3 \cdot 6\text{H}_2\text{O}$ and $\text{Y}(\text{NO}_3)_3 \cdot 6\text{H}_2\text{O}$ } in aqueous solution using excess deionized water, and kept stirred overnight to commence hydrolysis and polycondensation of metal alkoxides. This was followed by spray drying of the solutions at a feed flow rate of 10 ml/min, inlet air temperature of 160 °C and outlet air temperature of 80 °C using a 190 mini spray-dryer (BÜCHI, Switzerland). The spray-dried powders were calcined by means of a Ney 650 vacuum oven (Ney-Barkmeyer, USA) through sequential heating schedules at 200, 500 and 700 °C for 2 h. Finally, the calcined powders were melted in an uncovered platinum crucible at 1350 °C for 3 h in a high temperature furnace (Thermolyne Corporation, USA), followed by quenching in iced-water to obtain the glass frits.

Table 3-1: Chemical composition (wt%) of the experimental glasses

Glass component	SiO_2	Al_2O_3	CaO	CaF_2	K_2O	B_2O_3	P_2O_5	CeO_2	Y_2O_3
G-A	55	2	17	12	5	3	1.5	1.5	3
G-B	59	1	15	12	5	3	2	0	3
G-C	50	2	20	12	7	3	3	0	3

3.2.2 Differential Thermal Analysis

Crystallization kinetic parameters of the glasses (G) were determined using SDT Q600 V20.5 Build 15 (TA Instruments, USA) at different five heating rates (10-50 °C/min), starting from room temperature up to 1200 °C under air atmosphere; for each heating rate, three-independent runs were carried out ($n=3$). The average sample weight was 20 mg and an equivalent weight of $\alpha\text{-Al}_2\text{O}_3$ was used as a reference. The activation energy (ΔE) was calculated from the plot of $\ln (T_p)^2/\emptyset$ vs. $1000/T_p$ using the Kissinger equation,¹⁴ where T_p is the exothermic peak (°C) as determined from the DTA spectra and \emptyset is the heating rate (°C/s). The Avrami exponent (n_A) was calculated using the Augis-Bennett equation¹³ from the full width at the half maximum of the exothermic peak at 20 °C/min. n_A is related to the directionality of crystal growth, lower values (≈ 1) of n_A reflected surface crystallization, whereas n_A values above 1.5 indicated bulk crystallization.¹⁵

3.2.3 Glass-Ceramics Preparation

Glass powders were mixed with 4% polyethylene glycol as a binder and ball-milled using a planetary ball mill, Pulverisette 7 (Laval Lab, USA). Cylindrical ingots (6 mm x10 mm) and disk specimens (11 mm x 1 mm) of the glass powders were produced by cold pressing using a Carver laboratory cold press (Carver, USA) in stainless steel dies at 40 MPa. Pressed glass specimens were heated for 1h at the glass transition temperature that was obtained from DTA spectra for the nuclei formation. Afterward the temperature was subsequently raised to the crystallization temperatures determined from the DTA exothermic peaks and held for 4 h, Table 3-2.

Table 3-2: Optimal heat treatment schedules for the experimental glass ceramics based on the DTA data.

Samples	Heating rate* (°C/min)	Heat Treatment	
		Temperature (°C)	Holding time* (h)
GC-A	20	700	1
		950	4
GC-B	10	750	1
		1000	4
GC-C	10	700	1
		950	4

* Heating rate and holding time were experimental and not based on DTA data

3.2.4 X-Ray Diffraction

Crystalline phases of the GCs were analyzed by XRD using a Rotaflex RTP 300 RC (Rigaku Co, Japan) operating on CoK α radiation at 45 kV and 160 mA. Spectra were collected in the 2 θ range between 2 and 82°, with 0.05° step and 10°/min scan speed. Bragg's Law was used to calculate 2 θ for equivalent CuK α radiation.¹⁶

3.2.5 Microstructure

Prior to SEM analysis, samples were mounted on aluminum stubs with silver paint and then coated with 3 nm osmium metal (Filgen OPC 80T). The fracture surfaces of the glasses and GCs were examined using LEO 1540XB FIB/SEM (Zeiss, Germany) equipped with an energy dispersive X-ray spectroscopy (EDX) system.

3.2.6 Dynamic Elastic Constants of the GCs

The dynamic elastic properties of the synthesized GCs and yttria-stabilized zirconia (YZ) ceramic control (Vita Zahnfabrik, Germany) were evaluated by ultrasonic method.¹⁷ The density of each specimen (ρ) was determined using the Archimedes method in deionized water at room temperature. The dynamic elastic moduli and Poisson's ratios ($n=3$) were calculated from the velocities of the longitudinal (V_L) and shear (V_S) waves which were determined using lithium niobate crystals that were used for transmitting and receiving waves at 10 MHz resonant frequencies. The equations used for the calculation are reported elsewhere.^{17,18}

3.2.7 True Hardness and Fracture Toughness Evaluation

The true hardness (H_o) and the fracture toughness (K_{IC}) of the GCs and YZ specimens were determined using a Buehler Micromet 5114 Knoop and Vickers micro hardness indenter, (Buehler, USA), respectively. The specimens were embedded in resin and polished ($n=3$). To calculate the H_o , a series of Knoop indentations were performed on each specimen at six consecutive loads (0.49-9.9 N). The average diagonal lengths of the Knoop indentations were measured using Buehler OmniMet^{MH} T7.2 Rev.2 optical microscope equipped with a digital camera and computer software (Buehler, USA). Indentation lengths were plotted vs. the square root of the different load values, and H_o was calculated from the slope of the linear regression line.¹⁹ K_{IC} of the GCs and YZ were determined by measuring the diagonals of the Vickers indentation and the crack lengths using the Lankford equation.²⁰ The average K_{IC} value was calculated from 45 indentations performed on three specimens at a load of 9.8 N.

3.2.8 Chemical Durability

The ISO standard 6782²¹ was used for assessing the chemical durability of the GCs and YZ. Triplicate samples were washed in distilled water in a digital ultrasonic bath (Eumax, China) and dried in a Temp Master “A” furnace (JELRUS, USA) at 150 ± 5 °C for 4 h. The weight of the samples and the total surface area were determined to the nearest 0.1 mg and 0.1 cm^2 , respectively. Specimens were soaked in 20 ml of pre-heated (80 °C) 4 % acetic acid (AC) solution in glass bottles. The bottles were placed in a vacuum oven (VWR, USA) at 80 °C for 16 h. Then the specimens were washed with distilled water in the ultrasonic bath, dried at 150 ± 5 °C until a constant weight was reached. The chemical durability was analyzed by measuring of the specimens weight loss/ unit area (wt/A; $\mu\text{g}/\text{cm}^2$). Later, to assess the effect of the chemical dissolution on the mechanical properties of the materials, the K_{IC} were re-measured for chemically tested specimens.

3.2.9 Degradation Testing

The degradation testing was performed according to ISO standard 10993-14.²² The test is based on a buffered solution that simulates the body’s normal pH level. TRIS-HCl buffered solution (TBS) was prepared by dissolving tris (hydroxymethyl) aminomethane in water; the pH of the solution was adjusted to 7.4 ± 0.1 with an appropriate amount of 1 mol/L HCl acid at 37 °C. Triplicate specimens were washed in a digital ultrasonic bath (Eumax, China) and dried at 150 ± 5 °C in a Temp Master “A” furnace (JELRUS, USA). Samples’ weights were measured, and then the specimens were soaked in freshly prepared TBS in polypropylene containers. The bottles were placed in a MaxQ 5000 circular agitated controlled-temperature chamber (Thermo Scientific, USA) at 37 °C for different timelines (1, 3, 7, 30, 60, 90, and 120 days). At the predetermined time point the

specimens were washed with distilled water in the ultrasonic bath, dried to constant mass and weighed. The degradation of each sample was determined by calculating the percentage weight loss. In a similar manner as described above, the K_{IC} for the specimens that were soaked for 120 days in TBS were re-measured.

3.2.10 Machinability

Qualitative evaluation of the machinability of the GCs was conducted through drilling holes, grooves, bevels as well as preparing shoulder finish lines on GCs' ingots and discs of different thicknesses. Additionally, quantitative assessment was done by calculating brittleness index (BI), which is the ratio of the hardness to the fracture toughness. The lower the brittleness index, the higher the machinability.²³

3.2.11 Statistical Analyses

One-way analysis of variance (ANOVA) followed by Tukey's multiple comparisons test at a significance value of $p < 0.05$ was used to analyze differences among groups. Nonlinear regression analysis was used to evaluate the degradation rates at different timeline. The K_{IC} values for the chemically tested specimens at 120 days were analyzed with simple main effect analysis and Tukey's multiple comparisons test, $p < 0.05$.

3.3 RESULTS

The manufacturing process used in this study resulted in clear transparent amorphous glasses prior to any further heat treatment used to produce the final GCs.

3.3.1 Differential Thermal Analysis of the Glasses

The DTA spectrum of each glass displayed the glass transition temperature (T_g) as a shoulder endothermic peak, the crystallization temperature of the glass (T_p) as an exothermic peak, and the liquidus temperature (T_e), which resulted from decomposition and disintegration of the crystalline phases and illustrated as an endothermic peak, Figure 3-1A. Table 3-3 displayed the n_A values and the activation energies of crystallization of the glasses. G-A had two exothermic peaks and the n_A values for both peaks indicated bulk crystallization. On the other hand, G-B and G-C had one exothermic peak. The n_A value for G-B signified surface crystallization, while that for G-C of 1.8 denoted bulk crystallization. The activation energies of crystallization of the glasses (ΔE) were calculated from the slope of the regression lines, $\ln(T_p)^2/\emptyset$ vs. $1000/T_p$, as demonstrated in Figure 3-1B. The values of the glasses' ΔE ranged between 257 and 360 kJ/mole, and G-B exhibited the highest value.

Table 3-3: Avrami exponents and activation energies of the experimental glasses. Data are mean (SD) of three independent runs at 20°C/min. *Calculated from second exothermic DTA peak.

	Avrami Exponent (n_A)	Activation Energy (ΔE, kJ/mole)
G-A	1.7(0.06)	257(8)
G-A*	1.6(0.18)	308(23)
G-B	1.2(0.04)	360(16)
G-C	1.8(0.04)	317(14)

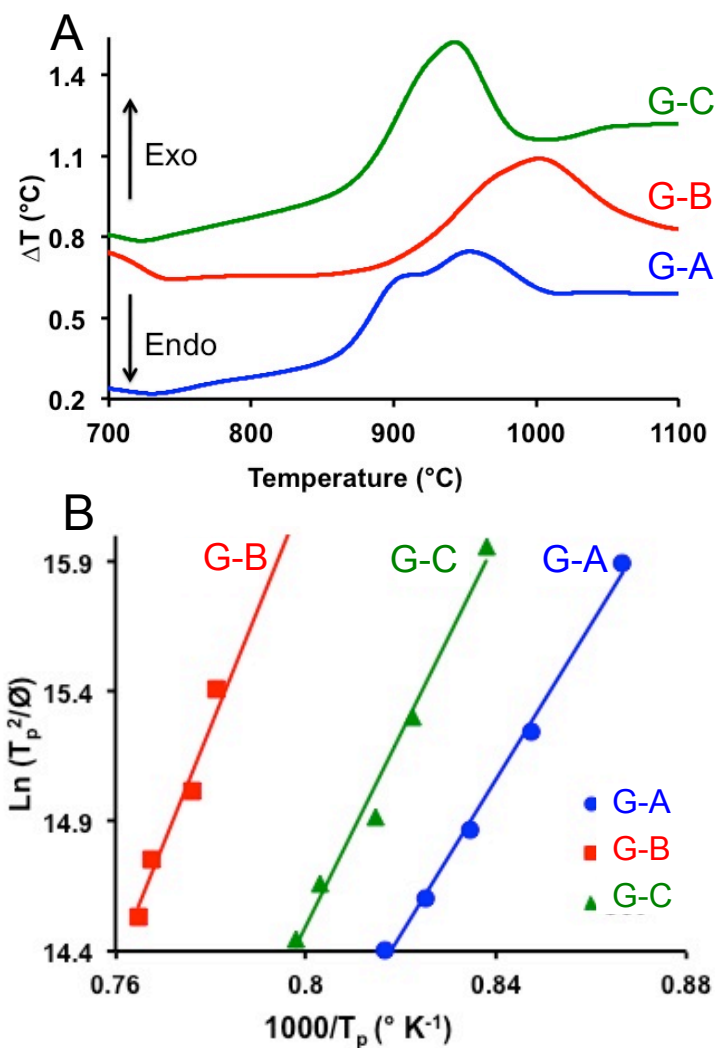


Figure 3-1: (A): Representative DTA curve of the G-A, G-B and G-C powders at 20 °C heating rate. (B) Typical DTA plots of $\ln T_p^2/\emptyset$ vs. $1000/T_p$ for the first peaks of the glasses at heating rates ranging between 10-50 °C/min. T_p is the exothermic peak as determined from the DTA spectra and \emptyset is the heating rate (°C/s). The coefficient of determination calculated from linear regression for G-A, G-B and G-C were 0.988, 0.983 and 0.996, respectively. Data are representative of 3 independent runs.

3.3.2 XRD Analysis of GCs

The principal crystalline phase for the GC-A and GC-C was wollastonite (CaSiO_3 / ICDD-PDF # 10-489), accompanied by hydroxyapatite ($\text{Ca}_5(\text{PO}_4)_3\text{OH}$ / ICDD-PDF # 9-432) and fluorite (CaF_2 / ICDD-PDF # 21-159) as shown in Figure 3-2A,C. The XRD spectrum of GC-B, Figure 3-2B, illustrated the same crystalline phases as GC-A and GC-C with an extra peak at $2\theta = 21.6^\circ$, indicating the presence of cristobalite (SiO_2 / ICDD-PDF # 39-1425) as an additional crystalline phase.

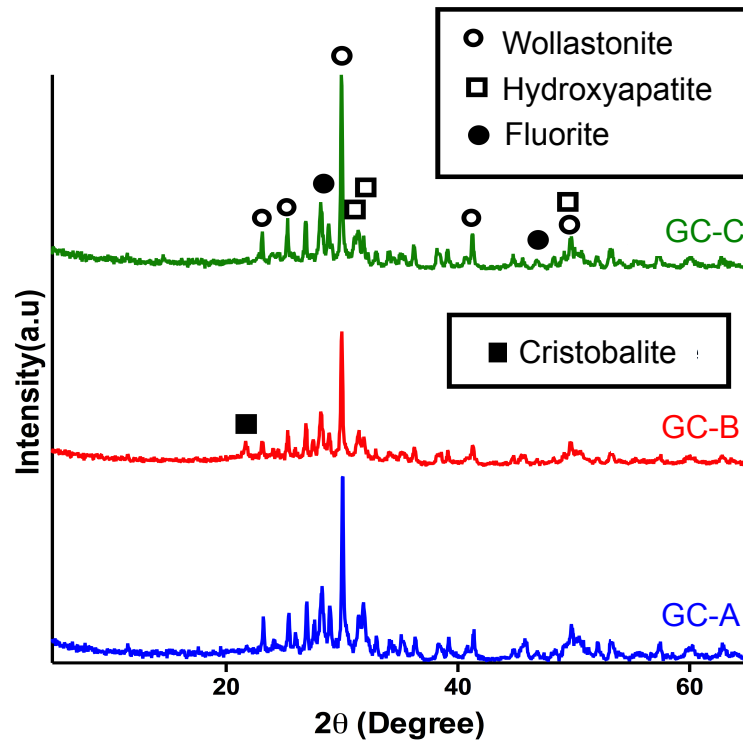


Figure 3-2: XRD analysis of GC-A, GC-B and GC-C.

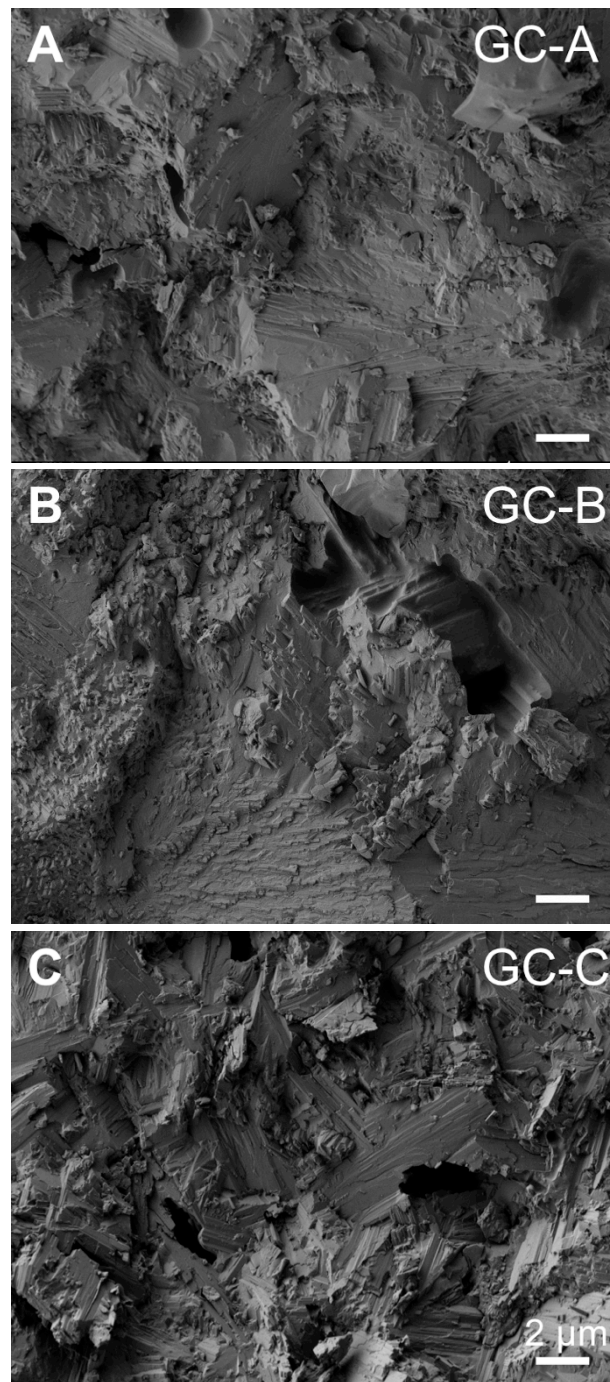


Figure 3-3: SEM micrograph of sintered GC-A (A), GC-B (B) and GC-C (C). Microstructure of the GCs showed acicular interlocking crystals

3.3.3 Microstructure of the GCs

Fracture surfaces of the GCs showed dense acicular interlocking log crystals, which are attributed to wollastonite crystals, Figure 3-3A-C.

3.3.4 Physical and Mechanical Properties

The density and Poisson's ratio for the GCs were 2656-2891 kg/m³ and 0.20-0.21, respectively. These values for YZ (the control material) – 6120 kg/m³ and 0.42, respectively, ($p < 0.05$) were significantly higher as shown in Table 3-4. The E values for the three GCs were 89-100 GPa; though, it was significantly higher for the YZ (212 GPa), $p < 0.05$. Furthermore, the H_o values were 4.85-5.17 GPa. These values were not significantly different among the three GCs, ($p < 0.05$). YZ had significantly higher H_o value of 9.64 GPa, $p < 0.05$. We note that there were significant differences among the measurements for the K_{IC} of GC-A, GC-B, GC-C and YZ that exhibited the significantly higher value of 10.02 MPa·m^{0.5}, ($p < 0.05$). BI of the GCs ranged between 0.99 and 1.16 $\mu\text{m}^{-0.5}$ indicating excellent machinability. This quality was confirmed by the quantitative assessment of crack-free and smooth preparation of GCs samples without fracturing or chipping.

3.3.5 Chemical Durability

The chemical solubility of GC-B samples in 4 % AC, pH=2, were significantly lower than those of GC-A and GC-C ($p < 0.05$) as shown in Table 3-4. The wt/A of GC-B satisfies the ISO specification (less than 100 $\mu\text{g}/\text{cm}^2$), which means that it can be exposed to the harsh oral cavity environments and it is comparable to the wt/A value for YZ. The significantly lower chemical durability for GC-A and GC-C (higher than 100 $\mu\text{g}/\text{cm}^2$ and

lower than $2000 \mu\text{g}/\text{cm}^2$) indicated that these GCs could be used as substructure ceramics that are veneered with other dental biomaterials and should not be exposed to the oral cavity environment. The K_{IC} values of the specimens following chemical durability testing in AC for 16 h were not significantly different when compared with the K_{IC} values of the original untested specimens (ANOVA $p < 0.05$), Figure 3-4.

Table 3-4: Physical, mechanical and chemical properties of the experimental glass ceramics and yttria-stabilized zirconia (YZ). Data are means (SD), $n = 3$. Different superscript letters denote that values are significantly different ($p < 0.05$) based on ANOVA and Tukey's multiple comparisons test.

Properties	GC-A	GC-B	GC-C	YZ
Density (ρ , kg/m^3)	2891(6.1) ^a	2656(20.8) ^b	2713 (38.5) ^b	6120(32.5) ^c
Poisson's ratio (ν)	0.20(0.020)	0.21(0.070)	0.20(0.009)	0.42(0.100)
Young's modulus (E, GPa)	89(1.27) ^a	90(2.98) ^a	100 (2.09) ^b	212(4.41) ^c
Fracture toughness (K_{IC} , $\text{MPa}\cdot\text{m}^{0.5}$)	4.62(0.04) ^a	5.58(0.32) ^b	4.91(0.26) ^a	10.02(0.50) ^c
True hardness (H_0 , GPa)	5.17(0.22) ^a	5.15(0.47) ^a	4.85(0.12) ^a	9.64(0.13) ^b
Brittleness index (BI, $\mu\text{m}^{-0.5}$)	1.12(0.06)	1.16(0.10)	0.99(0.06)	-----
Mass loss/Unit area ($\mu\text{g}/\text{cm}^2$)	1431(96.80) ^a	100(12.25) ^b	987(89.16) ^c	101(8.84) ^b

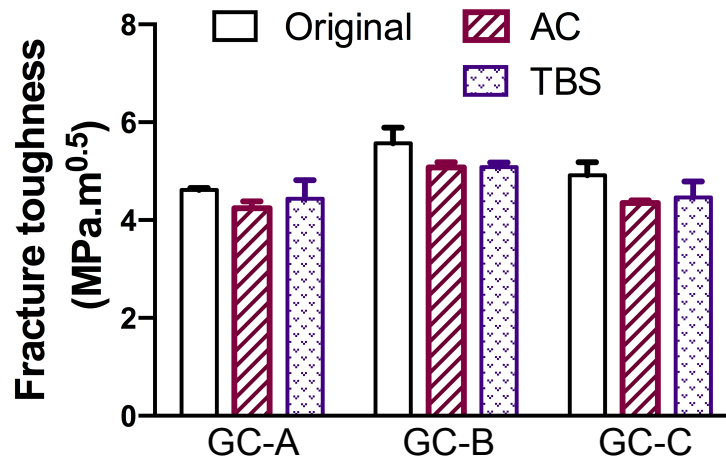


Figure 3-4: Fracture toughness values before and after soaking GCs specimens in 4 %acetic acid (AC) for 16 hours at 80 °C and tris buffered solution (TBS) for 120 days at 37 °C. Data are mean values (SD), $n=3$. ANOVA and Tukey's multiple comparisons test were used to analyze the results for each material ($p<0.05$). There was no significant difference between the original fracture toughness values and the values of chemically tested specimens in both solutions for GC-A, GC-B and GC-C.

3.3.6 Degradation Test

Figure 3-5A illustrates the variation of degradation rates of soaked GCs samples in TBS for different time durations starting from 1day up to 120 days. The percentage degradation increased incrementally as a function of soaking time. All GCs exhibited no weight loss at the first day. Afterward, the degradability values of the GCs increased slowly with different percentages. After 120 days, the GC-A had a weight loss of 2.9 % and it was significantly higher than that of GC-B and GC-C that were 0.36 % and 0.85 %, respectively, ($p<0.05$), revealing very low solubility of GC-B and GC-C, Figure 3-5B. The K_{IC} values of the specimens following chemical degradation testing for 120 days

were not significantly different (ANOVA $p < 0.05$) when compared with the K_{IC} values of the original untested specimens, Figure 3-4.

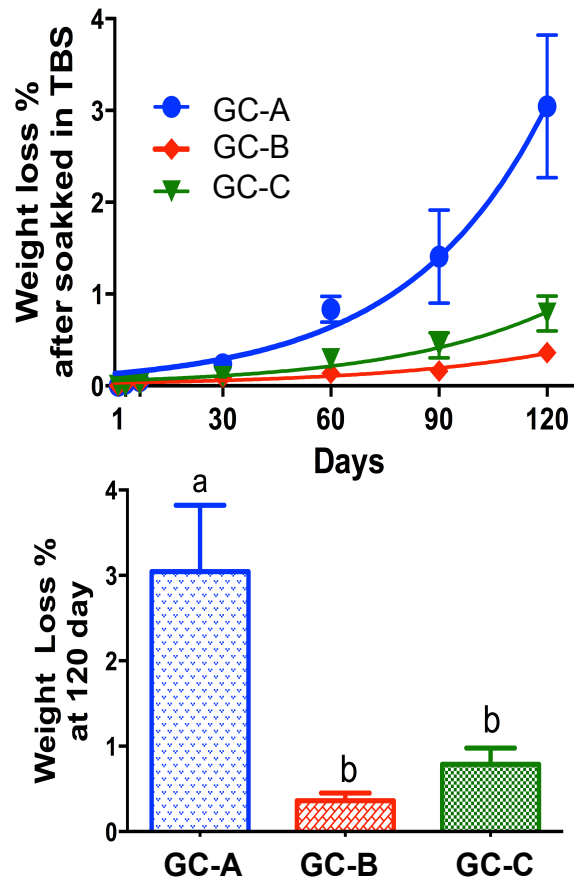


Figure 3-5: (A) Degradation test of the experimental GCs showing weight loss percentage of the GCs specimens after soaking in tris buffered solution from 1 day up to 120 days. Exponential growth equation was used to show nonlinear fit curve for the degradation rates at different timeline. **(B)** Weight loss percentages of the GC-A, GC-B and GC-C at 120 days time point soaking in tris buffered solution. GC-B showed the least weight loss percentage. Different letters represent significant statistical difference (Simple main effect analysis and Tukey's multiple comparisons test, $p < 0.05$). Data are mean values (SD), $n=3$.

3.4 DISCUSSION

The preparation of the precursor glass plays an important part in the properties of the manufactured GCs. In this study the glasses were synthesized by sol-gel chemistry, followed by spray drying and calcination, melting and quenching; all these steps improve the glass homogeneity and lead to good sintering characteristics of the resultant GCs.²⁴ The SEM images of the GCs confirmed the formation of dense acicular interlocking crystals that ascribed to wollastonite crystals. These blade-like crystals are thought to contribute to the strength and toughness of the GCs through blunting and crack seizing leading to the prevention of crack-propagation and achieve the high values of the fracture toughness.¹

The Young's modulus of elasticity (E) is of great importance for dental GCs, and it represents the stiffness of a material within the elastic range measurement of the stiffness biomaterials. A mismatch between the E for bone (4-20 GPa)^{25,26} and implant biomaterials could lead to stress shielding phenomenon.²⁷ The young's modulus of elasticity influences the ability of the implant to transmit stresses to the adjacent bone and sustains tissue vitality over time. The lower the Young's modulus of implant material, the better the load distribution to the surrounding tissue with the possible beneficial result of new bone formation.^{28,29} The E value of ~210 GPa for the commercial non-metallic dental implant "yttria-stabilized tetragonal zirconia"⁶ is similar to that of In-Ceram zirconia. These values are 10x higher than that of cortical bone tissue. The E value for the experimental wollastonite GCs (89-100 GPa) is half of that for zirconia dental material, but it still higher than that of bone tissue.

XRD data analysis revealed that all experimental GCs had wollastonite as the principal crystals along with different proportions of secondary crystalline phases. However, GC-B has cristobalite as additional crystalline phase, which is the stable form of silica (SiO_2). The formation of cristobalite in GC-B is due to the higher silica within its chemical composition.

One-piece dental implants should be chemically durable to withstand the aggressive oral environments e.g. diverse chemical fluids, broad range in pH and periodic high magnitude mechanical forces that may accelerate GC degradation by corrosion and surface wear.^{1,30} In this study, the chemical durability of the GCs was tested in 4 % AC (pH 2) for 16 h at 80 °C as well as in TBS (pH 7.4) up to 120 days at 37 °C to simulate the body conditions whether the material is exposed to the oral environments or implanted in bone and soft tissue. The chemical durability of GC-A and GC-C in AC was substantially higher than 100 $\mu\text{g}/\text{cm}^2$ but less than 2000 $\mu\text{g}/\text{cm}^2$. As a result, these GCs can be used as core materials but cannot be exposed to oral fluids.²¹ On the other hand; GC-B exhibited the least degradation rate (0.36% weight loss at 120 days soaking in the TBS) and the least wt/A (100 $\mu\text{g}/\text{cm}^2$) in AC. These results can be related to the cristobalite, which is the chemically stable crystalline phase.³¹ The wt/A of GC-B is comparable to that of YZ that is used for dental restoration and is considered to be a chemically stable dental material.² The wt/A and degradation rates of the three GCs were dissimilar because of the different initial chemical compositions (Table 3-1), which were reflected on the crystallization kinetics of the parent glasses and their mechanical and chemical properties.

In the current study, we tested the chemical stability of the GC in acidic environment and in balanced pH based on ISO 6872 (for dental ceramics) and ISO 10993-14 (Biological evaluation of medical devices). However, recent study revealed that basic pH buffer environment (pH of 10) resulted in a complete breakdown of the silica network of the dental ceramics.³² We plan to evaluate the chemical stability of the synthesized GC in basic solution in a future study.

The mechanical properties of the chemically tested GCs were re-measured to evaluate the effect of the degradation and dissolution on their mechanical behavior. E , H_0 and K_{IC} were assessed, but only the data of the K_{IC} were shown in this study for two reasons. First, the equation and the calculation of K_{IC} include both E and H_0 and hence any changes of these parameters will be reflected on K_{IC} .²⁰ Secondly, the K_{IC} is considered as an essential and starting point for the evaluation and selection of the biomaterials for clinical applications and it determines the aspects of brittle material mechanical behavior.¹² Interestingly, there was no significant difference between K_{IC} values for the original and chemically-tested specimens indicating that the mechanical behavior of the chemically-tested specimens were not affected in spite of the fact of different chemical degradation and wt/A of the GC samples. To our knowledge we are the first group who evaluated the K_{IC} of the GCs following chemical durability testing.

Boccaccini²³ proposed the brittleness index (BI) as a quantitative evaluation of machinability. The BI values of the wollastonite GCs were lower than $4.3 \mu\text{m}^{-0.5}$ indicating excellent machinability. These results were confirmed by cutting, milling and preparing GC specimens smoothly without developing cracks, Figure 3-6. Interlocking crystals contributed to the machinability of the materials by acting as barriers to suppress

crack propagation.³³ Machinable GC can be prepared by the CAD-CAM system that enables customization of implants for individual patients. Additionally, the upper part of the GC can be prepared inside patient's mouth to function as an abutment part and to receive the crown.

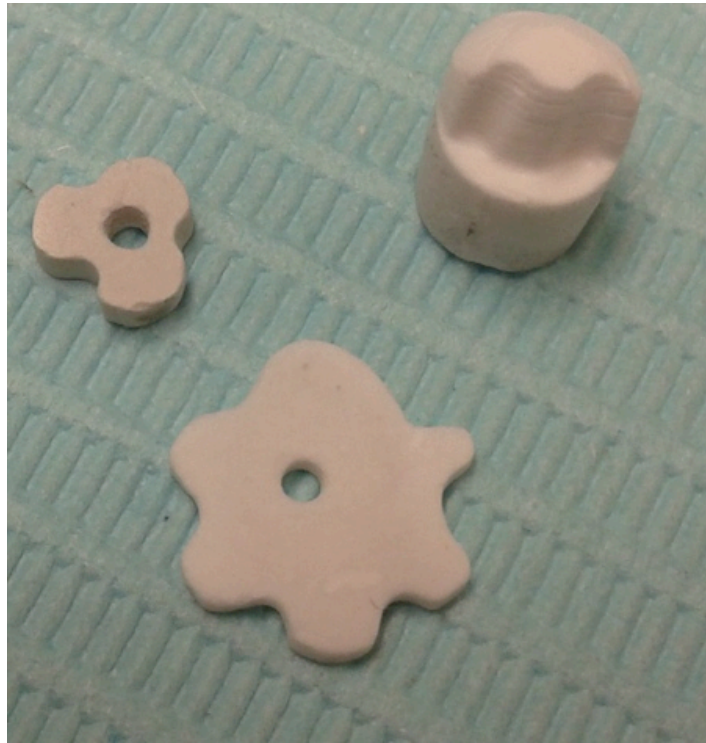


Figure 3-6: Representative image of machined GC-B specimens. Holes and grooves were cut on 1 mm thick disks and bevels with shoulder finish line were prepared on GC ingot. The preparation was going smooth without chipping or developing cracks.

3.5 CONCLUSIONS

High strength, chemically durable and machinable sintered GCs were prepared with different chemical compositions; the experimental GCs had different crystallization kinetics that affects the mechanical and chemical properties of the GCs. The wollastonite was the main crystalline phase with other secondary crystalline phases—hydroxyapatite ($\text{Ca}_5(\text{PO}_4)_3\text{OH}$) and Fluorite (CaF_2) for the three GCS. Yet, GC-B had an additional crystalline phase—cristobalite (SiO_2) that could be the main reason for showing an excellent chemical durability. Microstructures of GCs revealed acicular interlocking crystals that were responsible for the high K_{IC} and to the outstanding machinability. Machinable GC-B may be considered as a unique, convenient and propitious biomaterial for immediate non-metallic one-piece dental implant applications as alternative to the commercial dental implants.

3.6 REFERENCES

1. Höland W, Beall GH. Glass-Ceramic Technology. Westerville, USA: American Ceramic Society; 2002.
2. Hisbergues M, Vendeville S, Vendeville P. Zirconia: Established Facts and Perspectives for a Biomaterial in Dental Implantology. *J Biomed Mater Res.* 2009; 88 B (2): 519-29.
3. Wenz HJ, Bartsch J, Wolfart S, Kern M. Osseointegration and Clinical Success of Zirconia Dental Implants: A Systematic Review. *Int J Prosthodont.* 2008; 21 (1):27-36.
4. Chevalier J, Gremillard L, Deville S. Low-Temperature Degradation of Zirconia and Implications For Biomedical Implants. *Ann Rev Mater Res.* 2007;37:1-32.
5. Volpato CÂM, Garbelotto LGDA, Fredel M.C.and Bondioli F. Application of Zirconia in dentistry: Biological, Mechanical and Optical Considerations. In: Sikalidis C, editor. *Advances in Ceramics - Electric and Magnetic Ceramics, Bioceramics, Ceramics and Environment.* 1ST ed. Croatia: InTech; 2011. p. 397-420.
6. Piconi C, Maccauro G. Zirconia as a Ceramic Biomaterial. *Biomaterials.* 1999 1; 20 (1): 1-25.
7. Kokubo T. Bioactive Glass Ceramics: Properties and Applications. *Biomaterials.* 1991; 12 (2): 155-63.
8. Kokubo T, Kim H, Kawashita M. Novel Bioactive Materials with Different Mechanical Properties. *Biomaterials.* 2003 6;24 (13):2161-75.

9. Cannillo V, Colmenares-Angulo J, Lusvarghi L, Pierli F, Sampath S. In Vitro Characterisation of Plasma-Sprayed Apatite/Wollastonite Glass–Ceramic Biocoatings on Titanium Alloys. *J Eur Cera Soc* 2009; 29 (9):1665-77.
10. Zhang F, Chang J, Lin K, Lu J. Preparation, Mechanical Properties and In Vitro Degradability of Wollastonite/Tricalcium Phosphate Macroporous Scaffolds From Nanocomposite Powders. *J Mater Sci: Mater Med.* 2008;19 (1):167-73.
11. Zhu H, Shen J, Feng X, Zhang H, Guo Y, Chen J. Fabrication and Characterization of Bioactive Silk Fibroin/Wollastonite Composite Scaffolds. *Mater Sci Eng C.* 2010; 30 (1): 132-40.
12. Morena R, Lockwood PE, Fairhurst CW. Fracture Toughness of Commercial Dental Porcelains. *Dent Mater.* 1986; 2(2): 58-62.
13. Anusavice KJ, Zhang N. Chemical Durability of Dicor and Lithia-Based Glass-Ceramics. *Dent Mater* 1997; 13(1): 13-9.
14. Augis J, Bennett J. Calculation of the Avrami Parameters for Heterogeneous Solid State Reactions Using a Modification of the Kissinger Method. *J Therm Analysis.* 1978; 13(2):283-92.
15. Rizkalla AS, Jones DW, Clarke DB, Hall GC. Crystallization of Experimental Bioactive Glass Compositions. *J Biomed Mater Res.* 1996; 32 (1):119-24.
16. Fultz B, Howe JM. Diffraction and the X-ray Powder Diffractometer. In: *Transmission Electron Microscopy and Diffractometry of Materials.* 3rd ed. New York: Springer; 2008. p. 1-59.

17. Saadaldin SA, Dixon SJ, Costa DO, Rizkalla AS. Synthesis of Bioactive and Machinable Miserite Glass-Ceramics for Dental Implant Applications. *Dent Mater.* 2013; 29(6):645-55.
18. Schreiber E, Anderson O, Naohiro S. Elastic Constants and Their Measurement. New York: McGraw-Hill; 1973.
19. Rizkalla AS, Jones DW. Mechanical Properties of Commercial High Strength Ceramic Core Materials. *Dent Mater.* 2004;20(2):207-12.
20. Lankford J. Indentation Microfracture in the Palmqvist Crack Regime: Implications for Fracture Toughness Evaluation by the Indentation Method. *J Mater Sci Lett.* 1982;1(11):493-5.
21. International Standard. ISO 6782; Dentistry, Ceramic Materials. 2008.
22. International Standard. ISO 10993-14. Biological Evaluation of Medical Devices, Part 14; Identification and Quantification of Degradation Products From Ceramics. 2001.
23. Boccaccini AR. Machinability and Brittleness of Glass-Ceramics. *J Mater Process Tech.* 1997; 65(1):302-4.
24. Dorozhkin SV. Amorphous Calcium (Ortho) Phosphates. *Acta Biomater.* 2010; 6 (12):4457-75.
25. Park JB, Lakes RS. *Biomaterials: An introduction.* 3rd ed. New York; London: Springer; 2007.
26. Natali AN. *Dental Biomechanics.* London; New York: Taylor & Francis; 2003.

27. Pattanayak D, Rao B, Mohan T. Calcium Phosphate Bioceramics and Bioceramic Composites. *J Sol-Gel Sci Techn.* 2011; 59 (3):432-47.
28. O'Brien WJ. *Dental Materials and Their Selection.* 4th ed. Hanover Park, IL: Quintessence Pub. Co.; 2008.
29. Anusavice KJ. Degradability of Dental Ceramics. *Adv Dent Res.* 1992; 6 (1):82-9.
30. Şan O, Özgür C. Investigation of a High Stable β -Cristobalite Ceramic Powder from CaO–Al₂O₃–SiO₂ System. *J Eur Ceram Soc.* 2009 ;29(14):2945-9.
31. Esquivel-Upshaw JF, Dieng FY, Clark AE, Neal D, Anusavice KJ. Surface Degradation of Dental Ceramics as a Function of Environmental pH. *J Dent Res.* 2013;92(5):467-71.
32. Evan AG, Faber KT. Crack-Growth Resistance of Microcracking Brittle Materials. *J Am Ceram Soc.* 1984; 67(4):255-60.

CHAPTER 4

BIOACTIVITY AND BIOCOMPATIBILITY OF A NOVEL WOLLASTONITE GLASS-CERAMIC

This study was performed to further characterize the previously synthesized wollastonite GC. In this chapter, the bioactivity and biocompatibility of the wollastonite GC were evaluated and they were compared to those of In-Ceram yttria partially stabilized zirconia. The contents of this chapter have been submitted for publication.

4.1 INTRODUCTION

Zirconia dental implants were introduced as an alternative to titanium dental implants. In addition to fulfilling the patients' demand for a metal-free implant, zirconia dental implants overcome some aesthetic problems associated with titanium dental implants.¹ Zirconia implants exhibit unique and favorable physical, mechanical and optical properties, while also having excellent resistance to corrosion because of their chemical stability and bio-inertness.¹⁻⁵ Good biocompatibility of zirconia was attributed to biointegration, which "is the occurrence of continuity of ceramic implant to bone without intervening space at bone/implant interface",⁶ similar to the osseointegration obtained with titanium dental implants.^{4,6} Recently, various ceramic implant systems made of yttria-stabilized tetragonal zirconia polycrystals (Y-TZP) have become commercially available.^{5,7} However, adequate biological data on zirconia dental implants is not yet available due to the lack of long-term clinical studies.^{7,8}

The clinical usage of zirconia is limited for many reasons. First, machining and/or surface modifications of zirconia are difficult.^{5,9} Second, radioactive elements with long half-lives can accompany zirconia. The presence of segregated clusters of radionuclides could harm

the surrounding tissues.^{5,6,10} Third, Y-TZP is susceptible to aging through low-temperature degradation that compromises long-term clinical performance and increases the possibility of subsequent catastrophic implant failure.^{7,9}

Commercial dental implants (titanium and zirconia) are bioinert and lack bioactivity. Biomaterials researchers are interested in improving the bioactivity of implant materials through different techniques; the most common method is bioactive coatings that exhibit bone-bonding ability.¹¹⁻¹³ However, these coatings can de-bond at different locations on the implant surface or can undergo non-uniform degradation, which would impair osseointegration at the interface between the coated implant and bone.¹⁴ Another approach to improve bioactivity is to integrate HA as a composite within the implant material. As a result, the bioactivity and biocompatibility of the implant material is improved,¹⁵ but additional investigation is needed to evaluate the effect of the incorporated HA on the mechanical properties and clinical *in vivo* performance of these composite materials.⁹

Biocompatibility is the ability of a material to provide successful clinical service in a host without producing allergic or/and toxic reactions in the surrounding tissues or adverse systemic reactions.¹⁶ The biocompatibility of zirconia has been evaluated; the bone response of zirconia and the inflammation adjacent to zirconia have been shown to be satisfactory.² MCT3T-E1 osteoblastic cells displayed active cellular reactions on zirconia, including initial cell attachment, proliferation and differentiation.^{17,18} Other studies demonstrated that Y-TZP showed good attachment and proliferation of osteoblastic cells regardless of surface treatment or topography, with no signs of toxic or carcinogenic outcomes.¹⁹⁻²¹

Although commercial dental implants, both metallic and ceramic, have good clinical performance, both have the limitations of being non-bioactive and non-machinable.^{1,2} Our group has synthesized and characterized a novel WGC for one-piece dental implant applications (Saadaldin *et al*, accepted for publication, DEMA-D-13-00398R1) with the appropriate strength, chemical durability and machinability. In the current study, the bioactivity and biocompatibility of the WGC were evaluated and compared to In-Ceram yttria partially stabilized zirconia (YZ). WGC was found to be bioactive with biocompatibility comparable to that of YZ, making WGC a promising material for dental implant applications.

4.2 MATERIALS AND METHODS

4.2.1 Materials

The synthesis of a high strength, chemically durable and machinable WGC in the system ($\text{SiO}_2\text{-Al}_2\text{O}_3\text{-CaO-CaF}_2\text{-K}_2\text{O-B}_2\text{O}_3\text{-P}_2\text{O}_5\text{-CeO}_2\text{-Y}_2\text{O}_3$) and characterization of its mechanical and chemical properties were previously reported (Saadaldin *et al*, accepted for publication, DEMA-D-13-00398R1). In-Ceram yttrium partially stabilized zirconia (YZ, Zahnfabrik, Berlin, Germany) was used as a control.

4.2.2 Bioactivity

In vitro bioactivity of WGC and YZ was evaluated by soaking samples (11 mm x 1 mm) in simulated body fluid (SBF) under biomimetic conditions (37 °C, pH 7.24). The specimens were soaked for 1, 2 and 4 weeks in SBF that had inorganic ion concentrations similar to those of human blood plasma.²² SBF was refreshed every week. At the

scheduled time, the specimens were thoroughly rinsed, dried and then evaluated as described below.

4.2.2.1 Scanning Electron Microscopy (SEM) and Energy Dispersive X-ray Spectroscopy (EDX)

The surface layer of the WGC and YZ specimens was imaged before and after soaking in SBF using high resolution scanning electron microscopy (LEO 1540XB FIB/SEM Zeiss Nano Technology Systems Division, Germany) equipped with an EDX spectrometer. Prior to SEM and EDX assessment, all samples were coated with 3 nm osmium metal using a Filgen OPC 80T osmium plasma coater.

4.2.2.2 X-Ray Diffraction (XRD)

The formation of an apatite surface layer on the soaked specimens was assessed by XRD using a rotating anode X-ray diffractometer (Rotaflex RTP 300 RC, Rigaku Corp., Japan) operating on Co K α radiation at 45 kV and 160 mA. Spectra were collected in the 2θ range between 2° and 82° , with 0.05° steps and $10^\circ/\text{min}$ scan speed. 2θ for equivalent Cu K α radiation was calculated using Bragg's Law.²³

4.2.3 Biocompatibility

4.2.3.1 Osteoblast Attachment and Morphology

Newborn mouse calvaria-derived MC3T3-E1 Subclone 4 preosteoblastic cells were obtained from the American Type Culture Collection (ATCC, Manassas, VA, USA). MC3T3-E1 cells are similar to primary calvarial osteoblasts in their expression of Runx2, bone sialoprotein and osteocalcin, and their ability to form bone-like matrix *in vitro* and

in vivo.²⁴ WGC and YZ discs (11 mm x 1 mm) were cleaned and sterilized using an argon-based plasma cleaner PDC-32G (Harrick Plasma, Ithaca, NY, USA), placed in 24-well plates and then seeded with 5×10^3 cells/well. MC3T3-E1 cells were cultured in serum containing medium, as described elsewhere.²⁵ After 6 and 24 h incubation at 37 °C in a humidified atmosphere of 5%CO₂ in air, the cells were washed, fixed with 4% paraformaldehyde (PFA) in PBS, permeabilized with 0.1% Triton-X 100 in PBS for 5 min and then blocked using 3% bovine albumin (BSA) for 30 min. For visualization of vinculin and filamentous actin (F-actin), substrata were incubated with primary antibody against vinculin (1:100 in 3% BSA in PBS; Millipore, Billerica, MA, USA) for 1 h, rinsed three times with PBS and then incubated for 1.5 h with Alexa Fluor 488-conjugated goat anti-mouse IgG secondary antibody (1:200 dilution in 3% BSA in PBS; Life Technologies, Burlington, CA) and rhodamine-conjugated phalloidin (1:100 dilution in 3% BSA in PBS; Cytoskeleton Inc., Denver, CO, USA). To counterstain nuclei, Vectashield (Vector Laboratories, Burlingame CA) with 4', 6-diamidino-2-phenylindole dihydrochloride (DAPI) was used.

An Axio Observer Z.1 fluorescence microscope (Carl Zeiss, Jena, Germany) and AxioImager software was used to assess cell attachment, actin distribution and focal adhesion formation by capturing images from 10 randomly selected fields from each specimen. Cell attachment was analyzed by counting nuclei. The total number of focal adhesion per cell was measured by an impartial observer using ImageJ software (National Institutes of Health, USA). The average number of focal adhesions (based on vinculin labeling) was determined for 10 randomly selected cells on each sample. Three independent experiments were performed, each with triplicate specimens.

4.2.3.2 Cell Proliferation Assay

CyQuant[®] cell proliferation assay kit (Invitrogen, Burlington, CA) was used to assess the number of MC3T3-E1 osteoblastic cells on WGC and YZ discs at 1, 3, 5 and 7 days, according to the manufacturer's protocol.

4.2.3.3 Quantification of Alkaline Phosphatase Activity

Osteoblast differentiation was evaluated by monitoring alkaline phosphatase (ALP) activity. Rat calvarial osteoblasts (passage 2-3) were used for these experiments. Cells were generously provided by Dr. D.W. Hamilton (Schulich Dentistry, Western University). Cells were isolated from 0-5-day old neonatal Sprague Dawley rats according to a previously published protocol.²⁶ Animal procedures were approved by the University Council on Animal Care of Western University and were in agreement with the Canadian Council on Animal Care.

ALP was determined by measuring the cleavage of *p*-nitrophenyl phosphate (Sensolyte[®] *p*NPP colorimetric assay; ANASPEC, Fremont, CA, USA). Osteoblasts were incubated on WGC and YZ discs and cultured for 3 days in standard culture medium.²⁵ Afterwards, the medium was replaced by differentiation medium that consisted of standard culture medium supplemented with 50 µg/mL ascorbic acid and 2 mM β-glycerophosphate. Cells were incubated for an additional 1, 4 and 7 days, refreshing the medium every 2-3 days. At the scheduled times, the cell monolayer was washed and then lysed with lysis buffer containing 0.2% Triton X-100. The resulting suspension was sedimented at 2500 *g* for 10 min at 4°C, and the supernatant was collected and stored at -80 °C. Subsequently, 50 µL of each sample was mixed with 50 µL of *p*NPP solution on 96-well clear micro-

plate by gently shaking the plate for 30 sec, and incubated at 37 °C for 60 min. Reactions were terminated by adding 50 μ L of 0.05 M NaOH into each well and absorbance was read at 405 nm on a micro-plate reader (Tecan Safire, Morrisville, NC, USA). ALP activity was calculated according to a series of alkaline phosphatase standards. The protein concentration for each sample was calculated using BCATM protein assay kit (Thermo Scientific Pierce Biotechnology, Waltham, MA, USA), according to the manufacturer's instructions. ALP activity was normalized to total protein concentration and expressed as μ g *p*NP/h/ μ g total protein.

4.2.4 Statistical Analyses

Differences between two groups were evaluated by Student's *t*-tests. One-way analysis of variance (ANOVA) followed by Tukey's multiple comparisons test was used to evaluate differences among three or more groups. All statistical analyses were accepted as significant at $p < 0.05$. Data are expressed as means (SD) of three independent experiments ($n=3$), each with triplicate samples.

4.3 RESULTS

4.3.1 Bioactivity:

4.3.1.1 Scanning Electron Microscopy and Energy Dispersive X-Ray Spectroscopy

WGC and YZ displayed different behaviors when soaked in SBF. SEM revealed the surface features of WGC and YZ at 0 weeks before soaking in SBF (Figure 4-1). After 1 week soaking in SBF, WGC surface morphology changed with the precipitation of a partial thin coating. As the soaking time was increased, the formation of a uniform

surface layer with morphology similar to that of biomimetic HA^{27,28} was observed. The entire surface of the WGC was fully covered by that layer following 4 weeks of soaking. In contrast, no precipitate was observed on the YZ surfaces even after up to 4 weeks of soaking in SBF, indicating lack of bioactivity.

EDX elemental analysis spectra are shown in Figure 4-2. In the case of WGC, Ca and P peaks increased in intensity with the gradual reduction of the Si peak after soaking in SBF at the different time points. EDX analysis confirmed that the precipitate was Ca-P rich and that, at 4 weeks soaking time, Si was no longer detectable. To the contrary, there was no change in the EDX spectra of YZ for all the time points up to 4 weeks. The zirconium was the principal peak before and after soaking in SBF. Importantly, no phosphorus or calcium was detected, in spite of soaking in SBF up to 4 weeks, consistent with the SEM data.

4.3.1.2 X-Ray Diffraction

XRD patterns of WGC and YZ, before and after soaking in SBF, are shown in Figure 4-3. It can be observed that the XRD peaks associated with the starting material gradually diminished as soaking time was increased. After 4 weeks, only peaks attributable to carbonated HA were observed. The main peaks had 2θ values equal to 26° and 32° (Figure 4-3A), confirming the formation of an apatite layer.²⁹ In keeping with the SEM and EDX data, XRD did not reveal any carbonated HA on YZ surfaces at any time points (Figure 4-3B). Taken together, these findings establish that WGC supports the formation of a uniform, thick apatite layer in contrast to YZ, which is not bioactive.

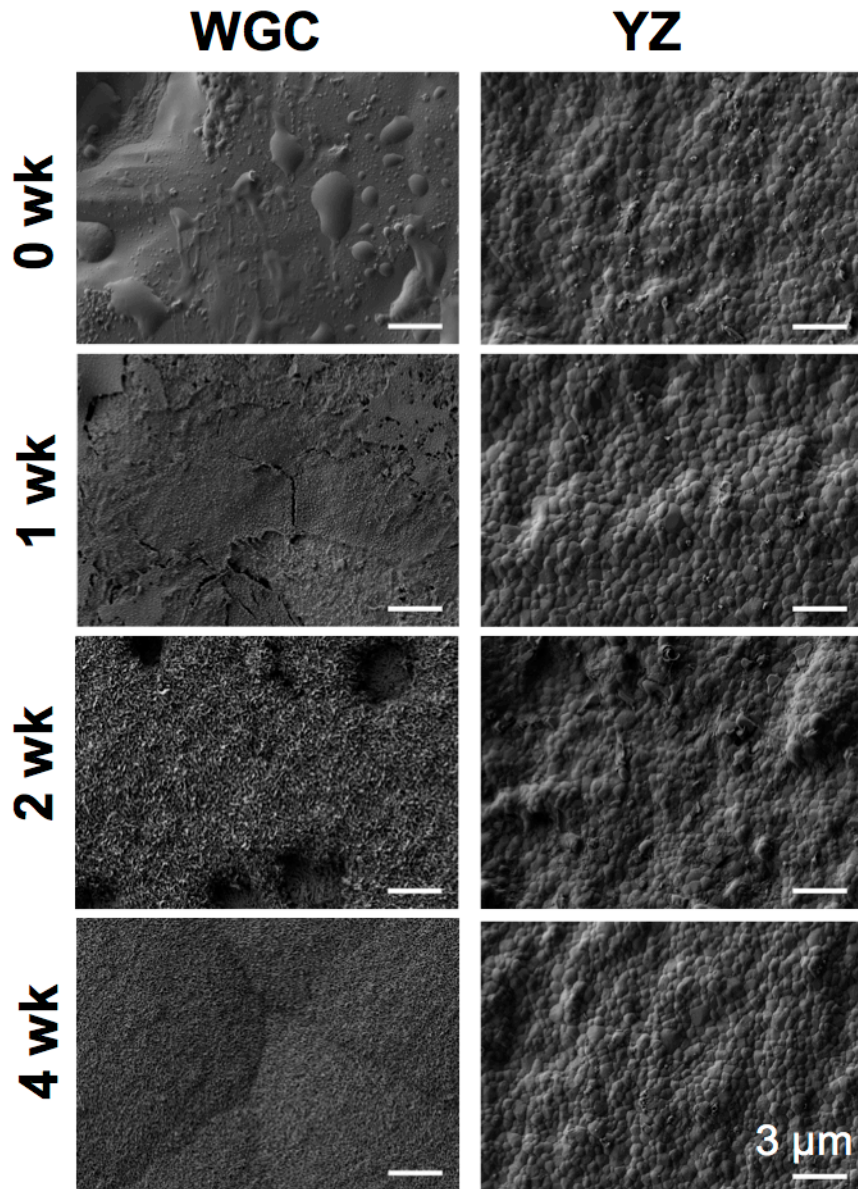


Figure 4-1: SEM images of wollastonite glass-ceramic (WGC) and In-Ceram yttria partially stabilized zirconia (YZ) before (0 week) and after (1, 2 and 4 weeks) soaking in simulated body fluid (SBF). SEM micrographs show the surface features of WGC and YZ before soaking in SBF (0 week), and the evolution of HA layer on the WGC surfaces (1, 2 and 4 weeks). There was no HA formed on YZ surfaces at any time. Scale bar = 3 μm in all panels.

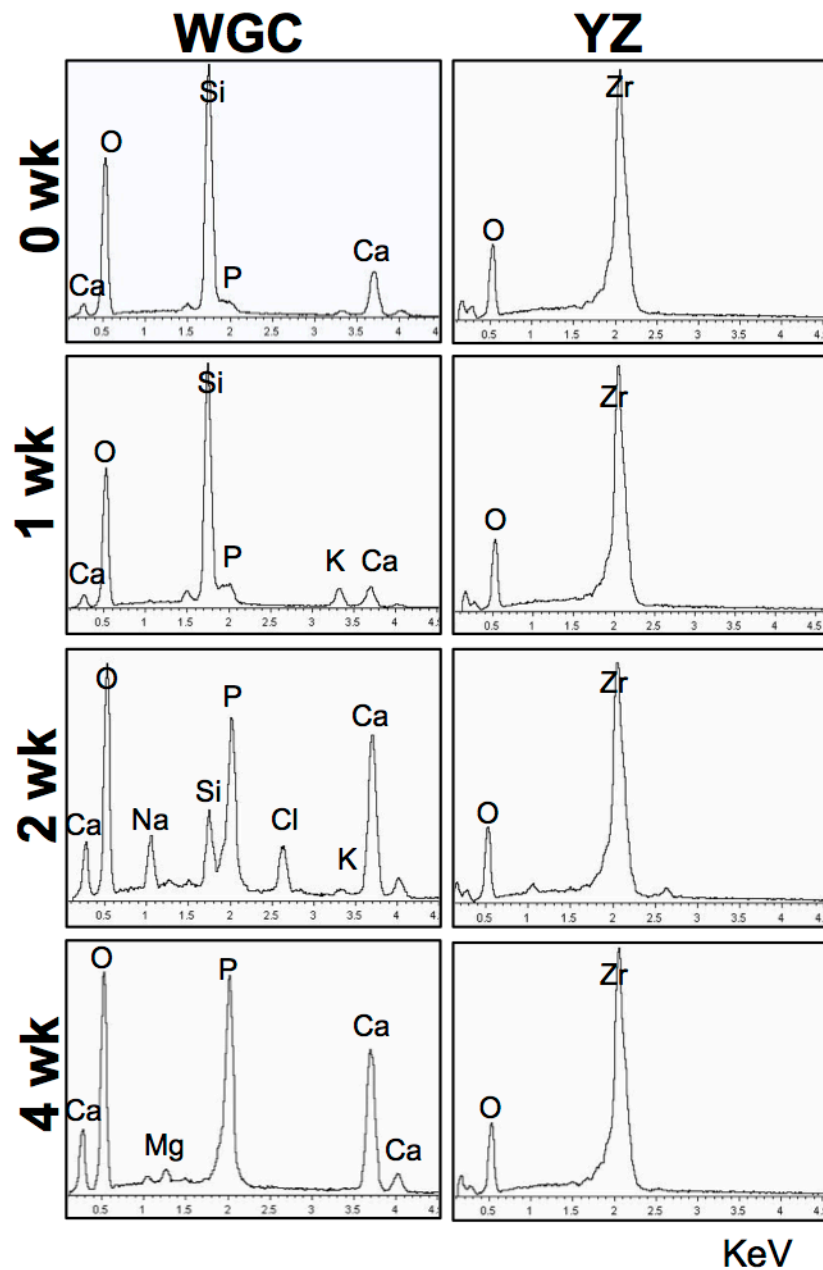


Figure 4-2: EDX spectra illustrating the elemental analysis of WGC and YZ surfaces after 0, 1, 2 and 4 weeks soaking in SBF. EDX spectra of WGC display the peaks of the main elements (Si, Ca, P) before and after soaking in SBF. YZ spectra indicate the lack of bioactivity by showing the same peak (Zr) at different time points. Spectra are representative of three different locations on the specimens' surfaces.

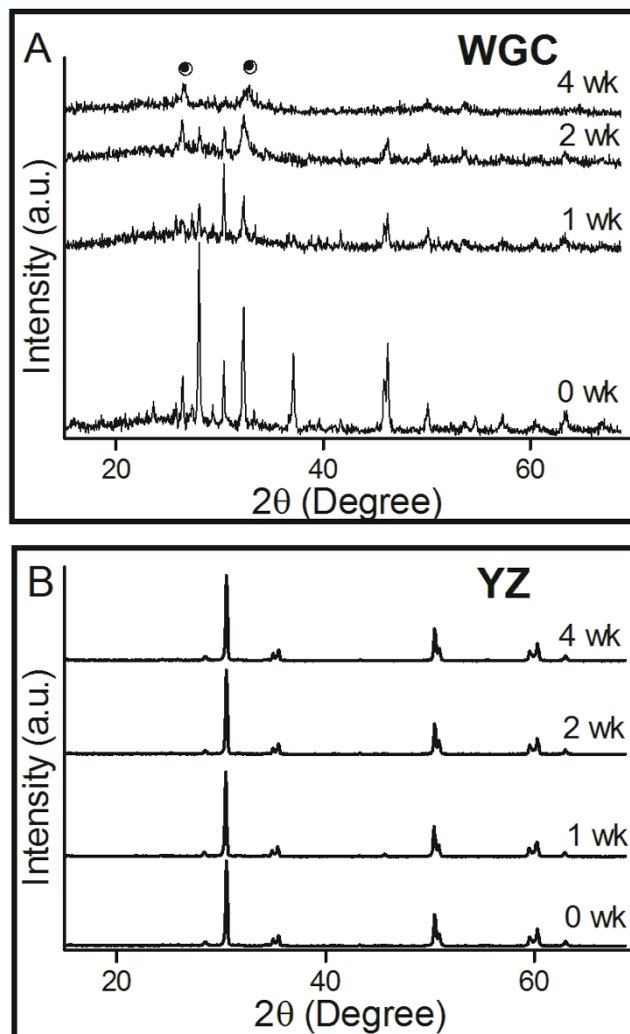


Figure 4-3: XRD pattern of WGC and YZ specimens before and after soaking in SBF. (A) XRD spectra of WGC confirmed the gradual formation of poorly crystalline HA surface layer. After 4 weeks, WGC is totally covered with HA layer, where XRD showed the spectrum of carbonated HA only (PDF # 19-272). The black circles above the spectra indicate the main peaks at 26° and 32°. (B) There were no changes in the XRD spectra of the YZ at the different time points.

4.3.2 Biocompatibility

4.3.2.1 Osteoblast Attachment and Morphology

To compare cell attachment and morphology on WGC and YZ surfaces, MC3T3-E1 osteoblast-like cells were cultured for 6 and 24 h. Fluorescence images indicated that cells attached and spread well on both substrata (Figure 4-4). After 6 h, cells had circular peripheries and there were no obvious stress fibers on either material (Figure 4-4B, D). However, after 24 h, the cells exhibited flattened polygonal morphology with multiple cytoplasmic extensions and highly organized actin stress fibers, consistent with extensive actin polymerization and adhesion to the substrata (Figure 4-4F,H).

Regarding cell attachment, there was no significant difference between the number of osteoblastic cells on WGC and YZ at either time point ($p>0.05$, Figure 4-5A). Focal adhesions were detected by immunofluorescence imaging of vinculin-labeled cells after 6 and 24 h of cell incubation (Figure 4-4). The focal adhesion counts on 10 randomly selected cells are displayed in Figure 4-5B. The number of the focal adhesion increased significantly from 6 to 24 h on WGC ($p<0.05$); however, there were no significant differences in the number of focal adhesions on WGC and YZ at either time.

4.3.2.2 Cell Proliferation Assay

The ability of WGC and YZ to support osteoblast proliferation was investigated using the CyQuant[®] cell proliferation assay. Cells were cultured for 1-7 days on both surfaces and the number of cells on each material was plotted (Figure 4-6A). Cells proliferated on

WGC and YZ and, by day 7, there was significantly higher cells count on both surfaces ($p < 0.05$).

4.3.2.3 Alkaline Phosphatase activity (ALP)

ALP is a classical marker associated with the early stages of osteoblast differentiation and it plays a critical role in promoting mineralization of the extracellular matrix.^{30,31} Calvarial cells were cultured on WGC and YZ discs in medium supplemented with ascorbic acid and β -glycerophosphate to induce osteoblastic differentiation. ALP activity was measured and normalized to the amount of protein per sample (Figure 4-6B). On both substrata, ALP activity increased with time. At day 7, the ALP activity was 2.4 fold higher than at day 1 for WGC and 1.5 fold for YZ. However, there was no significant difference between the ALP activity of cells on WGC and YZ at any time point ($p > 0.05$).

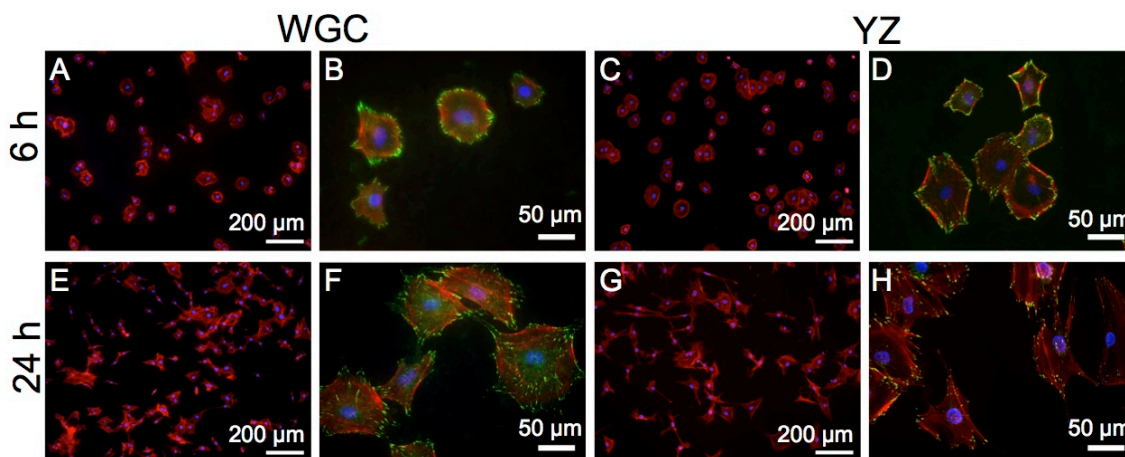


Figure 4-4: Representative fluorescence images of MC3T-E1 cell attachment, morphology spreading and focal adhesions on WGC and YZ substrata after 6 and 24 h of incubation. Images were captured at low (A, C, E and G) and high (B, D, F and H) magnifications. The nuclei were stained with DAPI (blue), F-actin with rhodamine phalloidin (red) and focal adhesions with vinculin (green).

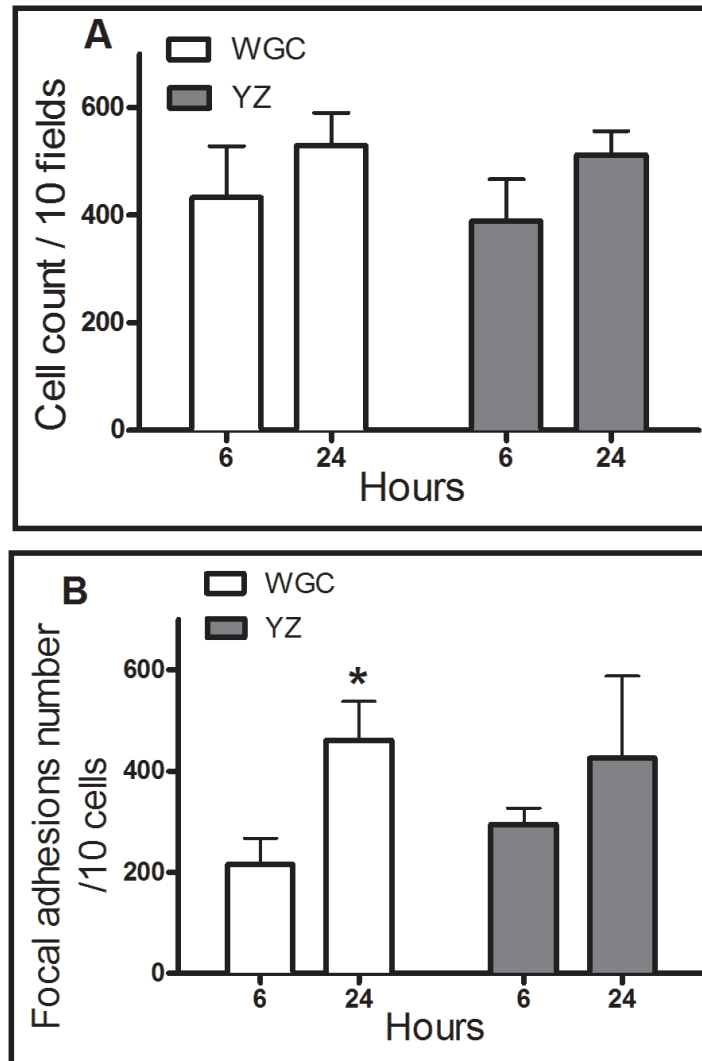


Figure 4-5: MC3T3-E1 cell count (A) and focal adhesion count (B) on WGC and YZ specimens after 6 and 24 h of incubation. There was no significant difference between cell count on both materials after 6 or 24 h incubation. On the other hand, focal adhesion count increased significantly on WGC after 24 h of incubation. The data are means (SD) of 9 samples from 3 independent experiments ($n=3$). *Indicates significant effect of time, analyzed by Student's *t*-test ($p<0.05$).

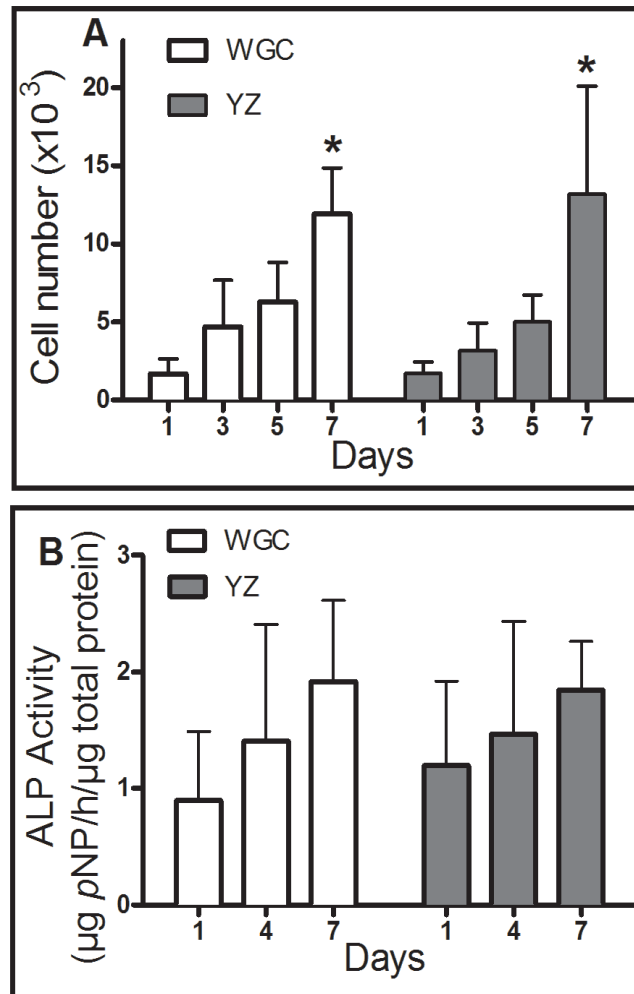


Figure 4-6: (A) MC3T3-E1 cell proliferation on WGC and YZ. CyQuant® fluorescence proliferation assay was used to quantify cell number up to 7 days. Data are means (SD), $n=3$. * Indicates that cell number at day 7 was significantly higher than that at day 1, 3, and 5 for both materials ($p<0.05$) based on ANOVA and Tukey's multiple comparisons test. (B) Calvarial osteoblasts were cultured on WGC and YZ specimens for 1, 4 and 7 days. Alkaline phosphatase activity was measured and normalized to total protein. Data are means (SD), $n=3$. There was no significant difference in ALP activity between materials at any time point (ANOVA and Tukey's multiple comparisons test, $p>0.05$).

4.4 DISCUSSION

Formation of bone-like apatite is an essential requirement for the bioactivity of materials. The first step for predicting in vivo bioactivity of a new material is soaking the material in SBF and evaluating the formation of apatite layer on its surface.²² In the present study, SEM, EDX and XRD analyses revealed the bioactivity of WGC and confirmed that YZ is not bioactive. A bioactive material creates an interface with the surrounding bone and promotes a long functional life of the dental implant.³²

Bioactivity mechanisms have been discussed thoroughly in the literature.³³⁻³⁵ It starts with apatite nuclei formation on the surface of the biomaterial that later grow over the entire surface by consuming calcium and phosphate ions from the SBF. Carbonate anions are later incorporated within the formed apatite, leading to formation of carbonated HA.^{22,33,35} In the present study, the WGC starting material showed various peaks attributed to the crystalline phases of WGC. In spite of the presence of apatite as a secondary crystalline phase in WGC (Saadaldin *et al*, accepted for publication, DEMA-D-13-00398R1), its bioactivity was ascribed to an apatite layer that formed on its surface after soaking in SBF. After soaking in SBF for increasing times, WGC peaks decreased in intensity until they totally disappeared at 4 weeks and were replaced with broad diffraction peaks of carbonated HA. These new broadened peaks indicate formation of a poorly crystalline structure, similar to bone apatite.³⁶ Kokubo³⁴ developed an apatite-wollastonite GC in an MgO-CaO-SiO₂-P₂O₅ glass system. This GC showed bioactivity with satisfactory mechanical properties. Kokubo established that, with bioactive materials, osteoblasts proliferate on formed apatite surfaces in preference to other cells. Consequently, the

surrounding bone comes into direct contact with the GC without intervention of fibrous tissue, establishing a strong chemical bond between the formed apatite and the bone apatite.^{34,37} Another study confirmed that bioactive GC could initiate biomineralization in osteoblast cultures, leading to a direct bond between the formed apatite layer on the bioactive GC and the mineralized extracellular matrix.³⁸ All these studies revealed the excellent osteoconductivity of HA layer.

Cell cultures provide an important tool to determine in vitro biocompatibility of biomaterials. Moreover, osteoblast attachment on the implant surface is a key factor for successful osseointegration to occur. We focused on the initial cell-implant interactions including attachment, focal adhesion formation, proliferation and ALP activity. We compared the behavior of WGC to that of a positive control YZ, which exhibits excellent biocompatibility, comparable to commercially used titanium dental implants.^{1,4,7,18,20,39,40} In the present study, cells exhibited favorable morphological features on WGC and YZ, indicating that WGC is comparable in its biocompatibility to YZ.

The formation of focal adhesions is considered to be one of the early steps essential for subsequent cell migration, proliferation and differentiation before formation of bone tissue.¹⁹ On both WGC and YZ, osteoblasts exhibited focal adhesions indicating that extracellular matrix proteins, membrane proteins and cytoskeletal proteins interacted together effectively.⁴¹ After 24 h, the focal adhesion number on WGC surfaces increased significantly compared to the number after 6 h, consistent with a positive enduring interaction between the cells and the substratum.⁴²

Both WGC and YZ supported cell proliferation. Various osteoblastic cells have been used previously to study proliferation kinetics on zirconia and apatite wollastonite composite glass ceramic materials. MC3T3-E1 and CAL-72 cell lines proliferated significantly on zirconia surfaces.^{18,41} Similarly, human osteoblasts proliferated and formed dense cell layers on zirconia surfaces.^{19,39} Also, apatite-wollastonite composite glass ceramic supported the proliferation of Saos-2 osteoblast-like cells.³⁹

Osteogenesis through osteoblast differentiation and extracellular matrix formation is required for subsequent implant osseointegration. In the current study, primary calvaria cells were used to evaluate ALP activity levels on WGC and YZ substrata. Primary cells were selected instead of the MC3T3-E1 cell line because most cell lines do not demonstrate a complete pattern of in vitro differentiation.²¹ ALP activity was maintained in osteoblasts on both materials at comparable levels. Similarly, previous studies have shown that zirconia surfaces, regardless of their roughness or topography, supported ALP expression by osteoblastic cells.^{18,43,44}

Overall, WGC and YZ had comparable interactions with cells. This can be attributed to two reasons. First, topography of material plays a critical role in cell-implant interaction^{26,41,45} and both WGC and YZ had relatively smooth surfaces due to the sintering process. Second, both of these materials are chemically durable; YZ was proved to be bioinert³ and WGC was found to be chemically durable (Saadaldin *et al*, accepted for publication, DEMA-D-13-00398R1). The possible toxicity of WGC and YZ is believed to be negligible because of their excellent chemical durability and insignificant degradation and dissolution rates. Further in vitro and in vivo studies will be required to

understand the effects of WGC on gene expression and to elucidate the interaction between oral tissues and the WGC implant material.

4.5 CONCLUSIONS

We established that WGC is bioactive and forms a complete apatite layer on its surface within 4 weeks in SBF. In vitro biocompatibility tests showed that WGC supported osteoblast attachment, focal adhesion formation, cell proliferation and ALP activity. The biocompatibility of WGC was comparable to that of the positive control, In-Ceram yttria partially stabilized zirconia. We have previously shown that WGC has chemical and mechanical properties – including machinability – suitable for the fabrication of one-piece dental implants (Saadaldin *et al*, accepted for publication, DEMA-D-13-00398R1), The results of the present study establish that WGC is bioactive and biocompatible and, thus, a promising material for non-metallic dental implants applications.

4.6 REFERENCES

1. Özkurt Z, Kazazoglu E. Zirconia Dental Implants: A Literature Review. *J Oral Implant.* 2011;37(3):367-76.
2. Anusavice KJ, Phillips RW, Shen C, Rawls HR. *Phillips' Science of Dental Materials.* 12th ed. St. Louis, Mo.: Elsevier/Saunders; 2013.
3. Hisbergues M, Vendeville S, Vendeville P. Zirconia: Established Facts and Perspectives For a Biomaterial in Dental Implantology. *J Biomed Mater Res.* 2009;88B(2):519-29.
4. Özkurt Z, Kazazoglu E. Clinical Success of Zirconia in Dental Applications. *J Prosthodont.* 2010;19(1):64-8.
5. Piconi C, Maccauro G. Zirconia as a Ceramic Biomaterial. *Biomaterials.* 1999 1;20(1):1-25.
6. Powers JM, Wataha JC. *Dental Materials: Properties and Manipulation.* 10th ed. St. Louis, Mo.: Mosby/Elsevier; 2013.
7. Wenz HJ, Bartsch J, Wolfart S, Kern M. Osseointegration and Clinical Success of Zirconia Dental Implants: A Systematic Review. *Int J Prosthodont.* 2008;21(1):27-36.
8. Kohal R, Att W, Bächle M, Butz F. Ceramic Abutments and Ceramic Oral Implants. An Update. *Periodontology 2000.* 2008;47(1):224-43.
9. Denry I, Holloway JA. Ceramics for Dental Applications: A Review. *Materials (1996-1944).* 2010 03;3(1):351-68.

10. Volpato CÂM, Garbelotto LGDA, Fredel M.C.and Bondioli F. Application of Zirconia in Dentistry: Biological, Mechanical and Optical Considerations. In: Sikalidis C, editor. *Advances in Ceramics–Electric and Magnetic Ceramics, Bioceramics, Ceramics and Environment*. First ed. Croatia: InTech; 2011. p. 397-420.
11. Dorozhkin SV. Amorphous Calcium (Ortho) Phosphates. *Acta Biomater*. 2010;6(12):4457-75.
12. Gross KA, Berndt CC. Biomedical Application of Apatites. *Rev Mineral Geochem*. 2002;48(1):631-72.
13. Cannillo V, Colmenares-Angulo J, Lusvarghi L, Pierli F, Sampath S. In Vitro Characterisation of Plasma-Sprayed Apatite/Wollastonite Glass–Ceramic Biocoatings on Titanium Alloys. *J Eur Ceram Soc*. 2009 ;29(9):1665-77.
14. Jayaswal GP, Dange SP, Khalikar AN. Bioceramic in Dental Implants: A Review. *J Ind Pros Society*. 2010;10(1):8-12.
15. Kong Y, Bae C, Lee S, Kim H, Kim H. Improvement in Biocompatibility of ZrO₂-Al₂O₃ Nano-Composite by Addition of HA. *Biomaterials*. 2005;26(5):509-17.
16. O'Brien WJ. *Dental Materials and Their Selection*. 4th ed. Hanover Park, IL: Quintessence Pub. Co.; 2008.
17. Ito H, Sasaki H, Saito K, Honma S, Yajima Y, Yoshinari M. Response of Osteoblast-Like Cells to Zirconia With Different Surface Topography. *Dent Mater J*. 2013.;32(1):122-9.

18. Lee D, Han J, Yang J, Lee J, Kim D. MC3T3-E1 Cell Response to Pure Titanium, Zirconia and Nano-Hydroxyapatite. *Int J Mod Phys B*. 2009;23(6-7):1535-40.
19. Josset Y, Oum'Hamed Z, Zarrinpour A, Lorenzato M, Adnet JJ, Laurent-Maquin D. In Vitro Reactions of Human Osteoblasts in Culture With Zirconia and Alumina Ceramics. *J Biomed Mater Res*. 1999;47(4):481-93.
20. Liu Y, Lee T, Lui T. Enhanced Osteoblastic Cell Response on Zirconia by Bio-Inspired Surface Modification. *Colloids and Surfaces B: Biointerfaces*. 2013;106(0):37-45.
21. Meyer U, Büchter A, Wiesmann H, Joos U, Jones D. Basic Reactions of Osteoblasts on Structured Material Surfaces. *Eur Cell Mater*. 2005;26(39):49.
22. Kokubo T, Takadama H. How Useful is SBF in Predicting In Vivo Bone Bioactivity? *Biomaterials*. 2006;27(15):2907-15.
23. Fultz B, Howe JM. Diffraction and the X-Ray Powder Diffractometer. In: *Transmission Electron Microscopy and Diffractometry of Materials*. 3th ed. New York: Springer; 2008. p. 1-59.
24. Smith KE, Hyzy SL, Sunwoo M, Gall KA, Schwartz Z, Boyan BD. The Dependence of MG63 Osteoblast Responses to Methacrylate-Based Networks on Chemical structure and Stiffness. *Biomaterials*. 2010;31(24):6131-4.
25. Saadaldin SA, Dixon SJ, Costa DO, Rizkalla AS. Synthesis of Bioactive and mMachinable Miserite Glass-Ceramics for Dental Implant Applications. *Dent Mater*. 2013; 29(6):645-55.

26. Costa DO, Prowse PDH, Chrones T, Sims SM, Hamilton DW, Rizkalla AS, *et al.* The Differential Regulation of Osteoblast and Osteoclast Activity by Surface topography of Hydroxyapatite Coatings. *Biomaterials*. 2013 10;34(30):7215-26.
27. LeGeros RZ. *Calcium Phosphates in Oral Biology and Medicine*. Basel; New York: Karger; 1991.
28. Costa DO, Allo BA, Klassen R, Hutter JL, Dixon SJ, Rizkalla AS. Control of Surface Topography in Biomimetic Calcium Phosphate Coatings. *Langmuir*. 2012;28(8):3871-80.
29. Joint Committee on Powder Diffraction Standards, American Society for Testing and Materials. *Selected Powder Diffraction Data for Minerals*. 1st ed. Swarthmore, Pa; 1974.
30. Aubin JE, Liu F, Malaval L, Gupta AK. Osteoblast and Chondroblast Differentiation. *Bone*. 1995;17(S1):S77-83.
31. Yadav M, Simão A, Narisawa S, Huesa C, McKee M, Farquharson C, *et al.* Loss of Skeletal Mineralization by the Simultaneous Ablation of PHOSPHO1 and Alkaline Phosphatase Function: A Unified Model of the Mechanisms of Initiation of Skeletal Calcification. *J Bone Miner Res*. 2011;26(2):286-97.
32. Ducheyne P, Ei-Ghannam A, Shapiro I. Effect of Bioactive Glass Templates on Osteoblast Proliferation and In Vitro Synthesis of Bone-Like Tissue. *J Cell Biochem*. 1994;56(2):162-7.
33. Kokubo T. Apatite Formation on Surfaces of Ceramics, Metals and Polymers in Body Environment. *Acta Materialia*. 1998;46(7):2519-27.

34. Kokubo T. Bioactive Glass Ceramics: Properties and Applications. *Biomaterials*. 1991;12(2):155-63.
35. Hench L. Bioceramics-From Concept to Clinic. *J Am Ceram Soc*. 1993;74(7):1487-510.
36. Li P, Ohtsuki C, Kokubo T, Nakanishi K, Soga N, Nakamura T, *et al*. Process of Formation of Bone-Like Apatite Layer on Silica Gel. *J Mater Sci: Mater Med*. 1993;4(2):127-31.
37. Kokubo T, Kim H, Kawashita M. Novel Bioactive Materials With Different Mechanical Properties. *Biomaterials*. 2003 6;24(13):2161-75.
38. Sautier J, Kokubo T, Ohtsuki T, Nefussi J, Boulekbache H, Oboeuf M, *et al*. Bioactive Glass-Ceramic Containing Crystalline Apatite and Wollastonite Initiates Biomineralization in Bone Cell Cultures. *Calcif Tissue Int*. 1994;55(6):458-66.
39. Möller B, Terheyden H, Açil Y, Purcz NM, Hertrampf K, Tabakov A, *et al*. A Comparison of Biocompatibility and Osseointegration of Ceramic and Titanium Implants: An In Vivo and In Vitro Study. *Int J Oral Maxillofac Surg*. 2012 5;41(5):638-45.
40. Popescu S, Popescu F, Burlibasa L. In Vitro Biocompatibility of Zirconia. *Metal Int*. 2010;15(4):14-25.
41. Bächle M, Butz F, Hübner U, Bakaliniš E, Kohal RJ. Behavior of CAL72 Osteoblast-Like Cells Cultured on Zirconia Ceramics With Different Surface Topographies. *Clin Oral Implants Res*. 2007;18(1):53-9.

42. Burridge K, Chrzanowska-Wodnicka M. Focal Adhesions, Contractility, and Signaling. *Annu Rev Cell Dev Biol.* 1996;12(1):463-519.
43. Aboushelib MN, Osman E, Jansen I, Everts V, Feilzer AJ. Influence of a Nanoporous Zirconia Implant Surface of on Cell Viability of Human Osteoblasts. *J Prosthodont.* 2013;22(3):190-5.
44. Hempel U, Hefti T, Kalbacova M, Wolf-Brandstetter C, Dieter P, Schlottig F. Response of Osteoblast-Like SAOS-2 Cells to Zirconia Ceramics With Different Surface Topographies. *Clinic Oral Implants Res.* 2010;21(2):174-81.
45. Le Guehennec L, Lopez-Heredia MA, Enkel B, Weiss P, Amouriq Y, Layrolle P. Osteoblastic Cell Behavior on Different Titanium Implant surfaces. *Acta Biomater.* 2008;4(3):535-43.

CHAPTER 5

GENERAL DISCUSSION

This chapter provides an overall summary of the important findings, their significance and general conclusions of the work. The limitations and future directions are presented.

Despite substantial gains in the discovery of new materials for dental applications in recent years¹ there is an ongoing search for dental implant materials to satisfy combined properties such as superior mechanical properties, biocompatibility, bioactivity, machinability, handling properties and cost. The main goal of this work was to develop GCs with suitable mechanical and biological properties for non-metallic one-piece dental implant applications. An implant can be the treatment of choice when natural teeth are lost and the masticatory function is diminished. Prevalence of partial and complete tooth loss is increasing among the population of different ages² due to many reasons:

1. Epidemic of dental caries and periodontal disease in modern societies.³
2. Traumatic dental injuries, as a result of various contributing factors (malocclusion, teeth grinding and clenching), physical trauma (motor vehicle accidents, fighting and sports injuries), in addition to inappropriate usage of teeth and oral piercing.⁴
3. Increased life expectancy and associated increase in older population, especially.⁵
4. Congenital missing teeth and other diseases, such as cancer.⁶

Patients have high expectations regarding the esthetics and biocompatibility of their dental restorations. Advanced ceramic materials such as zirconia and glass-ceramics (GC) have great potential as substitutes for metallic biomaterials. (GCs) have been used to fabricate different restorations including veneers, inlays, onlays, crowns and bridges.

GCs have become one of main interests for dental researchers to improve their esthetic outcomes and mechanical properties. GCs properties are determined largely by the number of the crystals formed from the base glass, their growth rate and size. To ensure superior mechanical performance the GCs, crystals should be numerous and uniformly distributed throughout the remaining glassy phase.⁷

To the best of our knowledge, we were the first group that synthesized precursor glasses by combining wet chemistry and spray drying (*Chapters 2 and 3*) to synthesize miserite and wollastonite GCs. Silicon alkoxides were hydrolyzed in an aqueous solution of metallic salts, the resulting sol was spray dried to produce multicomponent powder followed by calcination, melting, and quenching to obtain transparent glass frits. Spray drying is a well-established technique and a widely used industrial process that uses the aerosol phase to produce homogenous,⁸ highly reactive, and easily sintered glass powder.⁹ Sol-gel chemistry improved synthetic methods of the glasses by lowering the melting temperatures leading to better material properties.¹⁰

Pinckney *et al*¹¹ synthesized precursor glasses (to produce miserite GCs) using a conventional method: mixing batch components, ball-milling and then melting the powder at 1475-1500 °C. This method leads to fluorine loss from the melt; the amount of loss is varied and is associated with the difference in melting conditions.¹² It was

disclosed that the fluorine content in precursor glasses plays a significant role in improving the sintering and mechanical properties of GCs.^{13,14} In the current study, the sol-gel chemistry process lead to a lower melting temperature (1250 °C) of the glasses (*Chapter 2*) and kept the intended fluorine content. Differential thermal analysis (DTA) data was used to determine the ceramming temperature to produce the GCs. Different heat treatment schedules were used to study its effect on the microstructure and crystalline phases of the resultant GCs.

X-ray diffraction (XRD) of the GCs showed multi crystalline phases, including calcium fluoride silicate, xonotolite, hydroxyapatite and miserite. The GC that was produced by subjecting the glass to heat treatment up to 1000 °C exhibited miserite as the main crystalline phase and it was identified as GC4 in the study. GC4 exhibited a microstructure of tightly interlocking crystals that contributed to its toughness and strength and it is similar to that of miserite GC synthesized in a previous study.¹¹ In spite of having the same microstructure and the same main crystalline phase (miserite), their fracture toughness (K_{IC}) values were dissimilar. The K_{IC} of GC4 ($4.77 \pm 0.27 \text{ MPa}\cdot\text{m}^{0.5}$) is notably higher compared to the K_{IC} values reported by Pinckney *et al*¹¹ ($>3.5 \text{ MPa}\cdot\text{m}^{0.5}$). The dissimilarity of their K_{IC} can be attributed to the synthesis process of the parent glass that affected the mechanical properties of the resultant GCs.

Young's modulus (E) is an important mechanical property of implant materials that affects its osseointegration and compatibility with adjacent bone.¹⁵ In addition, E also contributes to the preservation of the vitality of the surrounding bone¹⁶ through effective transfer of forces to adjacent bone. The E values of the current dental implants such as titanium (100-116 GPa)¹⁷ and zirconia (200-210 GPa)¹⁸ were drastically higher than that

of human bone, which can range from 0.61 GPa to 17 GPa.^{17,19,20} GC4 has an E value of 96 ± 2.54 GPa, that is notably lower than that of titanium or zirconia, yet a long way from an ideal match to that of the human bone.

GC4 specimens (Chapter 2) exhibited excellent machinability; they were milled and machined using conventional drilling tools, indicating the possibility of introducing GC4 to CAD-CAM systems. The random interlocking microstructure of different GC crystals acts as a barrier against catastrophic crack propagation.²¹ The degree of the interlocking of the GC crystals will determine the ease of its machinability.²² Studies showed that some machinable materials could suffer from chipping defects, surface flaws, and microcracks, which reduce their mechanical strength and lifetime.²³ GC4 was milled and drilled to prepare different shapes such as marginal finish lines (shoulder, chamfer), grooves, holes and bevels without chipping or developing microcracks. The excellent machinability of GC4 was assessed quantitatively by calculating the brittleness index (BI). Boccaccini²⁴ proposed BI as a parameter for evaluating the machinability of brittle materials like glass and GCs, by combining both K_{IC} and the hardness values to evaluate the deformation and micro fracture phenomena responses of the materials. GC4 had a BI value of $1.11 \pm 0.05 \mu\text{m}^{-0.5}$ indicating excellent machinability.

Current dental implant materials, titanium and zirconia, have particular properties for direct functionability as implant materials, but they lack important features like osteogenic and osteoconductive capacity²⁵ or bioactivity.²⁶ Even though different mechanical and chemical modifications were applied to improve these qualities, and to prevent inflammatory reactions that could lead to fibrous encapsulation of the implant,

osteoconductive and bioactivity are still considered critical issues in any implant treatment.²⁵

GC4 specimens exhibited bioactivity; a successful deposition of continuous and compact HA layer was detected using XRD, EDX and SEM, after soaking in SBF for 4 weeks. The microstructure and chemical composition of the HA layer was similar to the mineral phase in bone; this result was in agreement with the outcome of bioactivity testing of other biomaterials.²⁷⁻³⁰ Formation of HA on the implant surfaces leads to direct bonding to living tissues without the formation of fibrous tissue that hinders the osseointegration.^{29,31} Alemany *et al*²⁹ disclosed the effect of the GC synthesis method and the microstructure on bioactivity; GC that was obtained by ceramming a glass that prepared by the sol-gel method formed HA layer sooner than that synthesized by the conventional method, although both of them exhibited bioactivity.

Implant biomaterials have to be biocompatible to surrounding cells and tissues, to prevent inflammation and osteolysis that occur as a result of toxic or corrosion products, and to promote osseointegration and mechanical stability.²⁶ It was shown in the current study that osteoblast-like cells attached, spread and proliferated on GC4 in a comparable level to biocompatible titanium materials,³²⁻³⁴ indicating its biocompatibility and the absence of toxic effects on cells. In spite of the favorable mechanical and biological properties of GC4, preliminary results of chemical stability were less promising (Appendix B). As a result, we were motivated to modify the composition of the GC to improve the chemical durability and to preserve its mechanical and biological properties.

In *Chapter 3* (Synthesis and characterization of wollastonite glass-ceramics for dental implant applications), three precursor glasses were synthesized following the same procedure executed in *Chapter 2*. Glass melting experiments were performed to prepare the glasses with the lowest melting temperature to prevent the loss of fluorine and to avoid uncontrolled crystallization. DTA was used to determine the crystallization kinetics of the GCs.

XRD of the GC specimens revealed that wollastonite was the main crystalline phase of all GCs accompanied with other secondary phases (hydroxyapatite and fluorite). One GC had cristobalite as an additional phase and was identified as WGC. Scanning electron microscopy (SEM) of the GCs showed dense acicular interlocking crystals. The K_{IC} of WGC was significantly higher ($p < 0.05$) than other GCs ($4.91 \pm 0.26 \text{ MPa}\cdot\text{m}^{0.5}$). All GCs exhibited excellent machinability. Young's modulus of WGC was $90 \pm 2.98 \text{ GPa}$. In summary, WGC had favorable properties with a lower E value and a higher K_{IC} than GC4 previously synthesized in *Chapter 2*.

One of the objectives in *Chapter 3* was to test the chemical stability of WGC. The results were very encouraging; the WGC weight loss/unit area in 4% acetic acid satisfied ISO 6872³⁵ specification for dental ceramics, indicating its superb chemical durability. The chemical stability was similar to the chemically durable YZ that is used widely to construct dental restorations.³⁶ Degradation testing (ISO 10993-14)³⁷ of the WGC showed insignificant degradation ranging from 0% at day 1 to 0.36% after 120 days of soaking in tris buffered solution. Assessment of the K_{IC} of WGC after the chemical stability tests showed no significant effect on the K_{IC} values ($p > 0.05$), providing support that soaking GC specimens in different solutions for various time periods did not affect mechanical

properties. In general, we concluded that WGC had both superior chemical stability and mechanical properties among the GCs in the study. As a result, it was selected for investigation of bioactivity and biocompatibility presented in *Chapter 4*.

In *chapter 4* (Bioactivity and Biocompatibility of a Novel Wollastonite Glass-Ceramic), bioactivity testing of WGC was performed by soaking specimens in SBF for different time. SEM, XRD and EDX revealed that WGC promoted the formation of bone-like HA on the surfaces of the specimens. These results were in agreement with other *in vitro* and *in vivo* studies of bioactivity of wollastonite GC.^{28,30,38-41} The synthesis procedures, chemical compositions, and mechanical properties of these GCs were different from the WGC that was synthesized in *Chapter 3*, but all of these GCs including WGC had wollastonite as the main crystalline phase. These studies showed that both wollastonite and pseudowollastonite GCs were bioactive. It was observed that the formation of apatite on wollastonite ceramics was faster than that on other bioglass or GCs in SBF.³⁰ Bioactivity of dental implants plays a critical role in improving its osseointegration,⁴² in which osteoblast proliferate on the formed apatite layer leading to direct contact between implant material and surrounding bone, thus establishing a strong chemical bond between the newly formed apatite and bone.^{28,43}

The biocompatibility of WGC was assessed in *Chapter 4* in comparison with the biocompatible zirconia (YZ).⁴⁴⁻⁴⁶ All tests compared forwardly to YZ, indicating the excellent biocompatibility of WGC and absence of any possible toxic reactions. Attached cells showed favorable morphological features of flattened polygonal morphology with multiple cytoplasmic extensions accompanied with highly organized actin stress fibers. Focal adhesion (FA) formations on WGC increased significantly with increased culture

time of the osteoblast cells, indicating a positive reaction of cells. FA is directly related to cell spreading under all conditions.⁴⁷ FA formation is also the indication of subsequent cell migration, proliferation, and differentiation that precedes new bone formation.⁴⁸ Lastly, WGC supported osteoblast proliferation; a result in agreement with other studies of osteoblast proliferation on apatite-wollastonite GC.^{44,49}

Alkaline phosphatase (ALP) is a widely recognized biochemical marker used to evaluate osteoblast differentiation, which is required for osteogenesis and subsequent implant osseointegration.⁵⁰ ALP activity was retained and increased with time on WGC specimens, indicating the ability of the osteoblast to differentiate – leading to *in vivo* initiation of bone calcification and consequent HA crystal formation.⁵¹ Overall, WGC showed positive interactions with osteoblasts by supporting their attachment, proliferation, and keeping up FA formation and ALP activity.

To the best of our knowledge, WGC is a novel material proposed for non-metallic, one-piece dental implant applications owing to its appropriate mechanical and chemical properties, machinability, bioactivity and biocompatibility. WGC is a promising biomaterial to satisfy the public as well as the dental profession new trend towards metal-free restorations.

5.1 LIMITATION OF THE RESEARCH AND FUTURE DIRECTIONS

5.1.1 Limitations

There are limitations encountered in the work done in the thesis:

1. In spite of superior mechanical properties, excellent bioactivity and biocompatibility, miserite GC exhibited inadequate chemical stability. Modifications of the chemical composition and/or heat treatment schedules are required to preserve the miserite as the main crystalline phase and to improve its chemical stability – either in accordance to ISO 6872 of dental ceramics and in accordance to ISO 10993-14.
2. Chemical durability of the GCs was evaluated based on ISO 6872 (on acidic environment) and on ISO 10933-14 (in neutral pH). Yet, recent study disclosed that basic pH buffer solution (pH of 10) resulted in a complete breakdown of the silica network of the dental ceramics.⁵²
3. Fatigue resistance is an essential property of dental implants. In vitro study disclosed that one-piece zirconia and titanium dental implant specimens failed after subjected to stepped fatigue-loading test.⁵³ The tests showed that the fatigue strength of zirconia was three times lower than that of titanium dental implants. Although Young's modulus, true hardness, and fracture toughness of WGC were considered suitable for dental implant applications, another critical property of dental implant such as fatigue resistance was not tested.
4. Mature osteoblasts influence osteoclastogenesis and normal bone remodeling.⁵⁴ Hence, further investigation in osteoblast marker gene expressions, mineral deposits in the osteoblast cultures and osteoclast activity on WGC specimens will be required.

5. The incidences of marginal infection, peri-implant mucositis, and peri-implantitis are increasing significantly. These incidences are considered being one of the fundamental factors of implant failure.⁵⁵ Therefore, evaluating the biocompatibility of implant materials with gingival fibroblast, bacterial adhesive properties on their surfaces, and their anti-inflammatory properties are the fundamental tests for dental implants.⁵⁶

5.1.2 Future Directions

This thesis provides the groundwork on the synthesis process, characterization, and potential application of a strong, chemically durable, machinable, bioactive, and biocompatible wollastonite GC for non-metallic one-piece dental implants. The following experiments are suggested to investigate further areas to set the stage for clinical applications:

1. Testing the dynamic fatigue strength of WGC using ISO 14801 standard to determine the functional loads of WGC under two different environments – dry and simulated body conditions.
2. Retesting the dynamic fatigue strength of WGC after the assessment of its chemical durability in 4% acetic acid for 16 h at 80 °C, and chemical degradation in TBS for 120 days at 37°C.
3. Assessment of other bone markers, including osteoblast gene expression markers and osteoclast cell activity.

4. Conducting *in vivo* studies in animal models such as dogs or monkeys to investigate WGC behavior when implanted in living bone and to ascertain its bioactivity and biocompatibility.
5. Testing the chemical stability of WGC in basic buffered solutions (pH of 10).

5.2 REFERENCES

1. Denry I, Holloway JA. Ceramics for Dental Applications: A Review. *Materials* (1996-1944). 2010;3(1):351-68.
2. Müller F, Naharro M, Carlsson GE. What Are the Prevalence and Incidence of Tooth Loss in the Adult and Elderly Population in Europe? *Clin Oral Implants Res.* 2007;18(s3):2-14.
3. Holm-Pedersen P, Lang NP, Müller F. What Are the Longevities of Teeth and Oral Implants? *Clin Oral Implants Res.* 2007;18(s3):15-9.
4. Glendor U. Etiology and Risk Factors Related to Traumatic Dental Injuries – A Review of the Literature. *Dent Traumatol.* 2009;25(1):19-31.
5. Moreira AN, Rocha ÊS, Popoff DAV, Vilaça ÊL, Castilho LS, de Magalhães CS. Knowledge and Attitudes of Dentists Regarding Ageing and the Elderly. *Gerodontology.* 2012;29(2):624-31.
6. Zarb GA, Fenton AH. *Prosthetic Treatment for Edentulous Patients: Complete Dentures and Implant-Supported pPostheses.* 13th ed. St. Louis, Mo. Elsevier Mosby; 2013.
7. Bergmann CP, Stumpf A. *Dental Ceramics Microstructure, Properties and Degradation* / Carlos P. Bergmann AS, editor. Berlin; New York: Springer; 2013.
8. Masters K. *Spray Drying Handbook.* 4th ed. New York: Halsted Press; 1985.

9. David LD, Anderson RM, Dynys JM, Goldsmith CC, Szule A. Synthesis and Characterization of Cordierite from Acetylacetonate/alkoxide Precursors. *J Mater Res.* 1993;8(7):1697-702.
10. Douy A. Synthesis of Cordierite Powder by Spray-Drying. *J Non Cryst Solids.* 1992;147/148:554-8.
11. Pinckney LR, Beall GH, and Andrus RL. Strong Sintered Miserite Glass-Ceramics. *J Am Ceram Soc.* 1999;82(9):2523-28.
12. Kiprianov AA, Karpukhina NG. Oxyhalide Silicate Glasses. *Glass Phys Chem.* 2006;32(1):1-27.
13. Banijamali S, Eftekhari Yekta B, Rezaie H, Marghussian VK. Effect of Fluorine Content on Sintering and Crystallisation Behaviour of CaO–Al₂O₃–SiO₂ Glass Ceramic System. *Advances in Applied Ceramics.* 2008;107(2):101-5.
14. Molla A, Basu B. Microstructure, Mechanical, and *In Vitro* properties of Mica Glass-Ceramics With Varying Fluorine Content. *J Mater Sci.* 2009;20(4):869-82.
15. Zhang Y, Wang J, Wang P, Fan X, Li X, Fu J, et al. Low elastic modulus contributes to the Osseointegration of Titanium Alloy Plug. *J Biomed Mater Res.* 2013;101B(4):584-90.
16. O'Brien WJ. *Dental Materials and Their Selection.* 4th ed. Hanover Park, IL: Quintessence Pub. Co.; 2008.
17. Natali AN. *Dental Biomechanics.* London; New York: Taylor & Francis; 2003.

18. Andreiotelli M, Wenz HJ, Kohal R. Are Ceramic Implants a Viable Alternative to Titanium Implants? A Systematic Literature Review. *Clin Oral Implants Res.* 2009;20(S4):32-47.
19. Bueno EM, Glowacki J. *Biologic Foundations for Skeletal Tissue Engineering.* San Rafael, CA.; 2011.
20. Park JB, Lakes RS. *Biomaterials: An Introduction.* 3rd ed. New York; London: Springer; 2007.
21. Alizadeh P, Eftekhari Yekta B, Javadi T. Preparation of Machinable Bioactive Mica Diopside-Fluoroapatite Glass-Ceramics. *Adv appl ceram.* 2010;109(1):56-61.
22. Grossman DG. Machinable Glass-Ceramics Based on Tetrasilicic Mica. *J Am Ceram Soc.* 1972;55(9):446-9.
23. Sindel J, Petschelt A, Grellner F, Dierken C, Greil P. Evaluation of Subsurface Damage in CAD/CAM Machined Dental Ceramics. *J Mater Sci Mater Med.* 1998;9(5):291-5.
24. Boccaccini AR. Machinability and Brittleness of Glass-Ceramics. *J Mater Process Tech.* 1997;65(1):302-4.
25. Ellingsen JE, Thomsen P, Lyngstadaas P. Advances in Dental Implant Materials and Tissue Regeneration. *Periodontol 2000.* 2006;41(1):136-56.
26. Choi A, Ben-Nissan B, Matinlinna J, Conway R. Current Perspectives: Calcium Phosphate Nanocoatings and Nanocomposite Coatings in Dentistry. *J Dent Res.* 2013;92(10):853-9.

27. Hench L. Bioceramics-from Concept to Clinic. *J Am Ceram Soc.* 1991;74(7):1487-510.
28. Kokubo T. Bioactive Glass Ceramics: Properties and Applications. *Biomaterials.* 1991;12(2):155-63.
29. Alemany MI, Velasquez P, de la Casa-Lillo MA, De Aza PN. Effect of Materials' Processing Methods on the '*In Vitro*' Bioactivity of Wollastonite Glass-Ceramic Materials. *J Non Cryst Solids.* 2005;351(19–20):1716-26.
30. Liu X, Ding C, Chu PK. Mechanism of Apatite Formation on Wollastonite Coatings in Simulated Body Fluids. *Biomaterials.* 2004 5;25(10):1755-61.
31. Kokubo T. Apatite Formation on Surfaces of Ceramics, Metals and Polymers in Body Environment. *Acta Materialia.* 1998;46(7):2519-27.
32. Wang RR, Li Y. *In Vitro* Evaluation of Biocompatibility of Experimental Titanium Alloys for Dental Restorations. *J Prosthet Dent.* 1998 10;80(4):495-500.
33. Ayyala Somayajula D. Biocompatibility of Osteoblast Cells on Titanium Implants [Dissertation]. USA: Cleveland State University; 2008.
34. Gahlert M, Röhling S, Wieland M, Sprecher CM, Kniha H, Milz S. Osseointegration of zirconia and titanium dental implants: A Histological and Histomorphometrical Study in the Maxilla of Pigs. *Clin Oral Implants Res.* 2009;20(11):1247-53.
35. International. ISO standard 6782; Dentistry, Ceramic Materials. 2008.

36. Hisbergues M, Vendeville S, Vendeville P. Zirconia: Established Facts and Perspectives for a Biomaterial in Dental Implantology. *J Biomed Mater Res.* 2009;88B(2):519-29.
37. International ISO Standard. 10993-14. Biological Evaluation of Medical Devices, Part 14; Identification and Quantification of Degradation Products from Ceramics. 2001.
38. Zhu H, Shen J, Feng X, Zhang H, Guo Y, Chen J. Fabrication and Characterization of Bioactive Silk Fibroin/Wollastonite Composite Scaffolds. *Mat Sci Eng C.* 2010;30(1):132-40.
39. Park J, Ozturkk A. Bioactivity of Apatite-Wollastonite Glass-Ceramics Produced by Melting Casting. *Surf Rev Lett.* 2013;20(1).
40. De Aza PN, Guitian F, de Aza S. Bioactivity of Wollastonite Ceramics: *In Vitro* Evaluation. *Scripta Metallurgica et Materiala.* 1994;31(8):1001-5.
41. Xue W, Liu X, Zheng X, Ding C. *In Vivo* Evaluation of Plasma-Sprayed Wollastonite Coating. *Biomaterials.* 2005;26(17):3455-60.
42. Ducheyne P, Ei-Ghannam A, Shapiro I. Effect of Bioactive Glass Templates on Osteoblast Proliferation and *In Vitro* Synthesis of Bone-Like Tissue. *J Cell Biochem.* 1994;56(2):162-7.
43. Kokubo T, Kim H, Kawashita M. Novel Bioactive Materials With Different Mechanical Properties. *Biomaterials.* 2003 6;24(13):2161-75.
44. Möller B, Terheyden H, Açil Y, Purcz NM, Hertrampf K, Tabakov A, *et al.* A Comparison of Biocompatibility and Osseointegration of Ceramic and Titanium

- Implants: An *In Vivo* and *In Vitro* Study. *Int J Oral Maxillofac Surg*. 2012;41(5):638-45.
45. Liu Y, Lee T, Lui T. Enhanced Osteoblastic Cell Response on Zirconia by Bio-Inspired Surface Modification. *Colloids Surf B Biointerfaces*. 2013;106(1):37-45.
 46. Popescu S, Popescu F, Burlibasa L. *In Vitro* Biocompatibility of Zirconia. *Metal Int*. 2010;15(4):14-25.
 47. Petit V, Thiery J. Focal Adhesions: Structure and Dynamics. *Biol Cell*. 2000;92(7):477-94.
 48. Josset Y, Oum'Hamed Z, Zarrinpour A, Lorenzato M, Adnet JJ, Laurent-Maquin D. *In Vitro* Reactions of Human Osteoblasts in Culture With Zirconia and Alumina Ceramics. *J Biomed Mater Res*. 1999;47(4):481-93.
 49. Rea SM, Brooks RA, Best SM, Kokubo T, Bonfield W. Proliferation and Differentiation of Osteoblast-Like Cells on Apatite-Wollastonite/Polyethylene Composites. *Biomaterials*. 2004;25(18):4503-12.
 50. Pivodova V, Frankova J, Ulrichova J. Osteoblast and Gingival Fibroblast Markers in Dental Implant Studies. *Biomed Pap*. 2011;155(2):109-16.
 51. Harris H. The Human Alkaline Phosphatases: What We Know and What We Don't Know. *Clin Chim Acta*. 1990;186(2):133-50.
 52. Esquivel-Upshaw JF, Dieng FY, Clark AE, Neal D, Anusavice KJ. Surface Degradation of Dental Ceramics As a Function of Environmental pH. *J Dent Res*. 2013;92(5):467-71.

53. Foong JKW, Judge RB, Palamara JE, Swain MV. Fracture Resistance of Titanium and Zirconia Abutments: An *In Vitro* Study. *J Prosthet Dent.* 2013 5;109(5):304-12.
54. Thomas GP, Baker SUK, Eisman JA, Gardiner EM. Changing RANKL/OPG mRNA Expression in Differentiating Murine Primary Osteoblasts. *J Endocrinol.* 2001;170(2):451-60.
55. Algraft H, Borumandi F, Cascarini L. Peri-Implantitis. *Br J Oral Maxillofac Surg.* 2012;50(8):689-94.
56. Franková,J., Pivodová V, Růžička F, Tománková K, Šafářová K, Vrbková J, *et al.* Comparing Biocompatibility of Gingival Fibroblasts and Bacterial Strains on a different Modified Titanium Discs. *J Biomed Mater Res Part A* [24]. 2013;101(10):2915.

APPENDICES

APPENDIX A

COPYRIGHT PERMISSIONS

To view this email as a web page, go [here](#).

Do Not Reply Directly to This Email

To ensure that you continue to receive our emails, please add rightslink@marketing.copyright.com to your [address book](#).

RightsLink



Thank You For Your Order!

Dear Dr. Selma Saadaldin,

Thank you for placing your order through Copyright Clearance Center's RightsLink service. Elsevier has partnered with RightsLink to license its content. This notice is a confirmation that your order was successful.

Your order details and publisher terms and conditions are available by clicking the link below:

<http://s100.copyright.com/CustomerAdmin/PLF.jsp?ref=fafa16c1-9862-427c-8d7b-5adb8c30a044>

Order Details

Licensee: Selma Saadaldin

License Date: Jul 18, 2013

License Number: 3192030075400

Publication: Dental Materials

Title: Synthesis of bioactive and machinable miserite glass-ceramics for dental implant applications

Type Of Use: reuse in a thesis/dissertation

Total: 0.00 USD

To access your account, please visit <https://myaccount.copyright.com>.

Please note: Online payments are charged immediately after order confirmation; invoices are issued daily and are payable immediately upon receipt.

To ensure we are continuously improving our services, please take a moment to complete our [customer satisfaction survey](#).

B.1:v4.2

+1-877-622-5543 / Tel: +1-978-646-2777



This email was sent to: ssaadal@uwo.ca

Please visit [Copyright Clearance Center](#) for more information.

This email was sent by Copyright Clearance Center
222 Rosewood Drive Danvers, MA 01923 USA

To view the privacy policy, please [go here](#).

**ELSEVIER LICENSE
TERMS AND CONDITIONS**

Oct 19, 2013

This is a License Agreement between Selma Saadaldin ("You") and Elsevier ("Elsevier") provided by Copyright Clearance Center ("CCC"). The license consists of your order details, the terms and conditions provided by Elsevier, and the payment terms and conditions.

All payments must be made in full to CCC. For payment instructions, please see information listed at the bottom of this form.

Supplier	Elsevier Limited The Boulevard, Langford Lane Kidlington, Oxford, OX5 1GB, UK
Registered Company Number	1982084
Customer name	Selma Saadaldin
License number	3192030075400
License date	Jul 18, 2013
Licensed content publisher	Elsevier
Licensed content publication	Dental Materials
Licensed content title	Synthesis of bioactive and machinable miserite glass-ceramics for dental implant applications
Licensed content author	Selma A. Saadaldin, S. Jeffrey Dixon, Daniel O. Costa, Amin S. Rizkalla
Licensed content date	June 2013
Licensed content volume number	29
Licensed content issue number	6
Number of pages	11
Start Page	645
End Page	655
Type of Use	reuse in a thesis/dissertation
Portion	full article
Format	both print and electronic
Are you the author of this Elsevier article?	Yes
Will you be translating?	No
Order reference number	
Title of your thesis/dissertation	Glass-ceramics for non-metallic dental implant applications
Expected completion date	Sep 2013

Estimated size (number of pages)

Elsevier VAT number GB 494 6272 12

Permissions price 0.00 USD

VAT/Local Sales Tax 0.00 USD / GBP

Total 0.00 USD

[Terms and Conditions](#)

INTRODUCTION

1. The publisher for this copyrighted material is Elsevier. By clicking "accept" in connection with completing this licensing transaction, you agree that the following terms and conditions apply to this transaction (along with the Billing and Payment terms and conditions established by Copyright Clearance Center, Inc. ("CCC"), at the time that you opened your Rightslink account and that are available at any time at <http://myaccount.copyright.com>).

GENERAL TERMS

2. Elsevier hereby grants you permission to reproduce the aforementioned material subject to the terms and conditions indicated.

3. Acknowledgement: If any part of the material to be used (for example, figures) has appeared in our publication with credit or acknowledgement to another source, permission must also be sought from that source. If such permission is not obtained then that material may not be included in your publication/copies. Suitable acknowledgement to the source must be made, either as a footnote or in a reference list at the end of your publication, as follows:

“Reprinted from Publication title, Vol /edition number, Author(s), Title of article / title of chapter, Pages No., Copyright (Year), with permission from Elsevier [OR APPLICABLE SOCIETY COPYRIGHT OWNER].” Also Lancet special credit - “Reprinted from The Lancet, Vol. number, Author(s), Title of article, Pages No., Copyright (Year), with permission from Elsevier.”

4. Reproduction of this material is confined to the purpose and/or media for which permission is hereby given.

5. Altering/Modifying Material: Not Permitted. However figures and illustrations may be altered/adapted minimally to serve your work. Any other abbreviations, additions, deletions and/or any other alterations shall be made only with prior written authorization of Elsevier Ltd. (Please contact Elsevier at permissions@elsevier.com)

6. If the permission fee for the requested use of our material is waived in this instance, please be advised that your future requests for Elsevier materials may attract a fee.

7. Reservation of Rights: Publisher reserves all rights not specifically granted in the combination of (i) the license details provided by you and accepted in the course of this licensing transaction, (ii) these terms and conditions and (iii) CCC's Billing and Payment terms and conditions.

8. License Contingent Upon Payment: While you may exercise the rights licensed immediately upon issuance of the license at the end of the licensing process for the transaction, provided that you have disclosed complete and accurate details of your proposed

use, no license is finally effective unless and until full payment is received from you (either by publisher or by CCC) as provided in CCC's Billing and Payment terms and conditions. If full payment is not received on a timely basis, then any license preliminarily granted shall be deemed automatically revoked and shall be void as if never granted. Further, in the event that you breach any of these terms and conditions or any of CCC's Billing and Payment terms and conditions, the license is automatically revoked and shall be void as if never granted. Use of materials as described in a revoked license, as well as any use of the materials beyond the scope of an unrevoked license, may constitute copyright infringement and publisher reserves the right to take any and all action to protect its copyright in the materials.

9. **Warranties:** Publisher makes no representations or warranties with respect to the licensed material.

10. **Indemnity:** You hereby indemnify and agree to hold harmless publisher and CCC, and their respective officers, directors, employees and agents, from and against any and all claims arising out of your use of the licensed material other than as specifically authorized pursuant to this license.

11. **No Transfer of License:** This license is personal to you and may not be sublicensed, assigned, or transferred by you to any other person without publisher's written permission.

12. **No Amendment Except in Writing:** This license may not be amended except in a writing signed by both parties (or, in the case of publisher, by CCC on publisher's behalf).

13. **Objection to Contrary Terms:** Publisher hereby objects to any terms contained in any purchase order, acknowledgment, check endorsement or other writing prepared by you, which terms are inconsistent with these terms and conditions or CCC's Billing and Payment terms and conditions. These terms and conditions, together with CCC's Billing and Payment terms and conditions (which are incorporated herein), comprise the entire agreement between you and publisher (and CCC) concerning this licensing transaction. In the event of any conflict between your obligations established by these terms and conditions and those established by CCC's Billing and Payment terms and conditions, these terms and conditions shall control.

14. **Revocation:** Elsevier or Copyright Clearance Center may deny the permissions described in this License at their sole discretion, for any reason or no reason, with a full refund payable to you. Notice of such denial will be made using the contact information provided by you. Failure to receive such notice will not alter or invalidate the denial. In no event will Elsevier or Copyright Clearance Center be responsible or liable for any costs, expenses or damage incurred by you as a result of a denial of your permission request, other than a refund of the amount(s) paid by you to Elsevier and/or Copyright Clearance Center for denied permissions.

LIMITED LICENSE

The following terms and conditions apply only to specific license types:

15. **Translation:** This permission is granted for non-exclusive world **English** rights only unless your license was granted for translation rights. If you licensed translation rights you may only translate this content into the languages you requested. A professional translator must perform all translations and reproduce the content word for word preserving the integrity of the article. If this license is to re-use 1 or 2 figures then permission is granted for non-exclusive world rights in all languages.

16. Website: The following terms and conditions apply to electronic reserve and author websites:

Electronic reserve: If licensed material is to be posted to website, the web site is to be password-protected and made available only to bona fide students registered on a relevant course if:

This license was made in connection with a course,

This permission is granted for 1 year only. You may obtain a license for future website posting,

All content posted to the web site must maintain the copyright information line on the bottom of each image,

A hyper-text must be included to the Homepage of the journal from which you are licensing at <http://www.sciencedirect.com/science/journal/xxxxx> or the Elsevier homepage for books at <http://www.elsevier.com> , and

Central Storage: This license does not include permission for a scanned version of the material to be stored in a central repository such as that provided by Heron/XanEdu.

17. Author website for journals with the following additional clauses:

All content posted to the web site must maintain the copyright information line on the bottom of each image, and the permission granted is limited to the personal version of your paper. You are not allowed to download and post the published electronic version of your article (whether PDF or HTML, proof or final version), nor may you scan the printed edition to create an electronic version. A hyper-text must be included to the Homepage of the journal from which you are licensing at <http://www.sciencedirect.com/science/journal/xxxxx> .

As part of our normal production process, you will receive an e-mail notice when your article appears on Elsevier's online service ScienceDirect (www.sciencedirect.com). That e-mail will include the article's Digital Object Identifier (DOI). This number provides the electronic link to the published article and should be included in the posting of your personal version. We ask that you wait until you receive this e-mail and have the DOI to do any posting.

Central Storage: This license does not include permission for a scanned version of the material to be stored in a central repository such as that provided by Heron/XanEdu.

18. Author website for books with the following additional clauses:

Authors are permitted to place a brief summary of their work online only.

A hyper-text must be included to the Elsevier homepage at <http://www.elsevier.com> . All content posted to the web site must maintain the copyright information line on the bottom of each image. You are not allowed to download and post the published electronic version of your chapter, nor may you scan the printed edition to create an electronic version.

Central Storage: This license does not include permission for a scanned version of the material to be stored in a central repository such as that provided by Heron/XanEdu.

19. Website (regular and for author): A hyper-text must be included to the Homepage of the journal from which you are licensing at <http://www.sciencedirect.com/science/journal/xxxxx> . or for books to the Elsevier homepage at <http://www.elsevier.com>

20. Thesis/Dissertation: If your license is for use in a thesis/dissertation your thesis may be submitted to your institution in either print or electronic form. Should your thesis be published commercially, please reapply for permission. These requirements include permission for the Library and Archives of Canada to supply single copies, on demand, of the complete thesis and include permission for UMI to supply single copies, on demand, of the complete thesis. Should your thesis be published commercially, please reapply for

permission.

21. Other Conditions: Permission is granted to submit your article in print and electronic format. This license permits you to post this Elsevier article online if it is embedded within your thesis. You are also permitted to post your Author Accepted Manuscript online however posting of the final published article is prohibited. Please refer to Elsevier's Posting Policy for further information:

<http://www.elsevier.com/wps/find/authors.authors/postingpolicy>

v1.6

If you would like to pay for this license now, please remit this license along with your payment made payable to "COPYRIGHT CLEARANCE CENTER" otherwise you will be invoiced within 48 hours of the license date. Payment should be in the form of a check or money order referencing your account number and this invoice number RLNK501069322.

Once you receive your invoice for this order, you may pay your invoice by credit card. Please follow instructions provided at that time.

**Make Payment To:
Copyright Clearance Center
Dept 001
P.O. Box 843006
Boston, MA 02284-3006**

For suggestions or comments regarding this order, contact RightsLink Customer Support: customercare@copyright.com or +1-877-622-5543 (toll free in the US) or +1-978-646-2777.

Gratis licenses (referencing \$0 in the Total field) are free. Please retain this printable license for your reference. No payment is required.



Dear Selma Saadaldin

We hereby grant you permission to reprint the material detailed below at no charge **in your thesis** subject to the following conditions:

1. If any part of the material to be used (for example, figures) has appeared in our publication with credit or acknowledgement to another source, permission must also be sought from that source. If such permission is not obtained then that material may not be included in your publication/copies.
2. Suitable acknowledgment to the source must be made, either as a footnote or in a reference list at the end of your publication, as follows:

“This article was published in Publication title, Vol number, Author(s), Title of article, Page Nos, Copyright Elsevier (or appropriate Society name) (Year).”
3. Your thesis may be submitted to your institution in either print or electronic form.
4. Reproduction of this material is confined to the purpose for which permission is hereby given.
5. This permission is granted for non-exclusive world **English** rights only. For other languages please reapply separately for each one required. Permission excludes use in an electronic form other than submission. Should you have a specific electronic project in mind please reapply for permission
6. This includes permission for the Library and Archives of Canada to supply single copies, on demand, of the complete thesis. Should your thesis be published commercially, please reapply for permission.

Yours sincerely

Jennifer Jones
Rights Associate

Elsevier Limited, a company registered in England and Wales with company number 1982084, whose registered office is The Boulevard, Langford Lane, Kidlington, Oxford, OX5 1GB, United Kingdom.

Sent: 27 October 2013 23:10
To: Rights and Permissions (ELS)
Subject: Obtain Permission - Book request

Title: Ms.
First name: Selma
Last name: Saadaldin
Institute/company: Western University
Address: 1151 Richmond St
Post/Zip Code: N6A 3K7
City: London
Country: Canada
Please select the type of publication: Book
Book - Title: Dental Implants
Book - ISBN: 978-1-4160-5341-5
Book - Author(s): Charles Babbush Jack Hahn Jack Krauser Joel Rosenlicht.
Book - Year: 2010
Book - Pages from: 2
Book - Pages to: 2
Book - Chapter Num: 1
Book - Chapter Title: The future news and demand for dental implants

I would like to use (please select one of the following options): Figures
If using figures/tables or illustrations please specify the quantity: 300 dpi
Are you the author of the material?: No
If not, is the author involved with your project: No
In what format will you use the material?: Print and Electronic
Will you be translating the material?: No
Information about your proposed use: thesis

Proposed use text: Dear I am a University of Western Ontario graduate student cc Doctorals thesis . I would like permission to allow inclusion c material in my thesis figure 1-1 from Dental Implant book.

Additional Can I have the copy right permission on Nov. 2nd 2013

RightsLink



Thank You For Your Order!

Dear Dr. Selma Saadaldin,

Thank you for placing your order through Copyright Clearance Center's RightsLink service. John Wiley and Sons has partnered with RightsLink to license its content. This notice is a confirmation that your order was successful.

Your order details and publisher terms and conditions are available by clicking the link below:

<http://s100.copyright.com/CustomerAdmin/PLF.jsp?ref=6979e8b6-e508-4184-8769-a16b47b6292a>

Order Details

Licensee: Selma Saadaldin

License Date: Oct 27, 2013

License Number: 3257400874425

Publication: Clinical Implant Dentistry and Related Research

Title: Fracture Strength of Zirconia Implants after Artificial Aging

Type Of Use: Dissertation/Thesis

Total: 0.00 USD

To access your account, please visit <https://myaccount.copyright.com>.

Please note: Online payments are charged immediately after order confirmation; invoices are issued daily and are payable immediately upon receipt.

To ensure we are continuously improving our services, please take a moment to complete our [customer satisfaction survey](#).

B.1:v4.2

+1-877-622-5543 / Tel: +1-978-646-2777





Title: Fracture Strength of Zirconia Implants after Artificial Aging
 Author: Marina Andreiotelli,Ralf-Joachim Kohal
 Publication: Clinical Implant Dentistry and Related Research
 Publisher: John Wiley and Sons
 Date: Jul 24, 2008
 © 2008, Copyright the Authors. Journal Compilation © 2008, Wiley Periodicals, Inc.

Logged in as:
 Selma Saadaldin
 Account #:
 3000675268

Order Completed

Thank you very much for your order.

This is a License Agreement between Selma Saadaldin ("You") and John Wiley and Sons ("John Wiley and Sons"). The license consists of your order details, the terms and conditions provided by John Wiley and Sons, and the [payment terms and conditions](#).

[Get the printable license](#).

License Number	3257400874425
License date	Oct 27, 2013
Licensed content publisher	John Wiley and Sons
Licensed content publication	Clinical Implant Dentistry and Related Research
Licensed content title	Fracture Strength of Zirconia Implants after Artificial Aging
Licensed copyright line	© 2008, Copyright the Authors. Journal Compilation © 2008, Wiley Periodicals, Inc.
Licensed content author	Marina Andreiotelli,Ralf-Joachim Kohal
Licensed content date	Jul 24, 2008
Start page	158
End page	166
Type of use	Dissertation/Thesis
Requestor type	University/Academic
Format	Print and electronic
Portion	Figure/table
Number of figures/tables	1
Original Wiley figure/table number(s)	Figure 1(b)
Will you be translating?	No
Total	0.00 USD



Copyright © 2013 [Copyright Clearance Center, Inc.](#) All Rights Reserved. [Privacy statement](#).
 Comments? We would like to hear from you. E-mail us at customer care@copyright.com

RightsLink



Thank You For Your Order!

Dear Dr. Selma Saadaldin,

Thank you for placing your order through Copyright Clearance Center's RightsLink service. John Wiley and Sons has partnered with RightsLink to license its content. This notice is a confirmation that your order was successful.

Your order details and publisher terms and conditions are available by clicking the link below:

<http://s100.copyright.com/CustomAdmin/PLF.jsp?ref=9e79c9f3-3c5b-457a-82a2-ba3912977000>

Order Details

Licensee: Selma Saadaldin

License Date: Oct 27, 2013

License Number: 3257400581518

Publication: Wiley Books

Title: Glass Ceramic Technology, 2nd Edition

Type Of Use: Dissertation/Thesis

Total: 0.00 USD

To access your account, please visit <https://myaccount.copyright.com>.

Please note: Online payments are charged immediately after order confirmation; invoices are issued daily and are payable immediately upon receipt.

To ensure we are continuously improving our services, please take a moment to complete our [customer satisfaction survey](#).

B.1:v4.2

+1-877-622-5543 / Tel: +1-978-646-2777





Book: Glass Ceramic Technology, 2nd Edition
 Author: Wolfram Holand, George H. Beall
 Publisher: John Wiley and Sons
 Date: Jun 1, 2012
 Copyright © 2012, John Wiley and Sons

Logged in as:
 Selma Saadaldin
 Account #:
 3000675268



Order Completed

Thank you very much for your order.

This is a License Agreement between Selma Saadaldin ("You") and John Wiley and Sons ("John Wiley and Sons"). The license consists of your order details, the terms and conditions provided by John Wiley and Sons, and the [payment terms and conditions](#).

[Get the printable license](#).

License Number	3257400581518
License date	Oct 27, 2013
Licensed content publisher	John Wiley and Sons
Licensed content publication	Wiley Books
Licensed content title	Glass Ceramic Technology, 2nd Edition
Book title	Glass Ceramic Technology, 2nd Edition
Licensed copyright line	Copyright © 2012, John Wiley and Sons
Licensed content author	Wolfram Holand, George H. Beall
Licensed content date	Jun 1, 2012
Type of use	Dissertation/Thesis
Requestor type	University/Academic
Format	Print and electronic
Portion	Figure/table
Number of figures/tables	3
Original Wiley figure/table number(s)	Figure 4-36, 4-53, 4-47(b)
Will you be translating?	No
Total	0.00 USD



Copyright © 2013 [Copyright Clearance Center, Inc.](#) All Rights Reserved. [Privacy statement](#).
 Comments? We would like to hear from you. E-mail us at customercare@copyright.com

RightsLink



Thank You For Your Order!

Dear Dr. Selma Saadaldin,

Thank you for placing your order through Copyright Clearance Center's RightsLink service. Elsevier has partnered with RightsLink to license its content. This notice is a confirmation that your order was successful.

Your order details and publisher terms and conditions are available by clicking the link below:

<http://s100.copyright.com/CustomAdmin/PLF.jsp?ref=74e39e52-4c83-4daa-a074-f6e8a27f62d9>

Order Details

Licensee: Selma Saadaldin

License Date: Oct 27, 2013

License Number: 3257401251093

Publication: Journal of Dentistry

Title: An overview of zirconia ceramics: Basic properties and clinical applications

Type Of Use: reuse in a thesis/dissertation

Total: 0.00 USD

To access your account, please visit <https://myaccount.copyright.com>.

Please note: Online payments are charged immediately after order confirmation; invoices are issued daily and are payable immediately upon receipt.

To ensure we are continuously improving our services, please take a moment to complete our [customer satisfaction survey](#).

B.1:v4.2

+1-877-622-5543 / Tel: +1-978-646-2777





Title: An overview of zirconia ceramics: Basic properties and clinical applications
 Author: Paolo Francesco Manicone, Pierfrancesco Rossi Iommetti, Luca Raffaelli
 Publication: Journal of Dentistry
 Publisher: Elsevier
 Date: November 2007
 Copyright © 2007, Elsevier

Logged in as:
 Selma Saadaldin
 Account #:
 3000675268



Order Completed

Thank you very much for your order.

This is a License Agreement between Selma Saadaldin ("You") and Elsevier ("Elsevier"). The license consists of your order details, the terms and conditions provided by Elsevier, and the [payment terms and conditions](#).

[Get the printable license.](#)

License Number	3257401251093
License date	Oct 27, 2013
Licensed content publisher	Elsevier
Licensed content publication	Journal of Dentistry
Licensed content title	An overview of zirconia ceramics: Basic properties and clinical applications
Licensed content author	Paolo Francesco Manicone, Pierfrancesco Rossi Iommetti, Luca Raffaelli
Licensed content date	November 2007
Licensed content volume number	35
Licensed content issue number	11
Number of pages	8
Type of Use	reuse in a thesis/dissertation
Portion	figures/tables/illustrations
Number of figures/tables/illustrations	1
Format	both print and electronic
Are you the author of this Elsevier article?	No
Will you be translating?	No
Order reference number	
Title of your thesis/dissertation	Glass-Ceramics for Non-Metallic Dental Implant Application
Expected completion date	Nov 2013
Estimated size (number of pages)	160
Elsevier VAT number	GB 494 6272 12
Permissions price	0.00 USD
VAT/Local Sales Tax	0.00 USD / 0.00 GBP
Total	0.00 USD



Copyright © 2013 [Copyright Clearance Center, Inc.](#) All Rights Reserved. [Privacy statement](#).
 Comments? We would like to hear from you. E-mail us at customercare@copyright.com

Dear Ms. Saadaldin:

Permission is hereby granted for the use requested subject to the usual acknowledgements (author, title, and copyright [year and owner]. And the statement "This material is reproduced with permission of John Wiley & Sons, Inc.").

Any third party material is expressly excluded from this permission. If any of the material you wish to use appears within our work with credit to another source, authorization from that source must be obtained.

This permission does not include the right to grant others permission to photocopy or otherwise reproduce this material except for accessible versions made by non-profit organizations serving the blind, visually impaired and other persons with print disabilities (VIPs).

Sincerely,

Sheik Safdar | Permissions Coordinator | P: 201-748-6512 | F: 201-748-6008

John Wiley & Sons, Inc. | 111 River Street | Hoboken, NJ | 07030 |
Mailstop: 4-02

A01_First_Name: Selma
A02_Last_Name: Saadaldin
A03_Company: Western University
A04_Address: 1151 Richmond Street
A05_City: London
A06_Province: Ontario
A07_Zip: N6A 3K7
A08_Country: Canada

A12_Reference_Number:
A13_Requestor_Name:
A14_Requestor_Phone: +15196612111
A15_Requestor_Fax:
A16_Product_Title: Anatomy and Physiology: From Science to Life

A17_ISBN: 0471770671

A18_Author_Name: Jenkins, Gail W; Kemnitz, Christopher P; Tortora, Gerard J

A19_Page_Number:

A20_Number_of_Copies:

A21_Semesters:

A22_Professor_Name:

A23_Course_Name:

A24_Organization_Name:

A25_Purpose_Reproduction: reuse in thesis

A26_Title_Your_Work: Glass-Ceramics for non-metallic dental implant applications

A26A_Resale:

A27_Print_Run:

A28_Publication_Date:

A29_World_Rights:

A30_Medium:

A31_Password:

32_Users:

A33_Duration_Posted_Web:

A34_CD_Print_Run: ,

APPENDIX B

Preliminary results of the Chemical stability of miserite GC (Chapter 2)

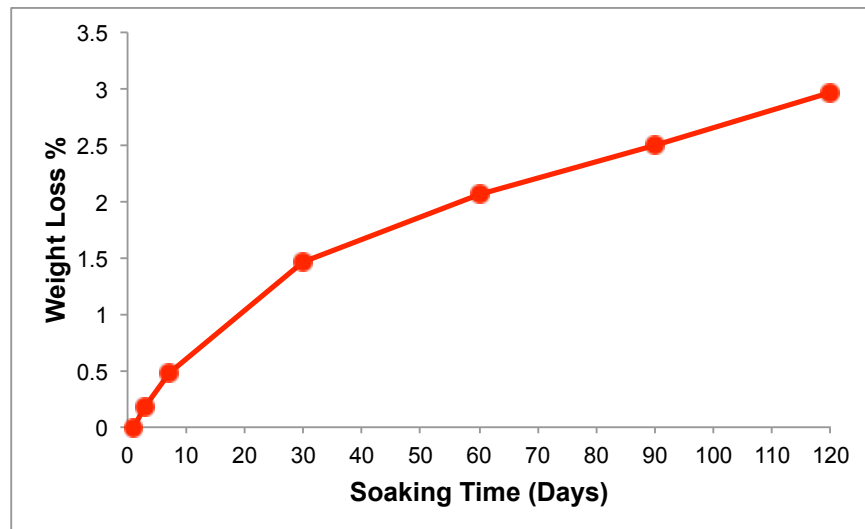
Chemical Durability of miserite GC

Chemical durability of the miserite GC (GC4) was evaluated by measuring mass loss/unit area after soaking the samples in 4% AC, pH=2, according to ISO standard 6782 for dental ceramics. Mass loss was significantly lower than the ISO specification (less than $100 \mu\text{g}/\text{cm}^2$), which means that GC4 cannot be exposed to the harsh oral cavity environments.

Properties	GC4
Mass loss/Unit area ($\mu\text{g}/\text{cm}^2$)	8332(490)

Chemical Degradation of miserite GC

Chemical Degradation of GC4 Degradation test of the experimental miserite GC showing weight loss percentage of the GC specimens after soaking in tris buffered solution (TBS) from 1 day up to 120 days. Weight loss percentage of the specimens was 3% after 120 days soaking in TBS Exponential growth equation was used to show nonlinear fit curve for the degradation rates at different timeline.



SALMA SAADALDIN

CURRICULUM VITAE

POST-SECONDARY EDUCATION

- 2008-2013** Doctor of Philosophy (Candidate)
Department of Medical Biophysics
Western University, London, Ontario
- 1996-1998** Masters of Prosthodontics Dentistry
University of Baghdad, Baghdad, Iraq
- 1985-1990** Bachelor of Dental Surgeon
University of Baghdad, Baghdad, Iraq

HONOURS AND AWARDS

- 2013** Dr. Alfred Jay Medical Biophysics Award - Runner Up
Western University, London, Ontario
- 2012** Three Minute Thesis competition – Finalist
Western University, London, Ontario
- 2008-2012** Schulich Graduate Scholarship - Recipient
Western University, London, Ontario
- 2006** The Outstanding Faculty Award –Winner
Ajman University of Science and Technology, Ajman, UAE
- 2002** Distinguished Teaching Award – Winner
Ajman University of Science and Technology, Ajman, UAE
- 1998** Prosthodontics Graduate Student Award of Excellence - Winner
University of Baghdad, Baghdad, Iraq
- 1990** Honor Student Award – Rank 5th among 197 students
University of Baghdad, Baghdad, Iraq

WORK EXPERIENCE

- 2012-Present** Adjunct Clinical Professor
Schulich School of Medicine and Dentistry
Western University, London, Ontario

- 2008-Present** Graduate Research Assistant
Schulich School of Medicine and Dentistry
Western University, London, Ontario
- 2000-2006** Lecturer
Ajman University of Science and Technology, Ajman, UAE
- 1999-2000** Dentist
Al-Mashriq Medical Centre, United Arab Emirates, Al-Ain
- 1996-1998** Graduate Student
University of Baghdad, Baghdad, Iraq
- 1993-1996** Instructor
University of Baghdad, Baghdad, Iraq
- 1990-1993** Dentist/ Internship
Ministry of Health, Baghdad, Iraq

PUBLICATIONS AND PRESENTATIONS

Papers:

1. ***Saadaldin, SA***; Dixon, SJ; Costa, DO and Rizkalla, AS. Synthesis of bioactive and machinable miserite glass-ceramics for dental implants applications. Dental Materials. 2013 Jun; 29(6): 645-655. doi: 10.1016/j.dental.2013.03.013.
2. ***Saadaldin, SA*** and Amin S Rizkalla. Synthesis and characterization of wollastonite glass-ceramics for dental implant applications. Dental Materials (Accepted for publication, Nov. 2013, Dental Materials).
3. ***Saadaldin, SA***; Dixon, SJ; Costa, DO and Rizkalla, AS. Bioactivity and cell-compatibility of wollastonite glass-ceramics. (Submitted).
4. Vinicius C. Bianco, ***Selma A Saadaldin*** Maria Jacinta M.C. Santos, José H. Rubo, Amin S. Rizkalla, Gildo C. Santos Jr. Fatigue testing of commercial CAD-CAM ceramic materials. Journal of Dentistry. (Submitted).

Presentations:

1. ***Saadaldin, SA***; Development of a High-Strength Machinable Bioactive Glass-Ceramics for Dental Implant Applications. London Health Research Day, London, Ontario, Canada, 2013.
2. ***Saadaldin, SA***, Dixon, SJ; Rizkalla, AS. Synthesis and Characterization of High-Strength Machinable Bioactive Glass-Ceramics for Dental Implant Applications. Annual Research Day, Schulich Dentistry, Western University, London, Ontario, Canada, 2013.

3. **Saadaldin, SA**; Dixon, SJ; Costa, DO and Rizkalla, AS. Machinable Bioactive Glass-Ceramics for Dental Implants. Careers in Academic Dentistry Workshop. Western University, London, Ontario, Canada, 2013.
4. **Saadaldin, SA**; Costa, DO; Dixon, JS and Rizkalla AS. Machinable Bioactive Glass-Ceramics for Dental Implants. Humboldt Colloquium, Toronto, Ontario, Canada, 2012.
5. **Saadaldin, SA**; Dixon, JS and Rizkalla AS. Development of a High-Strength Machinable Bioactive Glass-Ceramic for Dental Implant Applications. 24th Canadian Materials Science Conference. London, Ontario, Canada. 2012.
6. Mustaf, R and **Saadaldin, SA**. The Relationship of Tempromandibular Joint Dysfunction and Edentulous Cases. International Dental Conference. Dubai, UAE. 2006.
7. **Saadaldin, SA**. Improving the Stability of Complete Denture by Application of Neutral Zone Technique. International Dental Conference. Dubai, UAE. 2006.
8. **Saadaldin, SA**. Dentistry in Society/Denture Related Lesions. Lecture Presentation: Approach Seminar. AUST, Al-Ain, UAE. 2004

CERTIFICATES, WORKSHOPS AND TRAINING

2008-2013	Western Certificate in University Teaching and Learning Western University, London, Ontario
2012	Comprehensive Implant Training Program Hands-On-Institute, London Ontario
2008-2010	Continuous Dental Education Western University, London, Ontario